Bipedal Running with One Actuator per Leg

Neil Neville
Department of Mechanical Engineering
McGill University, Montreal, Canada

October 2005

A Thesis submitted to McGill University
in partial fulfillment of the requirements for the degree
of Master of Engineering.

Your file Votre référence
ISBN: 978-0-494-22659-9
Our file Notre référence
ISBN: 978-0-494-22659-9

Thesis Supervisor
M. Buehler and I. Sharf

Author
Neil Neville

Bipedal Running with One Actuator per Leg

Abstract

RHex is a cockroach-inspired hexapod robot capable of walking, running, and climbing. This thesis presents the development of a novel, three dimensional, bipedal running gait for RHex using only two actuated degrees of freedom (DOF), one per compliant leg. To the author's knowledge, there are no previous, two DOF bipeds capable of running. In this thesis it is experimentally demonstrated that only body pitch and leg angle sensing are required. The controller includes three levels of proportional derivative controls for balancing, forward speed and leg tracking, as well a leg trajectory generator and a means of forward speed estimation. With the addition of yaw angle feedback, high repeatability was obtained. Details of a platform upgrade are also presented. Finally, a simulation model of the robot was developed that, in conjunction with a genetic algorithm optimization used to tune the controller and gait parameters, produced a stable gait similar to those observed in experiment.

Directeurs de thèse
M. Buehler and I. Sharf

Auteur
Neil Neville

Résumé

RHex, un robot hexapode inspiré de la coquerelle, peut marcher, courir et même grimper. La présente thèse expose le développement d'une toute nouvelle démarche pour ce robot. En effet, il a été possible de faire courir RHex dans un environnement 3D en n'utilisant que deux de ses six pattes. À la connaissance de l'auteur, RHex serait le premier bipède ne possédant que deux degrés de liberté actionnés pouvoir courir. Pour cette nouvelle démarche, le robot n'a besoin de mesurer que les angles de ses pattes par rapport à son corps ainsi que le lancement de son corps. Trois régulateurs proportionnel-intégral-dérivé (PID) sont utilisés afin de contrôler: (a) l'équilibre du robot, (b) sa vitesse et (c) les angles de ses pattes. De plus, le contrôleur utilise une méthode de planification de la trajectoire des pattes ainsi qu'une méthode d'évaluation de la vitesse du robot. Il est aussi démontré dans cette thèse qu'en utilisant un régulateur sur l'angle de lacet, la reproductibilité de la démarche augmente. Certaines modifications aux systèmes mécaniques et électroniques du robot sont également proposées dans le but d'améliorer la démarche en mode bipède de RHex. Finalement, une simulation du robot est développée et utilisée conjointement à un algorithme d'optimisation afin de stabiliser la démarche.

Contents

List of Figures

List of Tables

List of Symbols

b	Leg width [m], p.79.
c	Dimensionless cycle time, $c \in [0, 1)$, p.22.
$c_1 \cdots c_9$	Constants.
d	Estimated lateral (sideways, X direction) displacement of the midpoint between the hips, p.47.
ds	Infinitesimal displacement.
dt	Infinitesimal period of time.
E	Elastic modulus [N/m^2].
$E_{flight,j}$	Energy input estimate over a flight phase for leg j, p.66.
$E_{stance,j}$	Energy input estimate over a stance phase for leg j, p.66.
f	Stride frequency [1/s], p.6.
F	Point on a leg where the foot is located, p.27.
g	Acceleration of gravity [m/s^2].
h	Leg thickness [m], p.80.
H	Hip point in a sagittal plane model of RHex, p.27.
I	Leg cross section second moment of area [m^4], p.80.
$\mathbf{I}$	RHex inertia matrix taken about body fixed frame xyz (p.28) located at COM [kg m^2], p.78.
i_{est}	Estimated motor current [A], p.40.

$i_{max,d}$	Maximum desired amplifier output current [A], p.82.
i_{max}	Maximum rated amplifier output current [A], p.82.
I_{pitch}	Moment of inertia about the pitch axis of body fixed frame xyz (p.28) [kg m^2], p.18.
I_{roll}	Moment of inertia about the roll axis of body fixed frame xyz (p.28) [kg m^2], p.18.
$\hat{I}_{roll}$	Dimensionless moment of inertia about the roll axis, p.42.
I_{yaw}	Moment of inertia about the yaw axis of body fixed frame xyz (p.28) [kg m^2], p.18.
j	Leg index.
k	Sample index for a digital system.
k_{dp}	Proportional gain for the lateral displacement term of the steering controller, p.47.
k_r	Radial leg stiffness [N/m], p.81.
$k_{rel,leg}$	Relative leg stiffness, p.69.
K_s	Motor speed constant [(rad/s)/V], p.33.
K_t	Motor torque constant [Nm/A], p.33.
k_{vp}	Proportional gain for the forward speed PD controller, p.30.
k_{vd}	Derivative gain for the forward speed PD controller, p.30.
$k_{\phi p}$	Proportional gain for the leg tracking PD controller, p.32.
$k_{\phi d}$	Derivative gain for the leg tracking PD controller, p.32.
$k_{\psi p}$	Proportional gain for the yaw term of the steering controller, p.47.
$k_{\theta p}$	Proportional gain for the pitch PD controller, p.30.
$k_{\theta d}$	Derivative gain for the pitch PD controller, p.30.
L	Half the hip spacing [m], p.42.
L_{arm}	Motor armature inductance [H], p.55.

l_{ave}	Average effective leg length in stance (estimated) [m], p.31.
l_e	Effective leg length [m], p.27.
ll_j	The lower limit below which a penalty is applied for parameter j in the genetic algorithm fitness function, p.85.
m	RHex robot mass [kg], p.18.
M	Bending moment [Nm].
n	Number of legs used in stance, p.69.
N	Gear ratio [(rad/s output)/(rad/s input)], p.33.
$\mathbf{p}$	Force applied to a leg at the foot, p.80.
P	Instantaneous power input to the robot [W], p.63.
P_{ave}	Average power input to the robot [W], p.63.
$\bar{P}_{flight,j}$	Average power input estimate over a flight phase for leg j, p.66.
p_j	Penalty assigned in the genetic algorithm penalty function for leg j, p.85.
$\mathbf{p}_r$	Radial leg force of magnitude P [N], p.80.
$\bar{P}_{stance,j}$	Average power input estimate over a stance phase for leg j, p.66.
$\bar{P}_{stride,j}$	Average power input estimate over a complete stride for leg j, p.66.
P_y, P_z	Forces applied to the leg at the foot in the y and z directions respectively, p.85.
q	Stride number
r	Undeflected leg radius [m].
R_{amp}	Motor amplifier resistance [Ω], p.55.
R_{arm}	Armature resistance [Ω], p.33.
T	Sampling period [s], p.22.
t_c	Stride period [s], p.6.

t_{end}	Simulated duration of a Simulink/ADAMS simulation trial [s], p.84.
t_f	Duration of the leg protraction (flight) phase [s], p.21.
t_{IIR}	Time constant of the forward speed estimation filter [s], p.38.
t_s	Duration of the stance phase [s], p.20.
U	Strain energy [J].
ul_j	The upper limit above which a penalty is applied for parameter j in the genetic algorithm fitness function, p.85.
V	Shear force [N].
$\bar{v}$	Estimated forward speed of the robot, taken at the midpoint between the hips [m/s], p.39.
v_{ave}	Average forward speed of the robot, taken at the midpoint between the hips [m/s], p.63.
v_d	Desired forward speed of the robot [m/s], p.30.
V_{EMF}	Motor back EMF voltage [V], p.33.
V_m	Motor voltage [V], p.66 and p.33.
$w_1 \cdots w_5$	Weighting constants in the genetic algorithm fitness function, p.85.
x	RHex body fixed coordinate axis.
X	Inertial frame coordinate axis.
y	RHex body fixed coordinate axis.
y_f, $y_{f\Delta}$, y_{f0}	Terms used in Controller #2, see p.36.
Y	Inertial frame coordinate axis.
z	RHex body fixed coordinate axis.
Z	Inertial frame coordinate axis.
α_v	Filter parameter for sweep velocity filter, p.38.
α_ψ	Filter parameter for yaw angle filter, p.45.
β	Duty factor; fraction of a cycle spent in the stance phase, p.6.

$\boldsymbol{\delta}$	Deflection of leg model at point F due to force P, p.80.
Δ	Steering controller output; fraction that a leg trajectory parameter is incremented or decremented for steering, p.47.
Δl	Compression of a "musculoskeletal spring" at mid-stance [m], p.69.
$\boldsymbol{\delta_r}$	Radial deflection of leg model at point F [m], p.80.
δ_y, δ_z	Deflection of point F with respect to H in the y and z directions, respectively [m], p.80.
ϵ	Specific resistance, p.63.
$\dot{\phi}_d$	Sweep velocity: desired angular velocity of hip joint during stance [rad/s].
$\bar{\dot{\phi}}_d$	Filtered version of $\dot{\phi}_d$, p.38.
$\bar{\dot{\phi}}_{d,k}$	Filtered version of $\dot{\phi}_d$ at sampling instant k, p.38.
ϕ_e	Effective leg angle [rad], p.27.
$\phi_{e,d}$	Desired effective leg touchdown angle [rad], p.36.
$\dot{\phi}_{max}$	Maximum angular speed attainable by the hip actuator [rad/s], p.24.
ϕ_o	Sweep offset: desired offset of the leg position trajectory from the reference position [rad], p.21.
ϕ_p	Desired hip joint rotation angle during the the leg protraction (flight) phase [rad], p.24.
ϕ_r, ϕ_l	Right and left hip angles [rad], p.32.
$\phi_{r,d}$, $\phi_{l,d}$	Desired right and left hip angles [rad], p.32.
$\dot{\phi}_{r,d}$, $\dot{\phi}_{l,d}$	Desired angular velocity of right and left hip joints during stance (right and left) [rad/s], p.22.
$\phi_{r,end}$, $\phi_{l,end}$	Total right and left hip rotation angles over the course of a simulation trial [rad], p.85.
ϕ_s	Sweep angle: desired hip joint rotation angle during the assumed stance phase [rad], p.21.
$\phi_{s,r}$, $\phi_{s,l}$	Sweep angle corresponding to the right and left legs [rad], p.47.

γ	Body fixed roll angle of the robot (frontal plane) [rad].
η	Gear efficiency [%], p.33.
ψ	Body fixed yaw angle of the robot [rad], p.45.
$\kappa_{ll,j}$, $\kappa_{ul,j}$	Weighting constants for the lower and upper limits outside of which a penalty is applied for parameter j in the genetic algorithm fitness function, p.85.
μ_s, μ_d	Static and dynamic coulomb friction coefficients, p.82.
θ	Body fixed pitch angle of the robot (sagittal plane) [rad], p.28.
σ	Pulse width modulation (PWM) amplifier duty cycle, p.55.
θ_b	Pitch angle at which the robot maintains constant forward velocity, p.30.
θ_d	Desired pitch angle [rad], p.30.
τ_{max}	Maximum torque output of the motor-gear assembly [Nm], p.82.
τ_r, τ_l	Torque produced by the right and left hip motors [Nm], p.32.
τ_{stall}	Stall torque of the motor gear assembly [Nm], p.82.
φ_F	Arc spanned by the leg from the hip to the foot [rad], p.80.
φ_m	Arc spanned by the leg from the hip to point "m" [rad], p.80.

Acknowledgments

I would like to express my appreciation to all those who have helped me through my research at McGill. In particular, I would like to thank:

- Dr. Martin Buehler, my thesis adviser, for his advice and guidance and for giving me the opportunity to work in his lab, the Ambulatory Robotics Lab (ARL).

- Prof. Inna Sharf, my thesis adviser, for her advice and guidance and for taking over after Prof. Buehler's departure from McGill. Her willingness to commit time to her students and her critical readings of my thesis drafts were most greatly appreciated.

- James Smith, Chris Prahacs, for their help and advice with all things lab related. I would also like to thank James for translating my abstract into French.

- Don Campbell and Dave McMordie for answering questions about RHex and electrical engineering when I first began in the ARL. I would also like to thank them for their great work on RHex.

- Prof. Koditschek, Prof. Rizzi, Prof. Full, Dr. Uluç Saranli and the rest of the RHex team at McGill, the University of Michigan, Carnegie Mellon University, and the University of California at Berkeley for creating the RHex robot and a team that taught me much about robotics and collaboration.

- Akihiro Sato, Julien Marcil, and Mike Tolley for their comments and criticism of various parts of my thesis draft.

- All the people I have had the opportunity to work with at the ARL: François Deschênes, Christine Georgiades, Ioannis Poulakakis, Aaron Saunders, Julien Marcil, Mike Tolley, John Sheldon, Akihiro Sato, Evgeni Kiriy, Enrico Sabelli, Shane Saunderson, Matt Smith, Neil Wyper, and Charles Steeves. I would like to thank these people for making the ARL interesting during my stay. I would also like to thank François Deschênes for correcting my French abstract.

- John Sheldon for teaching me how to manufacture composite RHex legs and for his work on the leg stiffness testing rig.

- Janet Sutherland for her thorough proof reading of my entire thesis and for providing valued support and encouragement towards the end of my degree.
- Amy Neville for reading thesis drafts of chapters 1, 2, 5 and 7.
- Cynthia Davidson, Marlene Gray, and Gen Vinois for their administrative assistance and for their part in keeping the ARL and CIM running smoothly.
- Joyce Nault for her help with registration and administration.
- Jan Binder and Danny Chouinard for maintaining the computer network and for answering computer related questions.

I would like to acknowledge and thank the Natural Sciences and Engineering Research Council of Canada (NSERC) for their financial support through a PGS scholarship.

Most of all, I would like to thank and express my deepest gratitude to my parents and sister, to whom I am most indebted, for their continual support and encouragement.

To my family.

Chapter 1

Introduction

1.1 Motivation

Legged robots have made great strides in the past two decades. One need only look at the extraordinary range of mobility present across the animal kingdom to appreciate the immense potential for legged robots in unstructured environments. One can envision a wealth of practical applications for legged technology related to emergency first response [65], mobile monitoring, inspection and surveillance in hazardous or hostile environments [83, 9], planetary exploration [66], and personal helper devices [23], to name a few. Further uses of legged robots exist in entertainment applications such as toys [22], movie and theme park creatures [20], and museum demonstration models [92].

As mobility is a key element in developing autonomous vehicles, legged robots will be of increasing significance as the trend towards more capable autonomous robots continues. Compared to wheeled and tracked vehicles, which require a suitable continuous path of support, legged systems require only isolated footholds. In spite of this, the current mobility standards of performance by man-made vehicles have been set by wheeled and tracked vehicles. Moreover, to date there have been virtually no significant practical applications of legged robots outside of the laboratory, with the exception of a number of entertainment robots [22, 29, 18].

In addition to their great potential as useful devices, legged robots provide in-

teresting applications of basic mechanics and control theory. Further motivation to study legged robots is that legged robots deal with similar dynamics and control issues as animals but are, in many respects, easier to study.

1.2 Biological Inspiration, RHex

This thesis presents the development of a novel 3D bipedal running behavior using a compliant hexapod, RHex [85, 5, 46]. Figure 1.1 shows RHex in hexapedal and bipedal configurations, respectively. RHex was inspired by R.J. Full's research on cockroach locomotion [24, 27]. Naturally, the results of millions of years of biological evolution can serve as inspiration for the design of legged robots. Such characteristics as its sprawled posture, low center of gravity, passive compliant legs, and clock-driven tripod gaits are biologically inspired. These characteristics, combined with scientific and engineering principles, have endowed RHex with a large repertoire of behaviors, including walking over irregular terrain [85], pronking[1] [58], stair climbing [61, 62], swimming [7, 74], flipping [86], and quadrupedal bounding[2] [12].

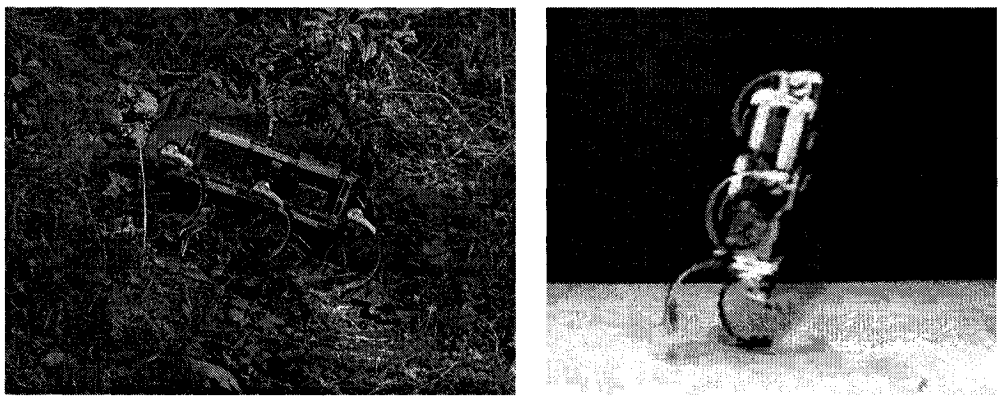

(a) (b)

Figure 1.1: (a) RHex outdoors, (b) RHex running bipedally

[1]Pronking is a one-beat running gait used by such animals as llamas, deer, and springboks in which the stance phases of all legs are coincident. [56]

[2]Bounding is a two-beat running gait used by such animals as dogs and squirrels that is characterized by the front and rear lateral leg pairs moving in phase.

Just as the overall robot design was inspired by Full's research on cockroach locomotion, so is the particular bipedal behavior studied in this thesis. Full and Tu [27] reported that the American cockroach, *Periplaneta americana*, can run bipedally on its hind legs at high speeds. Figure 1.2 shows a picture of a cockroach running bipedally.

Figure 1.2: Cockroach running bipedally [70]

1.3 Development of a Novel Bipedal Gait: Objectives and Contributions

Engineers have been building electronically controlled legged robots for approximately four decades. Currently there is a particularly large amount of research devoted to bipedal robots. Biped robots with a wide spectrum of morphologies, actuated degrees of freedom, and sensing capabilities have been developed. Some benefits of mechanical simplicity include reduced cost and weight and improved reliability. Minimalistic approaches, which aim to lower the complexity of the sensing and actuation schemes, raise several questions. What is the minimum number of actuated degrees of freedom necessary for dynamically stabilized bipedal locomotion? What sensing is necessary for dynamically stabilized bipedal locomotion? What are the characteristics of such a gait?

This thesis details the development of novel 3D dynamic bipedal running behavior using only two actuated degrees of freedom, one for each compliant leg. In addition, only body pitch and leg angle sensing are required. This work emphasizes simplicity and is in stark contrast to the approach employed in the vast majority of biped robot projects presented in the literature. By and large, these biped robots involve

six or more actuated degrees of freedom, extensive sensor suites, and low flexibility. Such characteristics generally reduce speed, mobility, and energy efficiency. To the author's knowledge, there are no (2D or 3D) bipeds with only one actuated degree of freedom (DOF) per compliant leg capable of dynamic running in existence. It is demonstrated in this thesis that in spite of the simplicity of the actuation, sensing, and control schemes and the fact that the experimental platform was designed for six legged locomotion, dynamically stabilized bipedal running is possible with the RHex robot. Furthermore, forward velocity, pitch, roll, and yaw can be successfully stabilized or controlled to some degree.

1.4 Thesis Organization

The concepts used in this study are obtained from the dynamics, control, and legged robotics literature as well as from the biomechanics literature. Both experimental and simulation results are presented. The primary methods of analysis used in the experimental work are analysis of measured data and video.

Chapter 2 presents a survey of the relevant literature that exists on bipedal robots and their control methods. Legged locomotion terminology and concepts used throughout the thesis are briefly presented. A description of the experimental platform is also included. Chapter 3 describes the overall control strategy in the sagittal plane and elaborates on the control of body pitch and forward speed. The leg trajectory generation scheme and the leg trajectory parameter choice and calculation are discussed. Frontal and transverse plane dynamics are then discussed in Chapter 4. The physical characteristics of the robot used to manipulate the dynamics in these planes are also discussed. A steering controller is also presented. Experimental results are given in Chapter 5 along with an outline of the parameter tuning procedure. Simulation results using MSC ADAMS of bipedal RHex are presented in Chapter 6 along with component models of the robot legs and body. The details of a genetic algorithm optimization used to tune the gait are included. Finally, Chapter 7 summarizes the research presented in this thesis and provides recommendations for future work.

Chapter 2

Background and Literature Review

This chapter provides context for the research presented in this thesis. A survey of the relevant work on legged machines is provided. Legged locomotion terminology and concepts used in this thesis are also briefly presented. Finally, this chapter includes a brief description of the mechanical, electrical, and software characteristics of the experimental platform used.

2.1 Legged Locomotion

Full and Koditschek described locomotion in the following way: "Locomotion results from complex, high-dimensional, non-linear, dynamically coupled interactions between an organism and its environment" [26]. Legged robots are variable structure dynamic systems. For example, a biped can have a ballistic flight phase with no legs contacting the ground, a single leg support phase with one leg contacting the ground, and a double leg support phase with both legs contacting the ground. Two additional key characteristics of legged systems are related to the nature of the joint formed by the foot and the ground. This joint is unilateral; no attractive forces are present [31]. It is also unactuated because no actuation or control input exists at this joint.

2.1.1 Concepts and Terminology

Terminology used throughout this thesis is discussed in this section. If a leg is in contact with the ground it is said to be in *stance phase*, otherwise, the leg is said to be in *flight phase*, or *swing* phase. The transition of a leg from flight phase to stance phase is known as *touchdown*, whereas the transition from stance phase to flight phase is known as *liftoff*.

Similar terminology can be used to describe the robot. A robot is said to be in flight phase when all its legs are in flight phase. Depending if there are zero, one, or two legs in contact with the ground, a biped robot can have three different phases: *flight phase*, *single support (stance) phase*, and *double support (stance) phase*.

A *gait* can be defined as "a manner of moving the legs in walking or running"[36]. A *stride* refers to a complete cycle of leg movements; for example, all the movements that occur between successive touchdown events of the same foot.

In addition, there are a number of quantities used to characterize a gait. The *stride frequency*, f, is the number of strides per second and the *stride period*, t_c equals $1/f$. The *stride length*, λ, equals the distance traveled in one stride. The *duty factor*, β, is the fraction of the total leg cycle that a particular leg is in contact with the ground and is typically assumed to be the same for each leg. In bipedal locomotion a double stance phase will exist if $\beta > 0.5$ and no flight phase will exist. In this case, the duration of the double stance phase as a fraction of a stride period is $2\beta - 1$. For a given leg, the angle traversed by the leg at the hip between touchdown and liftoff is called the *sweep angle*, ϕ_s. The *relative phase* will be defined as the fraction of the stride period between the touchdown event of a particular leg relative to that of a reference leg.

Anatomical terms are used frequently in the context of both natural and artificial legged locomotion. As shown in Figure 2.1, the *sagittal plane* divides the right and left parts of the body while the *frontal plane* divides the front and back of the body. Lastly, the transverse plane divides the top and bottom of the body. Front, back, left, right, top, and bottom are defined as they would naturally be for humans. Note that the orientation of these planes with respect to the robot body are different

for the hexapedal and bipedal configurations of RHex; however, only the bipedal configuration is relevant in this thesis.

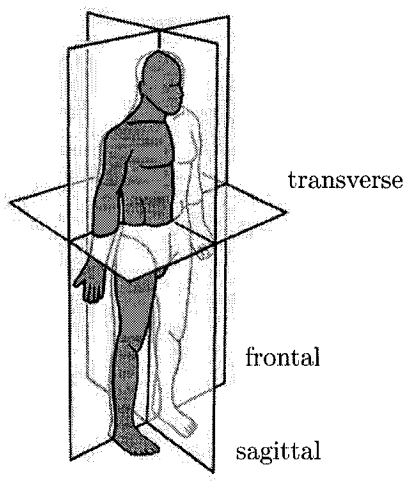

Figure 2.1: Anatomical Planes [95]

A common way of distinguishing walking from running is to determine whether a ballistic flight phase, during which no leg touches the ground, is present; this is equivalent to a duty factor less than 0.5 for bipeds. However, many researchers point out deficiencies with this type of definition because it does not apply for all animals [3], or under all conditions for a given animal [54, 55]. A more applicable definition is provided by Cavagna [13]: in walking, the center of mass (COM) of the body is highest at approximately mid-stance, while in running the COM is lowest at approximately mid-stance. Therefore, in walking changes in the kinetic energy associated with the forward motion and gravitational potential energy are out of phase. In running changes in gravitational potential energy and the kinetic energy associated with the forward motion are in phase and energy is stored in spring elements until approximately mid-stance and released thereafter.

2.1.2 Stability

Stability is a key issue in the study of legged robots and many stability definitions have been applied in this context. Legged machines are commonly categorized by their

stability characteristics: *statically stable*, *quasi-statically stable*, or *dynamically stable.* Static stability occurs when the ground projection of the center of mass lies within the region formed by the support feet, known as the support polygon. Generally, robots that maintain static stability require four or more legs, however, static stability can also be maintained using as few as two legs if the feet are large enough. Statically stable machines require large support polygons and are forced to move slowly so that momentum is negligible. In contrast, dynamically stable robots use feedback and dynamic forces to maintain balance [82]. Some create stable limit cycles that repeat with each stride. Lastly, quasi-static stability encompasses the possibilities between static stability and dynamic stability. For example, a quasi-static robot may maintain static stability for all but a short part of the stride cycle.

For the bipedal research presented here it is practical to separate and view stability in terms of body stability, body path stability, and gait stability as proposed by Vukobratovic [93]. Standard stability concepts apply to body stability and body path stability. Gait stability, on the other hand, requires the following quantities to be constant: average forward velocity, stride length, leg phasing, duty factor, and cycle period. This type of division will be useful in the discussion of the experimental results. Although the word *balance* is frequently used in the legged robotics literature to imply some types of stability, the concept of balance varies and no agreed upon definition is available.

2.1.3 Compliance in Legged Locomotion

Compliance plays a critical role in the current research. The use of compliance in legged locomotion is extensively documented in the biomechanics literature. Animals use tendons, ligaments, and muscles to absorb, store, and release energy as they run [21, 54, 4]. In fact, there are striking trends in musculoskeletal stiffness values across animals of vastly different sizes. More specifically, Full and Farley [25] report that the relative leg stiffness is approximately constant for runners, trotters, and hoppers having a wide range of morphologies and masses ranging over orders of magnitude. The simplest and most common model for running is the spring loaded inverted pendulum

(SLIP), see Figure 2.2(b). In addition to serving as a model for the aforementioned biomechanics work, SLIP has also served as basis for running robots (e.g [80, 32]).

Alexander [4] points out three uses of springs in legged locomotion. The first use is of the SLIP property, which he refers to as the "pogo stick principle". Resonant bouncing of the robot or animal's center of mass (COM) can be used to increase efficiency and generate higher speeds than are possible with walking. The second use is to make the leg swing motion more efficient. The final use compliance discussed by Alexander is as "foot pads" to aid foot contact by reducing impact forces and chattering between the foot and the ground.

In contrast, walking does not make significant use of compliance and is usually modeled as an inverted pendulum, see Figure 2.2(a). Due to the stiff behavior of the leg in walking and based on the assumption that the support foot remains in contact with the ground, a maximum walking speed can be determined for which the acceleration of the body in the vertical direction equals the acceleration of gravity, g. This maximum speed is $\sqrt{gl}$, where l is height of the COM at mid-stance.

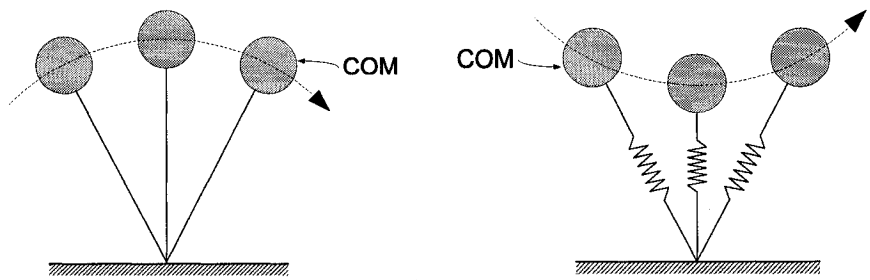

(a) (b)

Figure 2.2: (a) Inverted pendulum; (b) Spring loaded inverted pendulum (SLIP)

2.2 Survey of Dynamically Stable Biped Robots

As mentioned in the introduction, legged machines have been the subject of intense research in the last four decades. Much of the early work focused on statically

stable quadruped and hexapod machines (e.g. the work of Mosher [88], McGhee [52], Gurfinkel [33], Hirose [38]). Subsequently, work on quasi-static and dynamic bipeds emerged. Kato [43] built a biped whose "quasi-dynamic" gait was statically stable except for short periods when support was transferred between feet. Miura and Shimoyama [60] developed a biped that is generally considered to be the first dynamically stable biped. Raibert conducted ground-breaking research on dynamically stabilized hopping machines with one, two, and four legs [80]. McGeer [51] built a gravity powered biped[1] capable of walking down shallow slopes without active control. Since these pioneering works, a wealth of walking and running robots have emerged; an extensive on-line catalogue can be found in [10].

This section surveys the relevant work and the state-of-the-art for biped robots with emphasis placed on morphology and control approaches adopted for these systems. Due to the expansive nature of the literature, a complete review is outside the scope of this thesis and only key robots and control approaches will be considered.

2.2.1 Humanoid Robots, ZMP Approaches

The vast majority of bipedal robots have large feet, a rigid structure, and a relatively high number of actuated degrees of freedom. Humanoid robots (anthropomorphic robots) generally fall into this category and their designs follow a structural biomimesis philosophy. Manipulator theory is used to carefully control the motion of each of the many joints to achieve precise foot placement and the desired sequence of events. Approaches using static stability criteria can be used in some cases, however, the most common stability criteria are related to the *zero moment point* (ZMP), to be described shortly. The main disadvantage of this type of robot design is that the number of actuators, heavy limbs, and lack of compliance result in slow gaits. In addition, a high degree of mechanical complexity tends to reduce efficiency, mechanical robustness, and reliability.

The currently best known examples of the state-of-the-art in humanoid robots

[1]While passive walking toys have probably existed for centuries, McGeer initiated recent study of passive dynamic walking.

are the Honda Asimo [18] and the Sony QRIO [29]; both use ZMP based control approaches. The Honda Asimo is a 1.2 m tall 52 kg robot shown in Figure 2.3a. It has a top speed of only 0.44 m/s. Very stable but slow walking and stair climbing is achieved with 12 degrees of freedom (DOF) in the legs and hips. There are an additional 14 DOF in the arms, hands, and head. The Sony QRIO (7 kg, 38 DOF) is capable of dynamic walking, dancing, and throwing behaviors. It can also detect the inclination of the ground and adapt accordingly. QRIO can even run with a very short duration flight phase (0.23 m/s, 20 ms aerial phase [41]); Sony claims that QRIO is the first humanoid robot capable of running [89]. Many other notable, successful bipeds with stiff legs and large feet exist (e.g. HRP-2 [42], H6 [67], HOAP-2 [8], Johnnie [40], KHR-1 [69]) and some are even available commercially. These robots are shown in Figure 2.3.

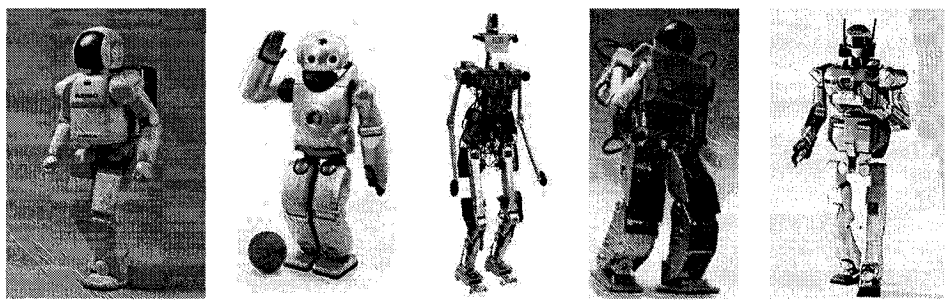

(a) (b) (c) (d) (e)

Figure 2.3: Humanoid robots: (a) Honda Asimo, (b) Sony QRIO, (c) Technische Universität München Johnnie, (d) Fujitsu HOAP-2, (e) Kawada Industries HRP-2.

The ZMP was first applied in the control of legged robots more than two decades ago and is still one of the most common frameworks used to control bipedal robots. This control method is applicable to robots with "large feet" (i.e. not "point" feet or large feet with rolling contact) and can be used for gait analysis, synthesis, and control. The ZMP is the point on the ground, within the support polygon, where the ground reaction moments in the ground plane are zero, i.e. the point on the ground through which the resultant ground reaction force acts. ZMP is a misnomer because only two components of the reaction moment need be zero. The existence of a ZMP

within the boundaries of the foot or support polygon is a necessary, but not sufficient condition for dynamic stability.

To calculate the ZMP, a location for the ZMP is computed using the static equilibrium condition applied to the stance foot. If this location falls outside the foot area, the ZMP is not defined and the ground reaction force acts on the edge of the foot. In this case, the foot will rotate about this edge due to the unbalanced moment. Figure 2.4 illustrates the ZMP concept. Goswami presents a detailed review of the ZMP and it's application in [31].

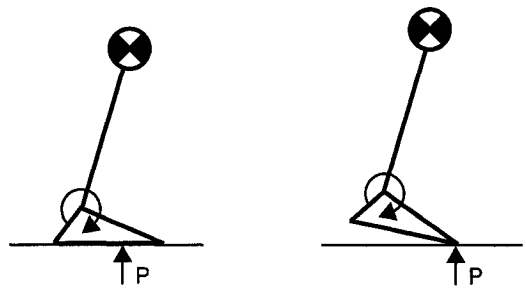

Figure 2.4: ZMP concept for a simplified, planar, inverted pendulum robot with actuated angle. Assume that adequate friction exists so that there is no sliding. (a) ZMP is within the foot boundaries, (b) foot rotates because the ZMP is not defined and the ground reaction force acts at the edge of the foot. [15]

To use the ZMP approach to control a biped, a walking algorithm generates desired trajectories for the ZMP. ZMP trajectories can be generated offline [37] or in realtime with some motion planning algorithm [68]. The joint angles of the legs and torso needed to produce the desired ZMP are then calculated.

The ZMP approach is similar to approaches used with statically stable machines in that this measure is used to maintain or evaluate equilibrium at every instant. Of course, it is not necessary or even desirable to impose equilibrium at every instant. Most running gaits in animals are not in equilibrium over the entire stride; for example, the flight phase of a running human, bounding squirrel, or galloping horse. In these examples the ZMP does not exist over the entire stride. In addition, ZMP

stability criteria would indicate that robots with point contact feet, *such as bipedal RHex*, cannot be stable; this points to another deficiency of this approach with respect to its application to the development of dynamically stable gaits. Other control methods using limit cycles do not attempt to maintain equilibrium at every instant; these will be discussed in later sections.

2.2.2 Passive Dynamic Walkers

Passive dynamics play an important role in many legged robots. For example, body pitch oscillations can be passively stable for bounding quadruped robots or, of direct relevance to the current research, roll oscillations for a bipedal running robot can be passively stable.

There is a class of robots that are entirely passive and require no control. These robots walk down shallow slopes and have walking as a natural mode. The pioneering engineering work in this domain was performed by McGeer [51] who built a 2D gravity-powered biped. Another example of notable work in this field is that of Ruina [17] whose lab built a 3D biped that walks with a natural looking gait. Both McGeer's and Ruina's robots have large curved feet that create a rolling contact with the ground (see Figure 2.5a,b). Mechanical simplicity is a key characteristic of such machines.

More recently, passive dynamic walking research groups at Cornell, Delft, and MIT have extended the principles of the gravity powered walkers to create robots capable of walking on flat surfaces [16]. These robots, including Tedrake's MIT learning biped and the Cornell biped shown in Figure 2.5c,d, walk with efficiencies similar to that of human walking. The Cornell and Delft bipeds require only ground contact sensors and motors that are issued on/off signals once per step. The rest of the motion is completely passive and governed by the natural dynamics of the mechanism.

2.2.3 Actively Driven Limit Cycle Based Approaches

The robots discussed in this section walk or run by creating stable limit cycles. Hopping robots and robots with "small" or "point" feet fall into this category.

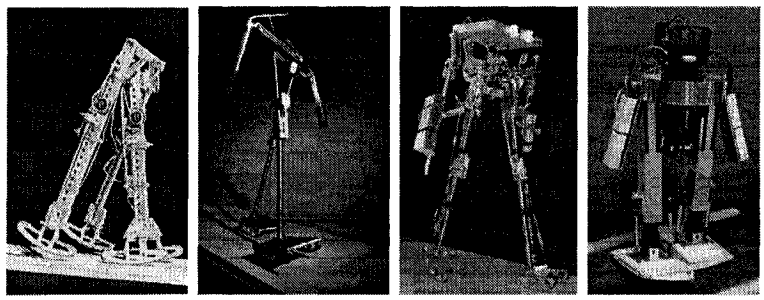

(a) (b) (c) (d)

Figure 2.5: Some passive dynamic robots: (a) McGeer's Passive Dynamic Walker [51], (b) Ruina-Wisse-Collins Cornell Walker [17], (c) Cornell Biped [16] (d) Tedrake's MIT Learning Biped [16]

Raibert conducted ground-breaking research on dynamically stabilized hopping machines with one, two, and four legs [80]. The principles developed generally apply to robots with significant leg compliance. Raibert found that simple controllers suited to the dynamics of the system could be used to effectively control running. He found that a decoupled three part controller could make 2D and 3D monopods run at a specified rate, leap over obstacles, follow a desired path, and balance themselves when disturbed. The 3D monopod, shown in Figure 2.6b, had a radially compliant prismatic leg with an air spring and hydraulic actuator, and two hydraulically actuated degrees of freedom at the hip. Body attitude, leg length, contact between the foot and the ground, joint rates and angles, and the pressure in the leg air cylinder were sensed.

Control of the monopod was decoupled into the tasks of hopping height, forward speed, and posture stabilization. Raibert's standard hopping controller aimed at delivering a fixed amount of energy with the prismatic leg during each stance phase. Because the energetic losses in the system were a monotonic function of the hopping height, an equilibrium hopping height existed for each fixed energy input. Posture control was effectuated during the stance phase. The attitude of the body was controlled by hip torques calculated using a proportional derivative (PD) control law. Forward velocity and acceleration were controlled by moving the leg to the appropriate touchdown angle during the ballistic flight phase. The touchdown angle has

a strong effect on the resultant forward body acceleration over the stride. Using an approximation of the system dynamics, it was possible to calculate the foot position at touchdown that would produce the desired net acceleration over the stride. Interestingly, Raibert also successfully showed an alternative three part controller in simulation that used forward foot placement for posture control, hip torque for forward velocity control, and leg thrust for hopping height control. Thus, a range of control algorithms exist for such robots; Raibert speculated that more complex non-decoupled, non-linear control strategies would provide optimized performance.

Following the success of the monopods, Raibert used the same ideas and the concept of virtual legs to control biped and quadruped robots. The 2D biped was capable of running at speeds up to 5.86 m/s. Both the 2D and 3D bipeds were capable of running, jumping over obstacles, climbing certain stairs, and performing somersaults.

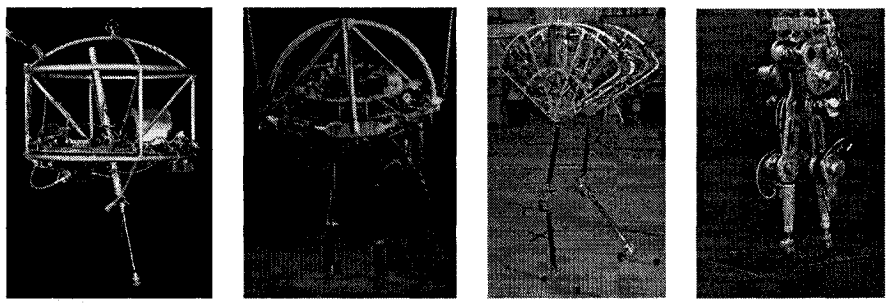

(a) (b) (c) (d)

Figure 2.6: (a) MIT 3D Monopod [47], (b) MIT 3D Biped [47], (c) MIT Spring Flamingo [47], (d) RABBIT [14]

One example of a 2D biped robot with "point" feet that walks using a limit cycle approach is RABBIT [14, 79]. Unlike the many heuristic approaches often used to control legged robots, RABBIT uses analytically derived controllers. The concepts of virtual constraints and hybrid zero dynamics are used to generate periodic walking motions that are provably asymptotically stable. Moreover, preliminary (unsustained) running results have been obtained in which a distinct flight phase is present [39]. This planar biped, shown in Figure 2.6d, consists of five links and

has four actuated degrees of freedom. Full state sensing is used and no significant compliance is included.

2.2.4 Other Control Approaches and Parameter Tuning

Many other approaches have been used to control legged robots, more in simulation than in practice. Iterative parameter tuning is often required for legged robots because of the lack of a model, modeling errors, and model parameter errors. In particular, complexities in realistically modeling impacts, friction properties, nonlinear stiffness and damping, actuators, gears, and complex ground-robot interactions make the development of realistic models suitable for analysis or controller development a problem for many systems. This is especially true for bipedal RHex. In addition, more options are available for controller development and parameter tuning in simulation environments because of the overhead required for experimental work. Learning and optimization techniques, such as reinforcement learning algorithms [71, 90] and genetic algorithms [6, 35], have been successfully implemented in the simulation of legged systems. Some have also been implemented using real robots [91, 45].

Pratt [75] developed an interesting framework called "virtual model control" to control legged robots without a dynamic model. Such a controller uses virtual components (e.g. springs, masses, dampers) that interact with the robot and generate virtual forces that are converted into real joint torques via suitable transformations. Virtual model control was used successfully to control walking gaits of two planar bipeds, Spring Turkey (5 link, 4 actuated DOF) and Spring flamingo (7 link, 6 actuated DOF, see Figure 2.6), on level and shallow sloped surfaces [76, 77].

One example of a very successful parameter optimization procedure applied to a real robot, the RHex hexapod robot, was the use of a modified Nelder-Mead direct search algorithm by Weingarten et al. [94]. For this procedure, the robot was run repeatedly over a test track with a different parameter set each time to minimize a performance index. The two performance indices used were the specific resistance (see Section 5.4) and the specific resistance divided by velocity squared. This eight dimensional space optimization resulted vast efficiency improvements and in speeds

more than three times higher than were possible by manual tuning.

2.3 RHex: The Robotic Hexapod

The RHex robot (Figure 1.1) was the experimental platform used to conduct this research. RHex is a power- and computation- autonomous[1,2] hexapod robot with compliant legs. This robot was the result of a collaborative research effort by teams at the University of Michigan, McGill University, University of California at Berkeley, and Carnegie Mellon University. This section briefly details relevant mechanical, electrical, and software characteristics of the platform. A summary of the physical parameters of the RHex robot are given in Table 2.1.

2.3.1 Mechanical, Electrical, Software Description

Compliant semicircular legs are constructed with layers of "S glass". Each leg is driven by one motor. High performance Maxon RE25 DC motors and 33:1 planetary gearheads are used. For some parts of the research detailed in this thesis, larger Maxon RE30 motors and 14:1 planetary gearheads were used (see Section 5.5.3). Leg angle measurement is performed by incremental optical encoders with 2000 counts per revolution. Hall effect sensors mounted in the hips detect a magnet embedded in the leg to provide an initial position for leg angle measurements. To predict the possibility of motor failure, sensors monitor the motor case temperature.

The robot contains nickel metal hydride (NiMH) batteries. In the standard configuration, the batteries have a nominal voltage of 24 V and an electric charge capacity of 3 A·h (10.8 kC). A custom amplifier board using Apex Microtechnology SA60 H-bridge pulse width modulation chips is used to drive the motors [57] with up to 10 A continuous and 15 A peak currents. A custom analog/digital input output board interfaces with the various sensors and actuators [11]. For control purposes, computation is performed by a 300 MHz Lippert CoolRunner II PC104 processor with

[1]Power supply resides on the robot.

[2]All computational hardware and software resides on the robot except for low bandwidth remote supervisory user interface.

256 M of RAM. Communication with the robot is accomplished via 802.11b wireless ethernet.

A three axis Fizoptika VG941-3D fiber-optic gyroscope is used to measure the orientation of the robot body. This gyroscope has a dynamic range of ±500 deg/s and low zero-input drift. Details on the attitude estimation system on RHex can be found in [57]. A color digital camera and vision system are also available on RHex but were not used in this research.

With respect to software, the QNX realtime operating system is used. RHexLib, a C++ library originally developed by RHex team members at the University of Michigan [44], is used to provide a control interface, sensor and hardware interfaces, timing controls, a framework for gait descriptions, data logging, etc.

	Property	Symbol	Value	Units
Dimensions	Body Length		0.48	m
	Body Height		0.13	m
	Body Width		0.30	m
Mass Properties	Body Mass	m	8.4	kg
	Moment of Inertia (COM, yaw axis)	I_{yaw}	0.06	kg m^2
	Moment of Inertia (COM, roll axis)	I_{roll}	0.23	kg m^2
	Moment of Inertia (COM, pitch axis)	I_{pitch}	0.18	kg m^2
	Leg Mass	m_l	0.08	kg
	Leg Moment of Inertia (hip axis)	I_{leg}	0.001	kg m^2
Motor Properties	Max. Hip Torque	τ_{max}	5	N m
	Max. Hip Speed	$\dot{\phi}_{max}$	5	rev/s
Leg Properties	Leg Length (unloaded)	$2r$	0.165	m
	Leg Spring Constant (radial, linear approximation)	k_r	1640	N/m

Table 2.1: RHex physical properties

Using the hardware described above, Chapters 3 to 5 present the development and testing of a bipedal gait for RHex. In terms of sensing and actuation, this bipedal gait is in strong contrast to the gaits described in this chapter. Further hardware details, including simplified component models, can be found in Section 6.2 (p. 77), in the context of a simulation of bipedal RHex.

Chapter 3

Sagittal Plane Running Controllers for Bipedal RHex

As described in the introduction, this thesis presents a three dimensional bipedal running gait for bipedal RHex. The dynamics in the sagittal, frontal, and transverse planes are considered separately. Compared to the robots described in the literature review of Chapter 2, the low number of actuators used by bipedal RHex places significant restrictions on solutions to the control problem of obtaining a stable gait. Accordingly, the relevant sensing and actuation issues are discussed in this chapter. Under these constraints, this chapter presents a sagittal plane balancing controller used to successfully create a bipedal gait on the RHex robot. Dynamics and control in the transverse and frontal planes are considered in Chapter 4. Experimental results obtained from this 3D, dynamic, stable running gait are presented, in depth, in Chapter 5.

3.1 Leg Trajectory Generation

Leg trajectory generation is a critical aspect of the bipedal RHex running controller. The leg trajectory parameter generation approach taken here was motivated by that of the standard hexapedal walking controller implementation on RHex, which uses open loop and clock-driven leg trajectories [85]. The leg stride cycle of hexapedal

RHex is parameterized by four independent *leg trajectory parameters*: stance time t_s, sweep angle ϕ_s, sweep offset ϕ_0, and stride period t_c. The desired leg position and velocity trajectories can be updated approximately twice per leg cycle. They consist of two phases linked by cubic splines: a constant velocity, *assumed* stance phase and a constant velocity, *assumed* flight phase, see Figure 3.1. The cubic splines provide a smooth transition between the fast and slow phases, but are omitted from Figure 3.1 for clarity. The stance and flight phases are "assumed" since there is no feedback indicating whether the leg is actually in contact with the ground. For bipedal RHex a similar set of four independent leg trajectory parameters is used to describe the leg cycle, but a slightly different implementation was desired.

Unlike hexapedal running, bipedal running is necessarily a closed loop gait, and provision to update the leg trajectories every sampling instant is required. Also, the bipedal gait is limited by the motor torque-speed capabilities and the inability of the robot legs to track the desired position and velocity trajectories consistently causes failure of the gait (e.g. a fall occurs). Thus, it was desired that the motor torque and velocity limitations be easily accounted for in the leg trajectory generator.

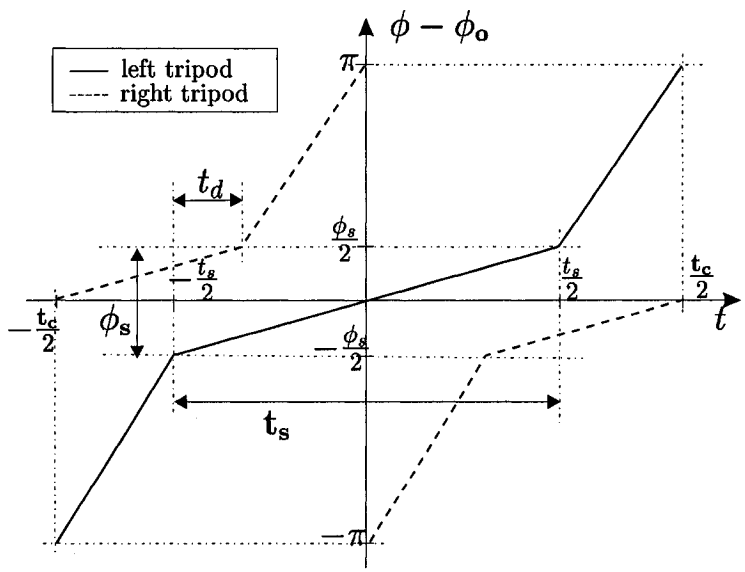

Figure 3.1: RHex hexapedal walking leg trajectory [84]. Cubic spline blending of chords omitted for clarity.

3.1.1 Leg Trajectory Parameters

For bipedal RHex, the following four leg trajectory parameters are used to specify the leg position and velocity trajectories: sweep angle ϕ_s, sweep offset ϕ_o, stance velocity $\dot{\phi}_d$, and duty factor β. The sweep angle, ϕ_s, is the desired hip joint rotation angle during the assumed stance phase. The sweep velocity, $\dot{\phi}_d$, is the desired angular rate of the hip joint during stance. The desired mid-stance position of the leg position trajectories are offset from the vertical by an angle of ϕ_0, the sweep offset. Recall that the duty factor, β, is the fraction of the total leg cycle that a particular leg is in stance phase. These parameters are easily related to alternative choices of parameters such as the stride period $t_c = \phi_s/(\dot{\phi}_d\beta)$, stance phase duration $t_s = \phi_s/\dot{\phi}_d$, or the flight phase duration $t_f = \phi_s(1-\beta)/(\dot{\phi}_d\beta)$, for example.

The values of leg trajectory parameters have a critical influence on the gait. The goal is to select parameters that produce stable limit cycles with respect to the body coordinates and orientation. The leg trajectory parameters are empirically chosen such that one full leg compression and decompression cycle occurs per leg per cycle. This creates roll and yaw oscillations with a frequency equal to the stride frequency, given by Equation (3.2), and vertical oscillations with twice this frequency. This makes the most out of the leg spring properties and promotes symmetry between strides. Such oscillations are also dependent on the physical configuration of the robot, including the spring-mass properties, mass moments of inertia, and robot geometry, which determine the natural response of the system. Relationships defining the leg trajectory parameters are controller dependent and are given in Sections 3.2.2 and 3.2.3.

$$t_c = \frac{\phi_s}{\beta\,\dot{\phi}_d} \tag{3.1}$$

$$f = \frac{1}{t_c} \tag{3.2}$$

Ideally, the stride frequency corresponds to the natural frequency of the system. However, in practice an empirical determination of the stride period is required for several reasons. The legs have highly nonlinear stiffness properties that are dependent on foot location on the leg (see Figure 3.5(b)) and direction of the applied force. The legs

can also deflect in three dimensions. Furthermore, the system is a variable structure system–stiffness depends on the number of legs in stance. To further complicate the issue, a torsional pose dependent compliance is introduced by the motor.

3.1.2 Clock Generated Trajectories

The leg position and velocity trajectories are updated every sampling instant. The resulting trajectories are smooth due to the fact that the changes in the trajectories are small in comparison with the sampling period, which is nominally $T = 1.5$ ms. The location of the legs in the stride cycle is based on the *cycle time*, $c \in [0, 1)$: $c = 0$ corresponds to the beginning of a stride while, $c = 1^-$ corresponds to the end. In order to maintain the correct phase relationship between the two legs, the cycle time corresponding to one leg is offset from that of the other leg by a constant relative phase equal to 0.5. Any other value would produce an asymmetric gait with respect to the sagittal plane. At each sampling instant, k, the cycle time is updated via Equation (3.3):

$$c_k = c_{k-1} + T/t_{c_k}. \tag{3.3}$$

Stance and flight phases are assumed based on the cycle time because of the absence of touch-down and lift-off sensors (real or virtual). In the leg trajectory generator, the desired leg positions ($\phi_{r,d}$, $\phi_{l,d}$) and velocities ($\dot{\phi}_{r,d}$, $\dot{\phi}_{l,d}$) corresponding to the right and left legs, respectively, are calculated based on the cycle time and the four leg trajectory parameters, as shown in Figure 3.2.

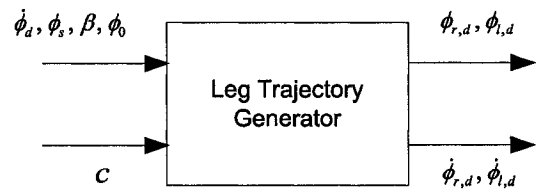

Figure 3.2: Leg trajectory generator signal flow diagram

For constant values of the four leg trajectory parameters, the leg velocity profile for the flight phase is trapezoidal, as shown in the top plot of Figure 3.3 and summa-

rized in Table 3.1. The calculation of T_a is provided in Section 3.1.3. The trapezoidal profile was chosen because of the ease in which the maximum velocity and maximum acceleration saturations are accounted for. The constant velocity portion of the flight phase exists only when the maximum velocity required by the trajectory exceeds a maximum velocity, $\dot{\phi}_{max}$, which is selected to be the no load speed of the hip joint.

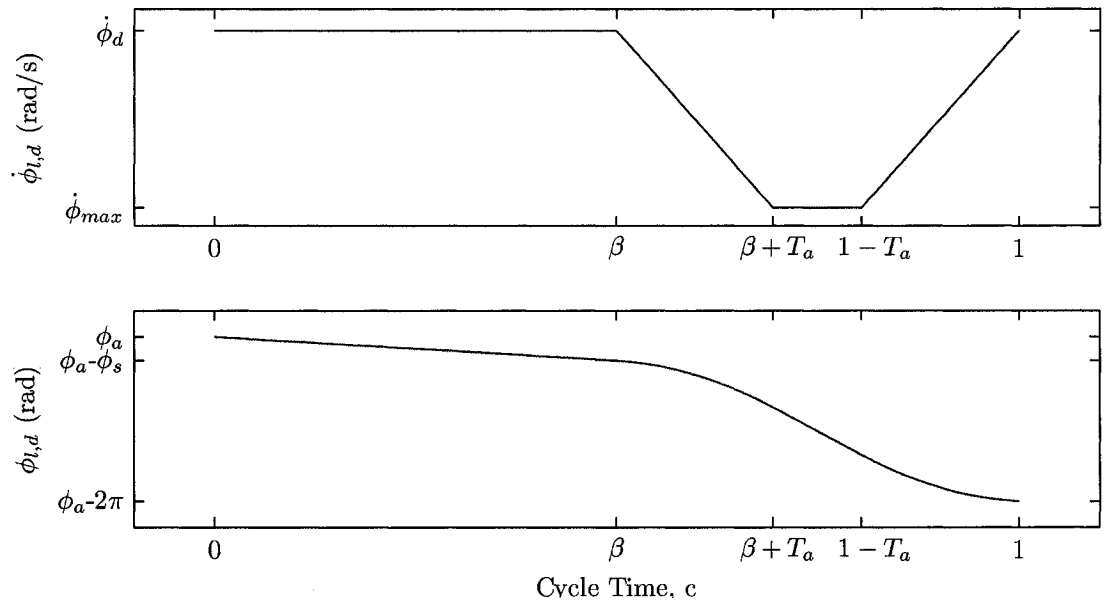

Figure 3.3: Reference leg trajectories for constant leg trajectory parameters in the robot body fixed frame

Assumed State	Phase Start		Phase End		Characteristic
	Event	Assumed Event	Event	Assumed Event	
Stance	$c = 0$	touchdown	$c = \beta$	liftoff	$\dot{\phi}$ = constant
Flight	$c = \beta$	liftoff	$c = \beta + T_a$		$\ddot{\phi}$ = constant
Flight	$c = \beta + T_a$		$c = 1 - T_a$		$\dot{\phi}$ = constant
Flight	$c = 1 - T_a$		$c = 1$	touchdown	$\ddot{\phi}$ = constant

Table 3.1: Leg trajectory description

3.1.3 Leg Position and Velocity Calculation

Details of the trajectory implementation are discussed in this section. First it is necessary to determine if the constant velocity portion of the flight phase is required due to motor speed limitations. Let ϕ_p ("p" for protraction) be the angle covered in the leg flight phase. The time required by the acceleration phases as a fraction of the stride period is $T_a \in [0, \frac{1-\beta}{2}]$. T_a is found by defining the integral of the velocity profile over the flight phase, as in Equation (3.5) below.

$$\phi_p = \int_{\beta t_c}^{t_c} \dot{\phi} dt \tag{3.4}$$

$$= 2\left(\frac{\dot{\phi}_{max} + \dot{\phi}_d}{2}\right) T_a t_c + \dot{\phi}_{max}(1 - \beta - 2T_a)t_c \tag{3.5}$$

This expression is solved for T_a yielding

$$T_a = \frac{\phi_p \dot{\phi}_d \beta / \phi_s - \dot{\phi}_d \beta - \dot{\phi}_{max}(1-\beta)}{\dot{\phi}_d - \dot{\phi}_{max}}, \tag{3.6}$$

using $t_c = \frac{\phi_s}{\dot{\phi}_d \beta}$. If $T_a < \frac{1-\beta}{2}$ then a constant velocity flight phase is required. On the other hand, if $T_a > \frac{1-\beta}{2}$ then no constant velocity flight phase is required, and the flight phase is composed of two constant acceleration phases with $T_a = \frac{1-\beta}{2}$. Moreover, if T_a is less than some minimum value corresponding to the maximum desired acceleration, then the desired trajectory is not feasible.

From the above, trapezoidal velocity profiles are easily constructed. The desired leg position relative to a reference position, ϕ_a, at any instant is obtained as the time integral of the velocity profile over the interval $[0, c]$. Let θ be the pitch angle of the robot body, shown in Figure 3.5(a). Then the reference position in the robot body frame is $\phi_a = \phi_s/2 + \phi_o + \pi/2 - \theta$. Note that $\phi_{l,d}(\mathrm{c}=0) = \phi_a$ and $\phi_{r,d}(\mathrm{c}=0.5) = \phi_a$.

3.1.4 Actuator Saturation and Modifications for "S" Shaped Legs

As already implied, actuator speed constraints are a major issue. This problem arises from the use of over-the-hip leg protraction (swing), which for the present

application has several advantages. Over-the-hip leg protraction is useful for obstacle clearance and eliminates the issue of "toe stubbing" during the leg flight phase. The latter, in turn, has the benefits of reducing the hip height required during the flight phase and/or the degree of actuation required. The major disadvantage of over-the-hip leg protraction is that the average flight phase velocities required are increased by a factor of $\frac{2\pi-\phi_s}{\phi_s}$. For example, for a typical stance sweep angle of $\phi_s = 1$ rad, over-the-hip leg protraction requires the average leg flight phase speed to be 5.28 *times* higher than for *under*-the-hip leg protraction. This places severe restrictions on the size of the achievable leg trajectory parameter space.

In order to reduce the high actuator speed requirements placed on the leg trajectory parameters by over-the-hip leg protraction, the legs were modified as follows: an additional, identical half-circle shaped leg was attached to each of the two hind legs, with a 180° offset, as shown in Figure 1.1(b) and 3.4. This "S" shape leg configuration reduces the actuator speed requirements when not in stance, but otherwise does not fundamentally change the dynamics or control of the system. The "S" leg configuration accommodates the standard RHex hip speed capabilities by reducing the average flight phase speed required by a factor of $\frac{2\pi-\phi_s}{\pi-\phi_s}$. The test results presented in this thesis were generated with the "S" shaped legs. However, in order to show that the regular "C" leg configuration is possible for bipedal RHex, the motors, gearhead, battery voltage, and amplifiers were modified to change the torque-speed capabilities of the system. The details of the corresponding design changes and experimental results are presented in Section 5.5.3.

For the "S" shaped legs, the previous leg trajectory algorithm can be used with the following modifications: ϕ_p must be changed from $2\pi - \phi_s$, for the "C" shaped leg configuration to $\pi - \phi_s$, for the "S" shaped leg case. Also, each time c reaches the limit of the interval $[0, 1)$, the reference position, ϕ_a, is rotated a half turn, $\phi_a = \phi_a + \pi$.

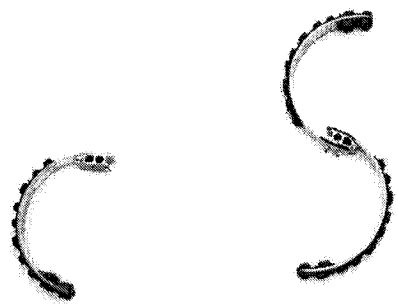

(a) (b)

Figure 3.4: Leg configurations: (a) "C" shape, (b) "S" shape

3.2 Running Controllers

This section presents two sagittal plane running controllers. These running controllers include the leg trajectory generator discussed in the previous section, inverted pendulum balancing and speed controllers, forward speed estimation, and a leg tracking controller. The first controller, Controller #1, uses the desired body pitch to regulate forward speed. This controller was extensively investigated experimentally and a detailed presentation of the resulting gaits is given in Chapter 5. A second controller, Controller #2, is inspired by hopping robot controllers and presented as a logical alternative for future work. Controller #2, however, was not implemented experimentally in the present work.

3.2.1 Requirements and Limitations

In the sagittal plane, the body of the robot acts like an inverted pendulum. Therefore, the equilibrium point about which the robot operates is unstable and must be stabilized by forces and torques transmitted to it at the hips. As stated in the introduction, one objective of this research is to study the feasibility of a minimalistic sensing and actuation approach. Therefore, it was desired to devise a controller that

uses one actuated degree of freedom per leg and a bare minimum of sensing. Ony body pitch and leg angle sensing are required for bipedal RHex.

Only steady state running gaits are considered in this thesis. Non steady state or aperiodic behaviors, such as the transition from hexapedal to bipedal configurations, or bipedal standing, are not considered. Simply stated, the control objective of the sagittal plane running controllers is to maintain an upright posture and control forward speed, given appropriate initial conditions.

Because bipedal RHex has only two control inputs – one actuated DOF per leg, the set of possible toe (tip of the leg) positions with respect to the robot body is limited to a small workspace. Actuator torques can only be exerted about one axis. This situation is in strong contrast with *all* the powered robots presented in the literature review of Chapter 2. In addition, the foot location (point where leg and ground contact) varies along the leg depending on the leg angle, leg deflection, and the ground profile; however, only flat horizontal ground is considered in this thesis. Thus, the effective length of the leg, l_e, and the effective leg angle, ϕ_e, vary according to leg angle and leg deflection and are shown in Figure 3.5(b).

Figure 3.5(a) contains a schematic of the robot showing relevant points and coordinate systems. The XYZ frame is the inertial frame. The inertial frame has the X and Y axes forming a plane parallel to the ground. Let xyz be a robot body fixed frame. The y axis passes through the robot COM and the midpoint between the hips, while the x axis is parallel to the hip axis. A leg fixed frame $x'y'z'$ is required with the x' axis perpendicular to the plane of the leg and the $-z'$ axis passing through the hip and the corresponding leg tip, as in Figure 3.5(b).

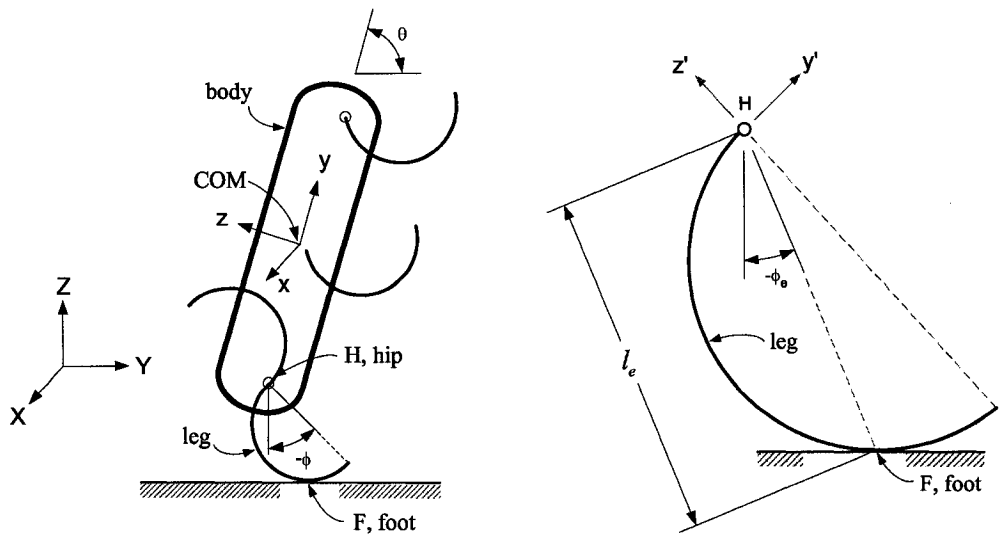

(a) (b)

Figure 3.5: Coordinate axes, variable and point definitions.

3.2.2 Controller #1

This sagittal plane running controller is hierarchical, with three levels of proportional-derivative (PD) controls for forward speed control, inverted pendulum balance control, and leg trajectory tracking. The primary motivation for using PD controllers is that they permit intuitive understanding of the control parameters that facilitates parameter tuning: stiffness and damping behavior correlate with the proportional and derivative terms, respectively. Parameter tuning is discussed further in Section 4.3. The elements of the overall block diagram, shown in Figure 3.6, are described in the following sections.

Forward Speed P Control

As already stated, the robot acts like an inverted pendulum in the sagittal plane. Gravity generates a "tipping" moment if the COM is not vertically aligned with the location of the ground reaction force. Thus, for a constant body pitch angle, this moment must be balanced by applied forces or moments. The forward speed

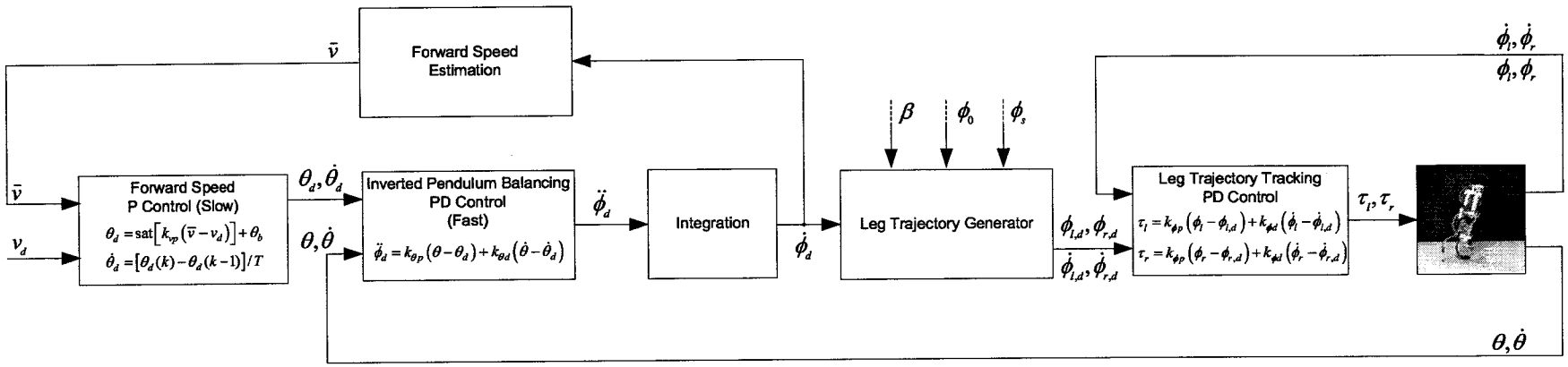

Figure 3.6: Controller #1 block diagram

controller manipulates this tipping moment to control the forward speed. The set-point of the forward speed controller is the desired instantaneous forward speed at the midpoint between the hips, v_d. The forward speed controller

$$\theta_d = \text{sat}\left[k_{vp}\left(\bar{v} - v_d\right)\right] + \theta_b \tag{3.7}$$

generates desired pitch angles, θ_d, which serve as inputs to the inverted pendulum PD balancing controller. In the above, $\bar{v}$ is the estimated forward speed and the saturation function is defined as:

$$\text{sat}(x) = \begin{cases} x_{min} & \text{if } x \leq x_{min} \\ x & \text{if } x > x_{min} \text{ and } x < x_{max} \\ x_{max} & \text{if } x \geq x_{max} \end{cases} . \tag{3.8}$$

The pitch angle that generates zero net horizontal acceleration (constant average velocity) in the forward direction over a stride is denoted by θ_b; this value is assumed constant and is empirically determined. Because of the non-linear nature of the system, the effectiveness of simple linear controllers diminishes rapidly as the system moves away from the equilibrium point for which it was designed. This is the reason why the desired *lean angle*, $\theta_d - \theta_b$, is limited using the saturation function in Equation (3.7). Since both speed and body pitch need to be controlled simultaneously, but only one control input to the robot is available via $\dot{\phi}_d$, the speed P control is set such that it responds more slowly than the more critical inverted pendulum balancing controller. More details on the choice of gain k_{vp} as well as gains for the other controllers will be presented in Section 4.3.

Inverted Pendulum Balancing PD Control

The linear PD control in Equation (3.9) is used to maintain the desired body pitch :

$$\ddot{\phi}_d = k_{\theta p}(\theta - \theta_d) + k_{\theta d}(\dot{\theta} - \dot{\theta}_d) \tag{3.9}$$

This equation generates the desired leg stance acceleration, $\ddot{\phi}_d$. The desired pitch rate, $\dot{\theta}_d$, is calculated online as the numerical time derivative of the desired pitch

angle commands:

$$\dot{\theta}_d = \frac{\theta_{d_k} - \theta_{d_{k-1}}}{T}. \tag{3.10}$$

Integration

The desired stance velocity, $\dot{\phi}_d$, is obtained via integration of the desired leg stance acceleration and the current leg stance speed estimate, via

$$\bar{\dot{\phi}}_d = \bar{v}/l_{ave} \tag{3.11}$$

$$\dot{\phi}_d = \bar{\dot{\phi}}_d + \ddot{\phi}_d T, \tag{3.12}$$

where l_{ave} is the average effective leg length and is determined experimentally, as discussed in Chapter 5.

Leg Trajectory Generator

The meaning of the leg trajectory parameters and how they are used to generate leg trajectories was described in detail in Section 3.1. This section presents relationships for the leg trajectory parameters that are specific to Controller #1. Several leg trajectory parameter relationships are considered and summarized in Table 3.2, where c_1 to c_7 are experimentally determined constants.

All results presented in this thesis use leg trajectory parameter scheme A, as given in Table 3.2. The functional relationships for ϕ_s and β in A are motivated by work done on hopping robots (e.g. [80]) and by biomechanics studies (e.g. [21, 54, 4]), which suggest that the sweep angle should be an increasing function of speed and that the duty factor a decreasing function of speed.

Leg trajectory parameter scheme B has been shown to be successful in experimental trials. In B, the choice of $t_f = c_6$ is based on the fact that the duration of the single support phase has a strong influence on the amplitude of the body roll angle oscillation. Thus, t_f was used to obtain an acceptable roll amplitude. The final leg trajectory parameter scheme, C is included in Table 3.2 because one might expect that it is the most logical given that linear spring theory and biomechanics

studies suggest the stride period, t_c, be constant with respect to forward speed. However, this approach results in poor performance because the resulting β values are, for reasons beyond the scope of this discussion, not well suited to the behaviour. A more detailed discussion about the experimental determination of the leg trajectory parameter values and their effect on the gait is given in Section 4.3.

Scheme	Leg Trajectory Parameter Functional Relationships
A	$\dot{\phi}_d \rightarrow$ Eq. (3.12) $\phi_s = c_1 + c_2\dot{\phi}_d$ $\phi_o = c_3$ $\beta = c_4 + c_5\dot{\phi}_d$
B	$\dot{\phi}_d \rightarrow$ Eq. (3.12) $\phi_s = c_1 + c_2\dot{\phi}_d$ $\phi_o = c_3$ $\beta = f(\dot{\phi}_d, \phi_s \mid t_f = c_6)$
C	$\dot{\phi}_d \rightarrow$ Eq. (3.12) $\phi_s = c_1 + c_2\dot{\phi}_d$ $\phi_o = c_3$ $\beta = f(\dot{\phi}_d, \phi_s \mid t_c = c_7)$

Table 3.2: Leg trajectory parameter relationships for Controller #1. The values depend on the hardware configuration. Specific values are given in Section 6.4, p. 86.

Leg Trajectory Tracking PD Control

The desired left and right leg position and velocity trajectories are tracked with a PD controller that generates the desired left and right hip torques according to:

$$\tau_l = k_{\phi p}(\phi_{l,d} - \phi_l) + k_{\phi d}(\dot{\phi}_{l,d} - \dot{\phi}_l) \tag{3.13}$$

$$\tau_r = k_{\phi p}(\phi_{r,d} - \phi_r) + k_{\phi d}(\dot{\phi}_{r,d} - \dot{\phi}_r). \tag{3.14}$$

The motor torque is related to motor current by $i = \frac{\tau}{K_t}$, where K_t is the torque constant $[\frac{Nm}{A}]$. The motor terminal voltage required to generate this desired motor current is calculated using the motor model shown in Figure 3.7. Thus, the desired

terminal voltages for the left and right motors are

$$V_{m,l} = \text{sat}\left[\frac{R_{arm}}{\eta N K_t}\tau_l + \frac{N}{K_s}\dot{\phi}_l\right] \tag{3.15}$$

$$V_{m,r} = \text{sat}\left[\frac{R_{arm}}{\eta N K_t}\tau_r + \frac{N}{K_s}\dot{\phi}_r\right] \tag{3.16}$$

where, R_{arm} is the armature resistance [Ω], η is the gearhead efficiency, K_s is the motor speed constant [$\frac{rad/s}{V}$], and N is the gear ratio. The pulse width modulation (PWM) amplifier duty cycle required to obtain the desired terminal voltage is then calculated using appropriate transformations, the details of which are not relevant here.

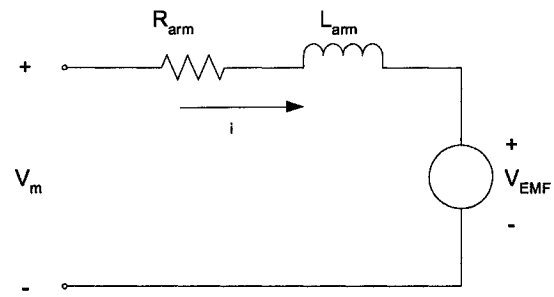

Figure 3.7: Simplified motor model

Beyond the objective of trajectory tracking performance the leg tracking control loop has a strong influence on the dynamics of the overall gait. In particular, the value of the proportional gain during stance is a *critical* factor in determining the dynamics of the gait. It introduces a pose dependent compliance that acts in series with the leg compliance. This issue is discussed in Section 4.3 in the context of parameter tuning. The PD leg tracking gains (i.e. $k_{\phi p}$, $k_{\phi d}$) are not constant; gain scheduling based on the cycle time, c, and the leg position is employed so that good trajectory tracking is achieved during the flight phase. A position requirement is included to ensure that the legs are *actually* off the ground because no touchdown or liftoff sensing is available on the robot.

State Estimation

Because no sensor is available on the robot to measure its forward speed, the forward speed is estimated using the desired sweep velocity, $\dot{\phi}_d$. Forward speed estimation is discussed in detail in Section 3.3.2.

3.2.3 Controller #2

Motivated by Raibert's pioneering work on hopping robots, an alternative controller is proposed that uses the desired foot position at touchdown to control forward speed. As in Controller #1, this controller uses an inverted pendulum balancing PD controller to generate motor torques that control the body pitch during the stance phase; however, in this case the desired pitch angle is fixed. For simplicity, a 2D sagittal plane version of the controller is considered; incorporating the roll and yaw angles into the calculations is straightforward. The control block diagram is given in Figure 3.8, and is described below.

Forward Speed Controller

As discussed in Chapter 2, the hopping robot literature emphasizes that the foot location at touchdown, relative to the robot COM, has a strong influence on the net horizontal acceleration of the robot COM produced during the stance phase. Following this line of thought, the leg trajectory parameters for this controller are selected so that the assumed touchdown event occurs at a desired distance ahead of the body COM.

Let y_f be the distance of the foot ahead of the projection of the COM on the ground at touchdown. Using Raibert's terminology, let y_{f0} be the neutral point that produces no net horizontal acceleration over a stride. For bipedal RHex, a function for the neutral point, $y_{f0} = f(\bar{v})$, would be determined experimentally. Then, y_f is the sum of the neutral point term and a control term, $y_{f\Delta}$, used to control the forward

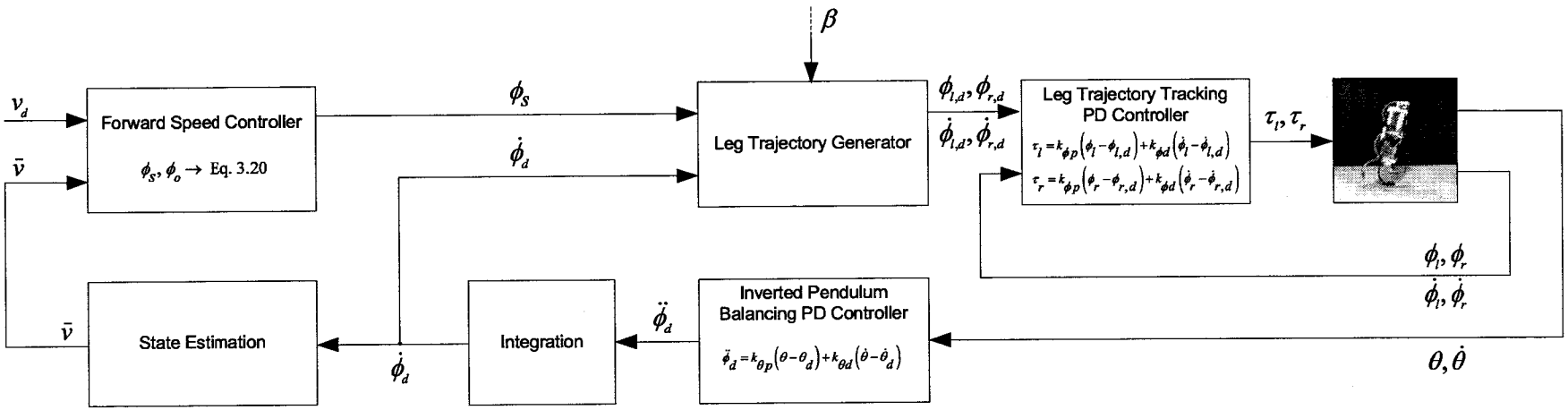

Figure 3.8: Controller #2 block diagram

speed. Equations (3.17) and (3.18) detail the calculation of y_f:

$$y_{f\Delta} = k_v(\bar{v} - v_d) \tag{3.17}$$

$$y_f = y_{f0} + y_{f\Delta}. \tag{3.18}$$

Let r be the perpendicular distance from the hip axis to the COM. The desired effective touchdown angle, $\phi_{e,d}$, can be found using (3.20):

$$y_{COM/H} = r\cos\theta \tag{3.19}$$

$$\phi_{e,d} = \sin^{-1}\left(\frac{y_f + y_{COM/H}}{l_e}\right). \tag{3.20}$$

As presented in Section 6.2 (p. 77), the effective leg angle (shown in Figure 3.5(b), p. 28) is $\phi_e = \phi/2$ for $0 < \phi < \pi/2$. Using this, and that the assumed touchdown angle occurs at $\phi = \phi_s/2 + \phi_o + \pi/2 - \theta$, the sweep angle ϕ_s and offset ϕ_o can be used to achieve the desired effective touchdown angle $\phi_{e,d}$:

$$\phi_s + 2\phi_o = 4\phi_{e,d} + 2\theta - \pi. \tag{3.21}$$

The relationship between ϕ_s and ϕ_o would have to be determined experimentally, such that it satisfies the above.

Leg Trajectory Generator

Proposed leg trajectory parameter relationships for this controller are summarized in Table 3.3, where c_8 and c_9 are constants.

Scheme	Leg Trajectory Parameter Functional Relationships
D	$\dot{\phi}_d \rightarrow$ Eq. (3.12) ϕ_s, $\phi_o \rightarrow$ Eq. (3.21) $\beta = c_8 + c_9\dot{\phi}_d$

Table 3.3: Leg trajectory parameter relationships for Controller #2

3.3 Sensing and State Estimation

The controllers discussed in this chapter use minimal feedback, in particular, leg angles with respect to the body and body pitch. It will be shown in Chapter 5 that a stable, 3D, dynamic, bipedal gait can be produced with only these measurements. This section discusses the sensing requirements and the estimation of forward speed for the controllers presented in the previous sections.

3.3.1 Requirements

For bipedal RHex, pitch angle sensing is required. It is conceivable to have a 3D bipedal running robot that does not require pitch sensing; this would require that the robot body COM lie below the hip axis. However, this potentially results in ground clearance problems. In such a configuration, the body would act like a pendulum and be passively stable. This approach was taken by Zeglin [96], who built a two-actuated DOF *planar monopod.*

In addition to pitch and leg angle measurements, body roll and yaw angle measurements are available, as described in Section 2.3. It was found that significant improvement can be made to the bipedal gait by including a yaw angle feedback loop in the controller. A steering controller is presented in Chapter 4 and the resulting performance is presented in Chapter 5.

3.3.2 Forward Speed Estimation

A forward speed measurement or estimate is required for both controllers presented in this chapter. There are a number of possible ways to measure the forward speed of the robot. Measurement options include on-board or off-board cameras, as well as various non-contact ranging systems (e.g. lasers). Further options include the use of a treadmill, moving harness, or ground contact mechanism, for example. However, for this application it was desired that the measurement or experimentation approach taken not confine the robot to a particular test area, not require equipment external to the robot, and not limit potential applications. Conceptually,

accelerometers are a desirable solution; however, accumulated error and drift over the approximately 10 s test are a problem. Yet further options for speed measurement involve leg re-design and instrumented legs. This type of option would require slip rings or some wireless signal transmission scheme to pass signals from the legs to the robot body. Such a system is the subject of development work on the RHex robot [48].

With the exception of the passive dynamics based walkers, all the robots discussed in the literature review of Chapter 2 have the ability to use joint angles and rates in conjunction with forward kinematics to determine the forward velocity of the robot. Of particular significance, large feet or non-rolling "point" contact feet have a stationary foot position (e.g. point F in Figure 3.5a, p. 28) with respect to the inertial frame during stance phase. In addition, joint deflections are known and can be measured in a straightforward manner because only rotational and prismatic joints are used.

In the interest of simplicity and reliability, and in order to determine if additional sensors were, in fact, *required*, forward speed estimation approaches using hip encoder measurements or no measurements at all were pursued. Bipedal RHex's half-circular leg geometry and un-instrumented legs introduce several complications. Neither the effective leg length nor angle are known because neither the leg deflection nor the foot position with respect to the leg are known. In addition, it is not known whether the leg is in contact with the ground. Slipping is another issue; experimental trials involving high frame rate video have shown that significant slipping occurs during portions of the stance phase.

It was found that no hip velocity measurement was necessary for forward speed estimation. The forward speed of the robot can be estimated based on the *desired* stance velocity, $\dot{\phi}_d$, alone. To this end, a single-pole low-pass infinite impulse response (IIR) filter is employed:

$$\bar{\dot{\phi}}_{d,k} = \alpha_v \dot{\phi}_{d_k} + (1 - \alpha_v)\, \bar{\dot{\phi}}_{d,k-1} \tag{3.22}$$

$$t_{IIR} = \frac{-T}{\ln(1 - \alpha_v)}, \tag{3.23}$$

where, $\bar{\dot{\phi}}_d$ is a filtered version of the sweep velocity, α_v is a parameter of the filter

found from Equation (3.23), t_{IIR} is the time constant of the filter, and k is the index of the sample (e.g. k and $k-1$ are T seconds apart). The time constant of this low pass filter was set to 1.0 s (approx. 3 stride periods) in the experiments presented in Chapter 5. The estimated forward speed is then

$$\bar{v}_k = \bar{\dot{\phi}}_{d,k} l_{ave}. \tag{3.24}$$

The resulting forward speed estimate is smooth and was implemented successfully in experiment.

Alternative approaches using hip measurements were also investigated. In practice, these approaches were not as well suited to the controllers presented in this chapter because the resulting speed estimate was not as smooth as with the open loop approach presented above. Other drawbacks of such approaches include the need for combining the data from the two legs, not knowing if a given leg is in contact with the ground, and the possibility of slipping between the foot and the ground.

3.3.3 Touchdown Detection

Touchdown event detection can be used in several ways. Reflex type control actions, which are common among hopping robots, can be employed. Touchdown detection could also be used to adaptively adjust the leg trajectory parameters so that the actual and assumed leg phases coincide. As mentioned previously, the leg state (stance or flight) can be assumed based on the cycle time, c. However, an approach was considered where the leg states were estimated based on a partial model of the system. Touchdown detection was not employed for any of the test results presented in this thesis, for reasons discussed in this section.

Touchdown detection was achieved on RHex in quadrupedal bounding and hexapedal pronking gaits [12, 58]. These gaits have considerable aerial flight phases that allow *under-the-hip* leg protraction. The algorithm used involved protracting the leg in flight to the desired touchdown angle and allowing adequate time for the leg motor currents to settle to zero. The touchdown event was then detected when the motor currents exceeded some threshold value.

In bipedal RHex, over-the-hip leg protraction results in high motor currents and velocities during the flight phase and it is not possible to stop the leg and wait for the motor currents to settle. Thus, an alternative approach was attempted. A closed loop flight phase model of the motor, gearhead, amplifier, and leg inertia was used to calculate the current expected to be drawn by the motor, i_{model}, in the absence of external disturbances. The inputs used to calculate i_{model} were the desired leg position and velocity, and the measured battery voltage. As no motor current sensors were available on the robot, the actual motor currents were estimated using a model of the motor and amplifier based on the measured battery voltage, leg velocity, and PWM amplifier duty cycle. The equation for estimated motor currents, i_{est}, is given by Equation (5.1), p. 55 . This model for i_{est} was identical to the one presented and validated in [59] for the RHex robot.

This touchdown detection approach is based on the fact that the flight phase model does not reflect any currents due to disturbance torques exerted by the ground on the leg. Thus, the disturbance torque can be calculated: $\tau_{dist} = K_t(i_{est} - i_{model})$, where K_t is the motor torque constant. With the necessary filtering, τ_{dist} was used to approximately detect the touchdown event.

Initial tests using high frame rate video revealed a delay in detection of up to 40 ms. (The duration of a typical stance phase is approximately 160 ms.) This delay, compounded by the fact that the high frame rate video equipment necessary to verify touchdown detection performance became unavailable, led to this touchdown detection approach being abandoned. One cause for the delay was filtering, which was required because of flight phase vibration of the leg. Another limitation was that, in some poses, the radial component of the leg force was much larger than the tangential force that generates load torques on the motors. A number of other touchdown detection approaches can be envisioned, but it was decided that the simplest approach, assuming the leg state based on the cycle time, was sufficient.

Chapter 4

Roll and Yaw Stability and Control

The controllers discussed in Chapter 3 deal with sagittal plane dynamics. The dynamics in the transverse and frontal planes (shown previously in Figure 2.1, p. 7) also have a strong contribution to the overall dynamics, and are critical to the success of the gait.

The dynamics in the frontal and transverse planes are naturally oscillatory due to the intermittent leg-ground contact and the wide hip spacing. Stable vertical oscillations at twice the stride frequency and roll angle oscillations at the stride frequency are desired in order to compress and decompress each leg once per stance phase. The yaw and roll angle dynamics are of particular importance to the stability of the gait.

Because only two actuated degrees of freedom are available to simultaneously control pitch, roll, yaw, and forward speed, passively stable roll oscillations are highly desirable. Passively stable roll oscillations can be encouraged by appropriate choice of the mass-stiffness properties, mass distribution, and hip spacing. Controller parameter values also have an important effect on the roll dynamics. Roll stability is discussed in Section 4.1.

The mean value of the yaw angle over a stride determines the forward direction of the robot. Experiments have shown that, once sufficiently disturbed, this angle is not stable and it increases exponentially until a fall failure occurs. Some turning is the result of, for example, uneven stiffness matching between the two legs, small mass distribution asymmetries, and motor asymmetries. However, once sufficiently

initiated, turning is unstable because the curvature of the robot's path results in an acceleration that causes the robot to "lean" more on the outside leg, resulting in a longer stance phase on one side. This generates an additional yaw moment that reinforces the turning motion. Steering, or yaw angle control, is accomplished by a differential modification of the leg trajectory parameters between the two legs, and is discussed in Section 4.2.

This chapter concludes with a discussion of the gait and controller parameter tuning procedure. Proper determination of the gait and controller parameters is critical to the success of the gait.

4.1 Roll Stability

Roll stability is addressed on two levels. The first level is the effect of mass distribution, hip spacing, and the mass-stiffness properties on the unforced response of the system. Secondly, controller parameter values determine the forced response of the system. No active roll stabilization (i.e. no explicit control) was implemented because of the limited number of actuated DOF available.

4.1.1 Passive Roll Stability

The mass distribution in the frontal plane is a critical factor in the roll dynamics. Murphy and Raibert [63] introduced a dimensionless group that they termed *dimensionless inertia*, in the context of their study of bounding and trotting of quadrupeds in the sagittal plane. In the current bipedal work, the concept of the dimensionless inertia is applied to study roll oscillations in the frontal plane. In this case, the dimensionless inertia, $\hat{I}_{roll}$, is defined as

$$\hat{I}_{roll} = \frac{I_{roll}}{mL^2}, \tag{4.1}$$

where I_{roll} is the mass moment of inertia of the robot body about the y (roll) axis, m is the mass of the robot, and L is half of the hip spacing. This concept is expanded upon in the following development adapted from [72] using the simplified frontal

plane model given in Figure 4.1. Small angles, a single leg stance configuration, and planar dynamics are assumed. Summing forces in the z direction, and denoting the magnitude of the spring force above the static deflection by F, yields $F = m\ddot{z}$. Ignoring gyroscopic effects, deemed negligible, the moment equation about the COM yields $F = I_{roll}\ddot{\gamma}/L$. Combining these two equations, rearranging, and dividing by the half hip spacing results in (4.2):

$$\frac{\ddot{z}}{\ddot{\gamma}L} = \frac{I_{roll}}{mL^2}. \tag{4.2}$$

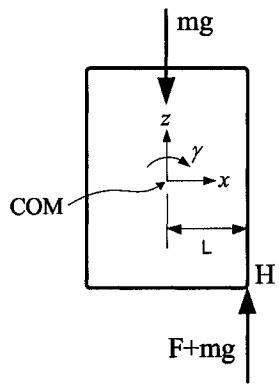

Figure 4.1: Simplified frontal plane model

The left hand side of Equation (4.2) is a ratio of the vertical acceleration of the hip, H, due to translation to the vertical acceleration of H due to rotation. Thus, intuitively, the dimensionless inertia is a measure of the "resistance" to rotation to the "resistance" to translation due to the mass distribution [72]. Figure 4.2 illustrates the interpretation of Equation (4.2). Murphy [64, 63] found that when $\hat{I}_{pitch} < 1$ the body pitch of a quadruped can be passively stabilized in a bounding gait. When the dimensionless inertia was greater than unity the gait would have to be actively stabilized.

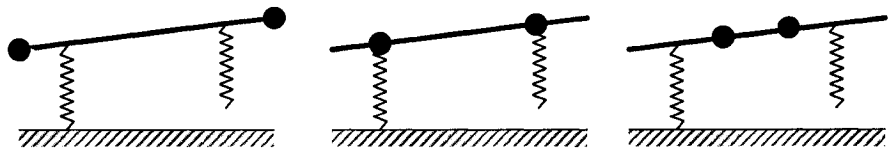

(a) (b) (c)

Figure 4.2: The concept of the dimensionless moment of inertia: (a) $\hat{I}_{roll} > 1$, (b) $\hat{I}_{roll} = 1$, and (c) $\hat{I}_{roll} < 1$. [80]

One might argue that minimizing roll oscillations using the mass distribution (e.g. $\hat{I}_{roll} > 1$) is a good option to achieve stable motion in the frontal plane (e.g. attempt to minimize the roll oscillation amplitude). However, in this case, disturbances causing the body to roll are more difficult to correct. In its standard configuration, bipedal RHex has a dimensionless moment of inertia of $\hat{I}_{roll} = 1.27$. Though close to one, this value indicates that the gait and controller parameters have to be carefully chosen so that the mass distribution of the robot does not have to be modified. Increasing the hip spacing can also lower $\hat{I}_{roll}$, but this has the undesired effect of changing the transverse plane dynamics. Otherwise, lowering $\hat{I}_{roll}$ is problematic without increasing the mass of the robot significantly. This leads to the need for stronger legs and increased hip actuator torque.

4.1.2 Forced Response

The frontal plane dynamics are also strongly dependent on gait and controller parameters, the determination of which are discussed further in Section 4.3. Firstly, the leg tracking PD control law causes the motor to act like a torsional spring. The proportional gain, $k_{\phi p}$, introduces a compliance that, depending on the robot's pose, can act in series with the leg compliance. In addition, the controller continually generates motor torques that allow the legs to track the desired position and velocity trajectories, which based on the leg trajectory parameters, determine the stride period, t_c. These leg motions create a forced response that is different from the natural

passive response. Ideally, the passive dynamics and controller forcing of the gait are compatible. For example, given the passive dynamics, the stride period dictated by the controller should, ideally, produce periodic roll oscillations with the same period.

Besides their role in determining the stride period, the leg trajectory parameters also determine the fraction of the stride during which double stance exists, if at all. Increasing the amount of double stance changes the average spring stiffness properties of the system over the stride. This has the effect of reducing the roll oscillation amplitude by reducing the duration of the single support phase.

4.2 Steering Controller

This section presents a steering controller devised for bipedal RHex. In Chapter 5 it will be shown that this steering controller is critical to achieving a high experimental success rate. This controller adds a yaw angle, ψ, feedback loop to Controller #1, presented in Chapter 3. The corresponding block diagram is presented in Figure 4.3.

The steering controller devised for bipedal RHex differentially changes the leg trajectory parameters between the left and right legs such that the stride period, t_c, is maintained by both the left and right leg. This ensures that the relative phase (defined in Section 3.1.2) between the legs is maintained.

The wide hip spacing of the robot results in a yaw oscillation with an amplitude of up to 6° and a period equal to t_c. Because this yaw angle oscillation is superimposed on the yaw angle defining the forward direction of the robot, some measure of the forward direction of the robot is required. To this end, the measured yaw angle ψ is filtered using a low pass single pole filter, producing $\bar{\psi}$, which is used in the control law as a measure of the direction of forward progress:

$$\bar{\psi}_k = \alpha_\psi \psi_k + (1 - \alpha_\psi)\bar{\psi}_{k-1}. \tag{4.3}$$

In the above, α_ψ is a parameter of the filter, and k is an index indicating the sample number. The time constant of the filter is $-T/\ln(1-\alpha_\psi)$, where T is the sampling period. The need for the yaw angle filtering, or some other means of accounting

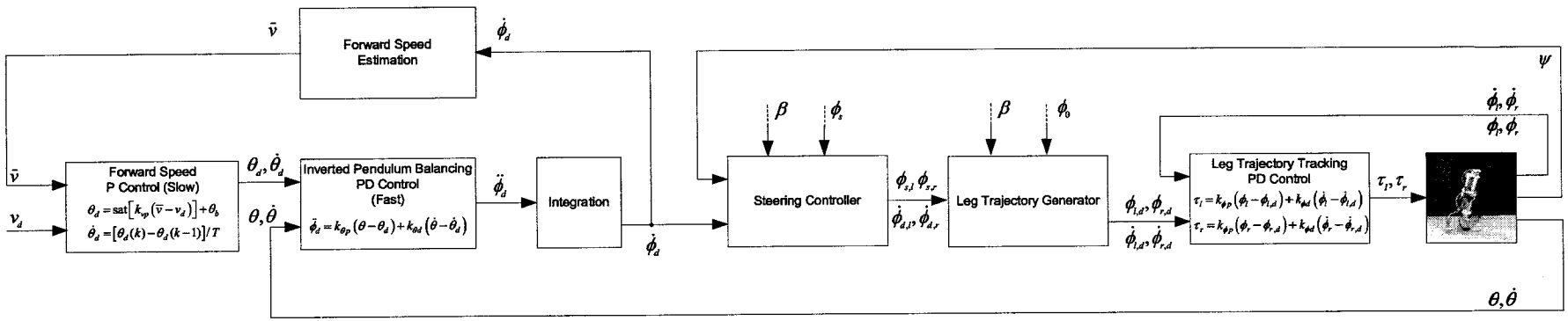

Figure 4.3: Controller #1 block diagram with steering controller

for the yaw oscillation over each stride, is clearly visible in the experimental data presented in Figure 5.5, p. 61.

To achieve steering, the desired left and right leg sweep velocities, $\dot{\phi}_{d,l}, \dot{\phi}_{d,r}$, are respectively incremented and decremented by Δ according to:

$$\Delta = \text{sat}\left[k_{\psi p}(\bar{\psi} - \psi_d)\right] \tag{4.4}$$

$$\dot{\phi}_{d,l} = (1 + \Delta)\dot{\phi}_d \tag{4.5}$$

$$\dot{\phi}_{d,r} = (1 - \Delta)\dot{\phi}_d, \tag{4.6}$$

where, ψ_d is the desired yaw angle, $\text{sat}(x)$ is the saturation function defined in Section 3.2.2, and the l and r are subscripts that refer to the left and right leg, respectively. The sweep angles for the left and right legs are then modified to maintain the correct stride period, $t_c = \frac{\phi_s}{\beta\dot{\phi}_d}$, as per

$$\phi_{s,l} = \dot{\phi}_{d,l}\beta t_c \tag{4.7}$$

$$\phi_{s,r} = \dot{\phi}_{d,r}\beta t_c. \tag{4.8}$$

Conceptually, it seems reasonable that other combinations of leg trajectory parameters could be used to achieve steering control. However, alternative combinations were not investigated in this thesis.

For the experimental testing presented in Chapter 5, it was desired that the robot travel in a straight line so that accurate average velocity calculations could be obtained from ground truth position and time measurements. In order to improve the steering performance for this application, a line tracking term was added to Equation (4.4):

$$\Delta = \text{sat}\left[k_{\psi}(\bar{\psi} - \bar{\psi}_d) + k_{dp}d\right]. \tag{4.9}$$

In the above equation, d is the estimated lateral displacement (displacement in the X direction) of the robot. The lateral displacement of the robot is estimated using the estimated forward speed, $\bar{v}$, and the yaw angle, ψ, according to

$$d = \sum_{0}^{k} \bar{v}_k \sin\left[\psi_k - \bar{\psi}_0\right]T, \tag{4.10}$$

where $\bar{\psi}_0$ is the filtered yaw angle at the beginning of the test. This lateral displacement estimation scheme was verified using a measuring tape attached to the floor parallel to the finish line of a 5 m test track. The accuracy of the lateral displacement estimate was found to be within the accuracy that a human observer could reasonably estimate the location of the ground projection of the midpoint between the robot hips using a measuring tape as the robot crossed the finish line, approximately ± 5 cm.

4.3 Parameter Tuning

The bipedal gait studied in this thesis is sensitive to small control parameter variations. The dependence of the gait on the gait parameters and controller parameters, combined with a lack of a practical framework to obtain suitable values for these parameters, is a weakness of the control approach. This circumstance is partly an outcome of the minimalist approach to the design of the platform, in particular, the use of minimal sensing and actuation for the robot. Complexities in realistically modeling friction properties, nonlinear stiffness and damping in the legs, and complex ground-robot interactions do not allow this task to be easily transferred to simulation. Thus, manual experimental parameter determination is required.

As discussed in Chapter 2, there have been several successful non-manual experimental approaches to parameter tuning of legged gaits that include on-line optimization and learning algorithms. As discussed in Chapter 2, a remarkably successful example is presented in [94] for a tripod gait on the RHex robot. However, such approaches are generally not feasible for the bipedal gait presented in this thesis because the gait is so sensitive to parameter variations that, even if an initial working gait is available as a starting point, an excessive percentage of unstable trials would result. This section discusses the manual tuning procedure adopted for the key parameters influencing the bipedal gait. The primary complication is the large number of parameters and the significant coupling that exists between them, in terms of gait performance. The result is a manual tuning procedure that is highly labor intensive, dependent on the operator's skill, and whose outcome is uncertain.

For a given forward speed set-point, v_d, the key gait and controller parameters

requiring tuning are listed below. Furthermore, a number of other less critical constants, not listed here, are required (e.g. bounds on variables).

- Balance angle, θ_b
- 2 PD leg tracking gains: $k_{\phi p}$, k_{ϕ_d}
- 2 PD gains for the inverted pendulum balancing (pitch) controller: $k_{\theta p}$, $k_{\theta d}$
- 1 P gain for the inverted pendulum forward speed controller: k_{vp}
- 1 P gain for the steering controller: $k_{\psi p}$
- 4 independent leg trajectory parameters, $\dot{\phi}_d$, β, ϕ_0, ϕ_s, and their functional relationships (see Table 3.2)
- 1 filter parameter for forward speed estimation: α_v
- 1 filter parameter for the steering controller: α_ψ

As discussed previously, a key desired characteristic of the gait is roll oscillation at the same frequency as the stride frequency. This allows smooth leg spring compression cycles to occur, making the most out of the spring properties of the leg and promoting symmetry between strides. As suggested in previous sections, such a roll oscillation is also a function of gait and controller parameters. Also, as discussed previously, yaw oscillations play an important role in the gait, particularly in body path stability. Therefore, one of the primary objectives of the tuning procedure is to obtain good frequency and phase relationships between these signals and the leg oscillation. Figure 4.4 shows power spectra for the roll, yaw, and leg velocity signals obtained using a Fast Fourier Transform (FFT) for a successfully tuned gait. This figure shows that the roll angle, yaw angle, and leg velocity signals each have one well defined frequency component. In addition, these values are approximately equal to each other. Such plots were used as a tool in the parameter tuning procedure. Not surprisingly, it has been observed that less smooth and less symmetric gaits have less well defined power spectra peaks, strong contributions from multiple frequencies, or

poor correspondence between the roll and leg velocity spectra. Correspondingly, such gaits also tend to be less stable.

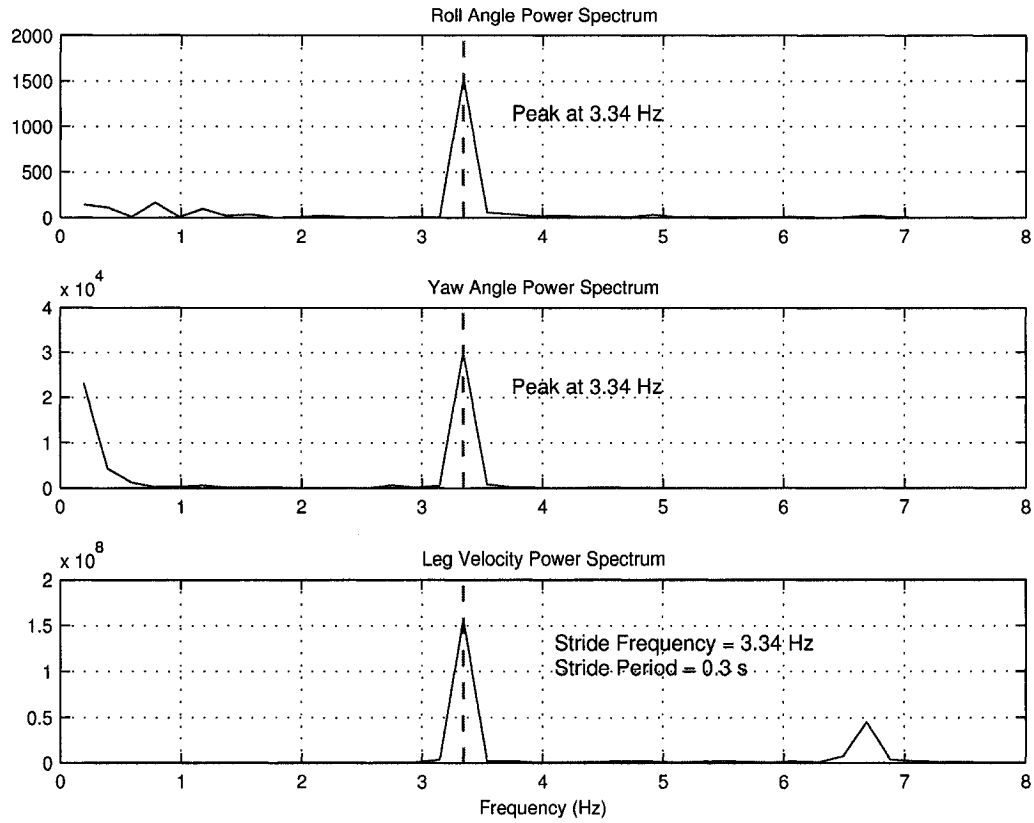

Figure 4.4: Roll, yaw, leg velocity power spectra plots.

The parameter tuning procedure is a highly iterative process. The remainder of the chapter outlines key elements of the tuning procedure. For the PD control loops, the standard stiffness and damping reasoning provides an intuitive way to tune the gait parameters. As mentioned previously, this is a primary reason for using PD control laws in this work.

Leg tracking PD gains play an important role in the gait. The P gain contributes to the stiffness of a fictitious spring (i.e. body spring) that extends from the body COM to the foot location. A lower limit exists for the P gain, at which the leg cannot track the desired trajectories. The preferred P gain is typically only slightly above this lower limit. The D gain can be chosen based on measured leg velocity data so

that the response is satisfactorily damped.

A preliminary determination of the leg trajectory parameters can be made with the balancing and speed controllers turned "off". To do so, experiments are performed in which the operator constrains the body pitch angle such that the robot approximately balances while moving at the forward speed set-point. All four leg trajectory parameters affect the timing and nature of the touchdown and liftoff events and an appropriate correspondence between the actual and assumed touchdown and liftoff events must be obtained. This procedure is constrained by actuator torque-speed capabilities, which limit the set of achievable leg trajectory parameter sets.

Once acceptable leg trajectory parameters and leg tracking PD gains have been obtained, a first determination of the PD balancing gains can made with the speed controller turned "off". The balance angle cannot be calculated using statics because the point where the ground reaction force acts is a function of the robot dynamics and it varies over the stride. The balance angle should be empirically chosen such that the magnitude of the forward acceleration of the robot is minimized. This value can be revised once the speed controller is enabled so that the desired lean angle (defined in Section 3.2.2) is zero for a constant forward speed. Next, with all controllers "on", the speed controller gains are chosen such that the dynamics of this controller are slower than the balancing controller.

After preliminary determinations have been made for all parameters, recorded experimental data and intuition are used to iteratively improve the gait. The steering controller can be tuned independently of the other controllers.

Chapter 5

Experimental Results

This chapter presents results obtained from analysis of recorded controller and sensor signals as well as video recordings from bipedal running experiments. Baseline results were obtained using the hardware configuration given in Table 5.1. Steering control and velocity control performance are then demonstrated with additional experimental data sets using the baseline hardware configuration. The effect of hardware modifications, including different radial leg stiffness values and increased lateral leg stiffness, are then considered. In addition, preliminary findings obtained using "C" shaped legs and upgraded power supply, amplifiers, and motors are presented. The following table outlines the physical configuration of the robot for experiments presented in this thesis.

Configuration	Radial Leg Stiffness (N/m)	Leg Width (mm)	Leg Shape	Power Supply, Motor, Gearhead Specifications
Baseline (Sec. 5.2)	1640	25	"S"	24V, RE25, 33:1
B (Sec. 5.5.1)	1492	25	"S"	24V, RE25, 33:1
C (Sec. 5.5.1)	2250	25	"S"	24V, RE25, 33:1
D (Sec. 5.5.2)	1620	34	"S"	24V, RE25, 33:1
E (Sec. 5.5.3)	1620	34	"C"	34V, RE30, 14:1

Table 5.1: Summary of hardware configurations

5.1 Experimental Method

Experimental results were produced by running the robot repeatedly over a test track. The test track consists of a standard linoleum floor marked with 2 m wide retro-reflective tape lines, spaced 5 m apart. Suitable initial conditions are provided by manually starting the robot in an upright posture at a distance of approximately 2 m from the start line. The robot senses the start and end reflective tape lines via a downward facing infrared (IR) sensor and records time data required for the calculation of the actual average forward speed, average power, and total lateral displacement.

Simple pragmatic criteria are used to assess body, body path, and gait stability. Two modes of failure were considered with respect to body stability. If the robot falls, the test is recorded as a fall failure. If the estimated forward velocity error is greater than 15% at the finish line, the trial is recorded as a speed controller failure. Body path stability is judged based on the total lateral displacement of the robot's path over the length of the test track. If the robot crosses the finish line with a lateral displacement greater than 1 m (d >1 m), the test is recorded as a steering failure. A run that does not fall into the any of the above categories is considered a successful run. A data set normally consists of a total of ten runs.

5.2 Baseline Results

This section presents results obtained with the baseline hardware configuration. First, the baseline test results are used to illustrate typical signal plots. These plots provide information about the gait dynamics and are useful in analysis of the controller. The performance of the forward speed and steering controllers are then presented.

5.2.1 Signal Plots

Figure 5.1 contains plots of the four standard leg trajectory parameters and the corresponding stride period over the 5 m test track (approximately 21 strides). The

leg trajectory parameters show some fluctuation but the mean values are constant, thus showing good gait stability. Note that the sweep velocity and sweep angle are slightly different for each leg; this is the result of the steering controller discussed in Sections 4.2 and 5.2.3.

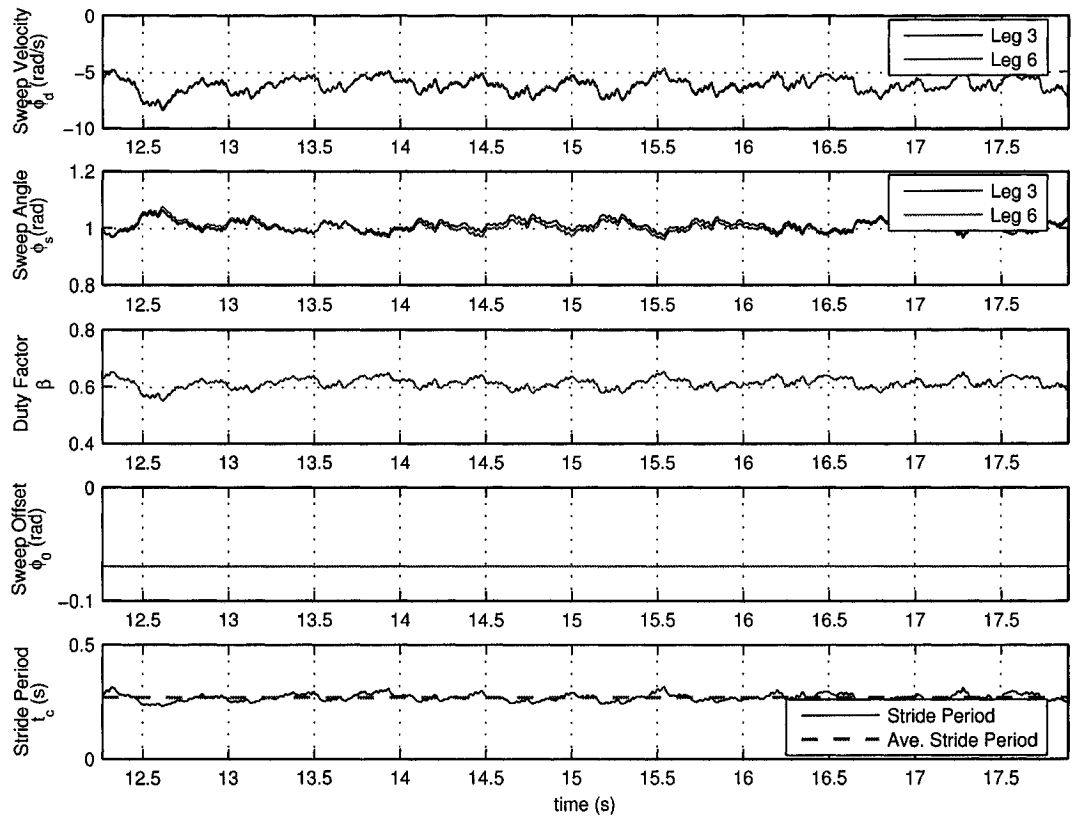

Figure 5.1: Leg trajectory parameter plot. Leg 3 is the left leg and Leg 6 is the right leg.

Figure 5.2 contains leg velocity and position profiles for two complete strides. Recall that leg rotation in the negative direction causes the robot to move forward. Background shading is used in the figure to emphasize the assumed phase. No shading corresponds to both legs in stance phase; light shading corresponds to the left leg (leg 3) in flight and the right leg (leg 6) in stance; darker shading corresponds to leg 6 in flight and leg 3 in stance. Thus, for baseline results, about 20% of the cycle is spent in the assumed double stance phase.

The lower plot of Figure 5.2 contains a plot of the estimated leg motor currents. The motor current is estimated via a simple motor, gearhead, and amplifier model given in Equation (5.1), where V_s is the supply voltage [V], K_s is the motor speed constant [(rad/s)/V], $\dot{\phi}$ is the leg velocity [rad/s], N is the motor gear ratio, σ is the commanded pulse width modulation (PWM) H-bridge amplifier duty cycle, R_{amp} is the resistance of the motor amplifier circuit [Ω], and R_{arm} is the motor armature resistance [Ω]. This model neglects the armature inductance ($L_{arm} = 0.12$ mH) and was presented and validated in [59]. The maximum possible current draw for a given speed is also included in the plot. It is calculated using Equation (5.2) for quadrants I and III of the torque-speed curve. In quadrants II and IV the full stall current is available, as long as the current does not exceed a 10 A limit imposed by thermal limitations of the motor amplifiers.

$$i_{est} = \frac{\sigma V_s - N\dot{\phi}/K_s}{R_{arm} + \sigma^2 R_{amp}} \tag{5.1}$$

$$i_{max} = \frac{V_s - N\dot{\phi}/K_s}{R_{arm} + R_{amp}} \tag{5.2}$$

Because motor current is proportional to the output torque of the motor, it provides insight into the leg-ground interaction and the gait dynamics. From the plot, it is apparent that the motors are saturated for a significant portion of the flight phase. However, no motor saturation occurs during stance. The estimated motor current provides a means to approximately assess how closely the *actual* phase matches the *assumed* phase of the gait. The plot shows that after the assumed liftoff event, there is a considerable velocity error and a negative current spike. This indicates that the leg is still on the ground when the assumed flight phase begins. The actual flight phase begins at the small upwards notch circled in the velocity profile. This notch occurs when any residual compression in the leg is released. The negative current spike at the beginning of the assumed stance phase, shortly after the flight phase braking of the leg, occurs after the touchdown event. Thus, the leg motor current plot suggests that the actual touchdown and liftoff events do not closely match the touchdown and liftoff events that are assumed in the trajectory controller. An effort was made to tune the gait parameters to achieve a closer correspondence

between the actual and assumed phase transitions; however, this had a detrimental effect on the stability of the gait, and this issue is discussed further in the following sections.

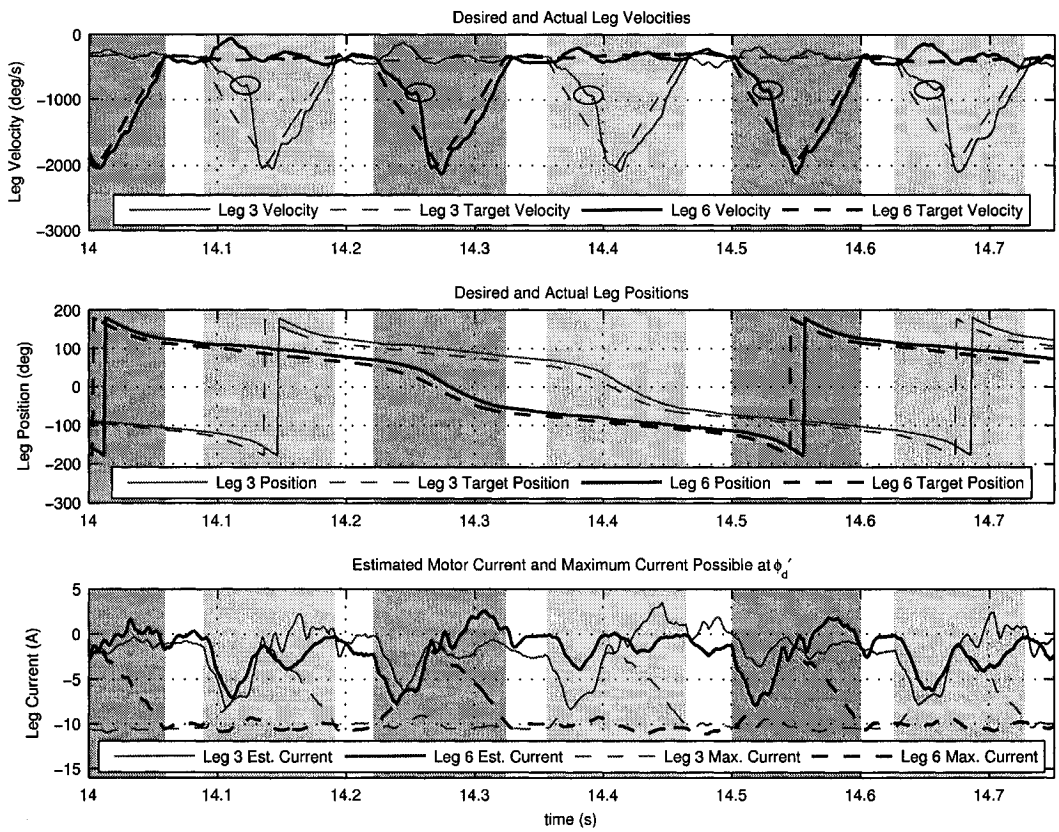

Figure 5.2: Leg velocity, position, and motor current plots

Figure 5.3 shows the tracking performance of the balancing controller and the corresponding desired acceleration, $\ddot{\phi}_d$. The top plot shows the desired and actual lean angles (angles from the specified balance angle, θ_b). The error is generally less than 2°, with spikes of about 3°. The forward speed of the robot is quite sensitive to the lean angle. In this case, the desired lean angle, θ_d is required to vary by less than 2° over the course of the test to stabilize the forward speed.

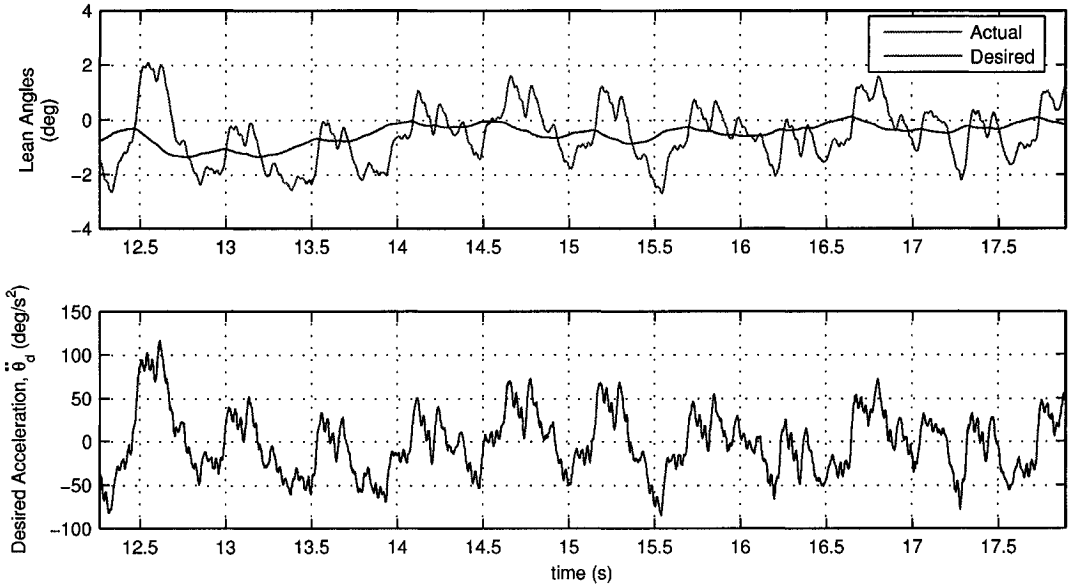

Figure 5.3: Balancing controller signal plot

As discussed in Chapter 3, the forward speed controller uses a forward speed estimate based on an approximate average leg length and a low pass filtered value of the desired sweep velocity. The average effective leg length during stance, used in the forward speed controller, depends on the stiffness of the legs. It was found to be 143 mm for the baseline legs, compared to an uncompressed length of 165 mm. The upper plot of Figure 5.4 shows velocity terms at the hip joint level: sweep velocity and the low-pass filtered sweep velocity. The time constant of the low pass filter used in the forward speed estimator is approximately 1 s (equivalent to approximately 3 strides). Interestingly, the desired sweep velocity fluctuates significantly. The resulting torques generated via the leg tracking PD loops are required to correct pitch and pitch rate errors. The lower plot shows the desired forward speed, estimated forward speed, average estimated forward speed, and the actual average forward speed. It shows good tracking of the set-point, v_d, with an average error of 2.6% between the estimated and desired forward speeds. Note that the actual average speed is calculated as the distance between the tape lines divided by the time taken to complete the test.

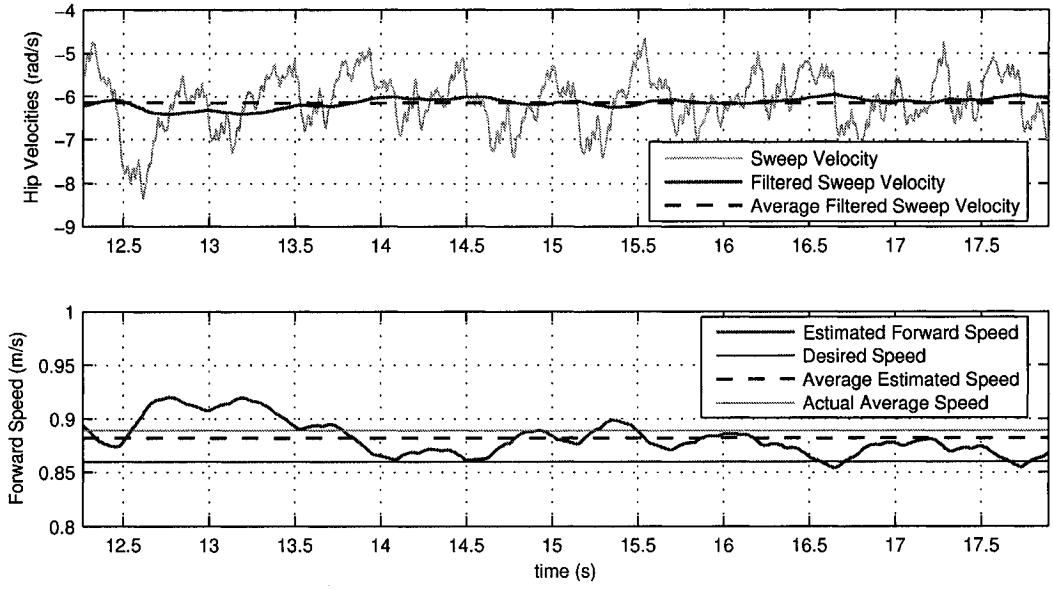

Figure 5.4: Forward speed controller signal plot

5.2.2 Speed Control

Forward speed control is demonstrated in this section. Experimental data sets, consisting of 10 runs each, were obtained for three speed set-points: 0.64, 0.86, and 1.15 m/s. This corresponds to nominal sweep velocities at the hip of 4.5, 6, and 8 rad/s, respectively. Additional experiments showed that, with the baseline hardware configuration, the minimum speed was 0.57 m/s, and the maximum speed was 1.26 m/s. Five data sets were produced for the aforementioned speed set-points, with the steering controller enabled. The data is presented in Table 5.2. The table also provides power consumption and efficiency data, which are discussed further in Section 5.4.

The mean error in average speed was 4.3% for the three 10 trial data sets. Over these 30 trials, the average error in the average estimated speed was 0.005 m/s with a standard deviation of 0.03 m/s. The maximum error was 0.05 m/s. These results demonstrate good tracking of the speed controller set-points.

Data Set Number	Speed Set-Point (m/s)	Actual Average Speed (m/s)	Speed Error (%)	Average Power (W)	Specific Resistance	# Trials / Success Rate
1	0.57	0.61	7.0	78.3	1.55	1 / 100%
2	0.64	0.67	4.7	78.9	1.42	10 / 100%
3	0.86	0.87	1.2	85.5	1.20	10 / 100%
4	1.15	1.07	-7.0	94.9	1.07	10 / 100%
5	1.29	1.28	-2.2	95.7	0.92	1 / 100%

Table 5.2: Forward speed controller experimental data.

5.2.3 Steering Control

In order to demonstrate the performance of the steering controller, a 10 trial experiment was performed under the exact same conditions as in data set #2 of Table 5.2, but with steering controller disabled. The lateral displacement, d, of the robot over the length of the track was used as a measure of controller performance. Using the stability criteria presented previously, 5 of 10 experiments resulted in steering failures.

From a stability standpoint, it is evident that the steering controller is an important component of the overall controller for the given hardware and velocity set-point. Table 5.3 presents the total lateral displacement over the length of the test track to further quantify the steering controller performance. Linear extrapolation was used to calculate the lateral displacement of the robot path when the robot left the track before completing the trial. This type of extrapolation is conservative because, once sufficiently initiated, turning is unstable, as discussed in Chapter 4. The data shows that the steering controller results in a vast improvement in the robot's ability to run in a straight line. It must be noted that the stability of the robot's direction depends on, for example, the forward speed set-point, leg characteristics and controller parameter values.

Steering Controller Enabled	Data Set Number	Speed Set-Point (m/s)	Specific Resistance ϵ	Mean Lateral Disp., d (m)	Standard Deviation of d (m)	# Trials / Success Rate
Yes	2	0.64	1.42	-0.09	0.24	10 / 100%
No	6	0.64	1.38	-0.69	0.87	10 / 50%[1]

Table 5.3: Steering performance tests. [1]Using a forward speed error of 10% (instead of the regular 15%) in the speed stability definition presented in Section 5.1 results in a 20% success rate.

Figure 5.5 illustrates the performance of the steering controller. The data set used is the same as in the baseline results section, Section 5.2. The middle plot shows lateral displacement as a function of the estimated distance traveled. Equally scaled axes essentially provide an aerial (i.e. plan) view representation of the body trajectory. The vertical dashed line represents the ground truth 5 m mark, providing an indication of the performance of the forward speed estimation. The upper plot shows the tracking performance of the steering controller with respect to forward direction. It also demonstrates the necessity of the low pass filter in the steering controller. In this case, the amplitude of the yaw oscillation is approximately 10°. Finally, the lower plot is the resulting steering controller output, Δ, which represents half the fractional difference in the desired sweep velocity between the two legs, as defined in Section 4.2. The value is small, generally on the order of 1%, and is limited to 3% by the controller.

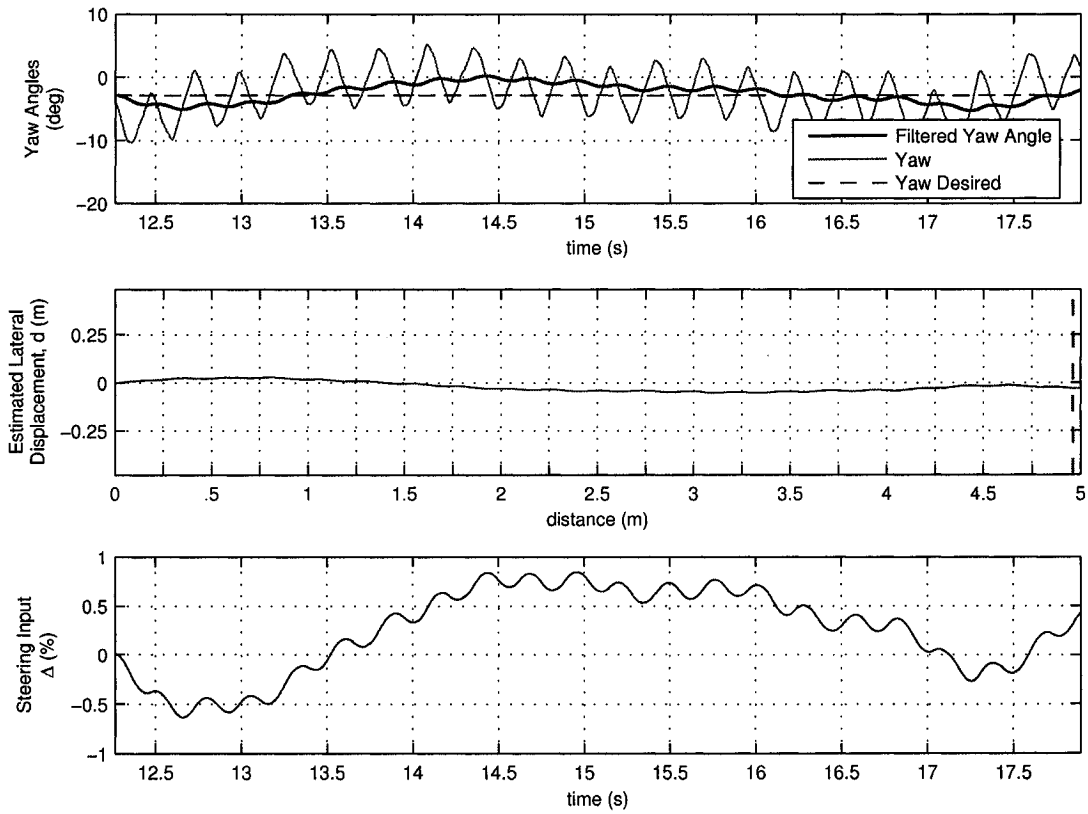

Figure 5.5: Steering plot. Yaw angles were obtained from gyroscope measurements. The time constant of the low pass filter was 0.5 seconds.

5.3 Qualitative Analysis of the Gait

As discussed in Chapter 2, the difference between running and walking is characterized by how kinetic and gravitational potential energies are exchanged, and in the role of elastic energy storage. In the bipedal gait currently under study, the hip height has been observed to reach its lowest point during stance. High frame-rate video analysis shows significant use of leg compliance, a characteristic of running. However, the gait also displays several characteristics normally associated with walking gaits. Most notably, this includes the existence of a double stance period. It is useful to break down the gait in terms of several characteristics used in the analysis of walking gaits: pelvic rotation (body yaw), pelvic tilt (body roll), and lateral displace-

ment. These are three of the six characteristics known as the determinants of normal walking gaits [53]. (The other three characteristics are not possible with RHex.) All three result directly from the spacing of the hips. Here, the lateral displacements discussed are small oscillations of the robot body in the x direction (See Figure 3.5) that repeat on a stride-to-stride basis, as opposed to the lateral displacement discussed in Section 5.2.3, which refers to the displacement of the robot path over the duration of the test.

Pelvic rotation

A yaw oscillation of approximately 9 to 12° peak-to-peak and period equal to t_c (see Figure 5.5) is observed in all data sets. During the single support phase, the hip corresponding to the flight leg swings forward relative to the other hip. This pelvic rotation increases the stride length by up to 15-20%, a significant increase.

Pelvic tilt

During the single support stance phase, the flight leg hip falls slightly during the single support phase. Over-the-hip leg protraction allows a gait with such a characteristic without any risk of toe-stubbing; no additional degrees of freedom are required. Pelvic tilt can lessen the vertical displacement required by the COM. Figure 5.6 contains a roll angle plot for a well tuned gait. For the experiments performed, the peak-to-peak roll amplitudes were typically 4-6°.

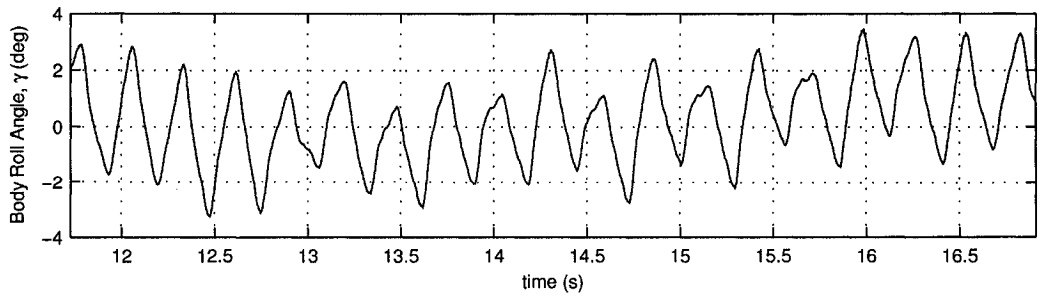

Figure 5.6: Body roll amplitude of a well tuned gait

Lateral displacement

Lateral displacement occurs when the robot's COM oscillates in the x direction. Because of the lack of accurate measurement data to this effect, only a qualitative assessment of the lateral displacement can be obtained using video recordings. Some degree of lateral displacement is inevitable given the spacing of the hips and feet. However, the displacement amplitude is increased greatly if the legs bend significantly out of a plane perpendicular to the hip axis. Lateral displacement was found to be detrimental to the gait, as will be discussed in Section 5.5.2.

5.4 Energetics

Energy efficiency is very important in most vehicle applications. This is particularly true for small electrically actuated robots, because currently available energy storage technologies carry significant size and weight penalties. This section attempts to answer energy related questions with the hope that the answers can lead to insights about the gait and how it can be improved. How is energy efficiency related to speed? How is energy efficiency related to controller parameter variations? Further motivation to look at energy efficiency in legged locomotion is that there is reason to believe that it correlates with stability because less stable gaits "waste" energy [94].

Specific resistance was proposed by Gabrielli and von Kármán [28] as a measure of energy efficiency to compare vehicles on the same scale, regardless of size, speed, or form. This dimensionless ratio can also be used to compare man-made vehicles to biological systems, a logical comparison when studying legged robots. Here, specific resistance is defined as

$$\epsilon = \frac{P_{ave}}{mgv_{ave}}, \tag{5.3}$$

where P_{ave} is the average power input, m is the mass of the system, g is the gravitational acceleration, and v_{ave} is the average speed. The definition of power input is an issue that must be addressed. One possibility is to use the mechanical power used by the actuators to generate the required motions. This directly addresses the performance of the gait, but neglects the cost of generating the actuator inputs. Al-

ternatively, the average total power input will be used in this analysis, an approach frequently employed in the literature. This approach facilitates the computation of specific resistance and generates a more practical, fair value for comparison.

Figure 5.7 shows how power and specific resistance are related to speed for the baseline configuration (see also Table 5.2). Although power requirements increase with speed, the specific resistance decreases significantly. This trend is also seen in other robots such as the ARL Monopod [32] and the ARL Scout II [73]. Note that the controller parameters were not tuned for each speed to generate the results for Figure 5.7.

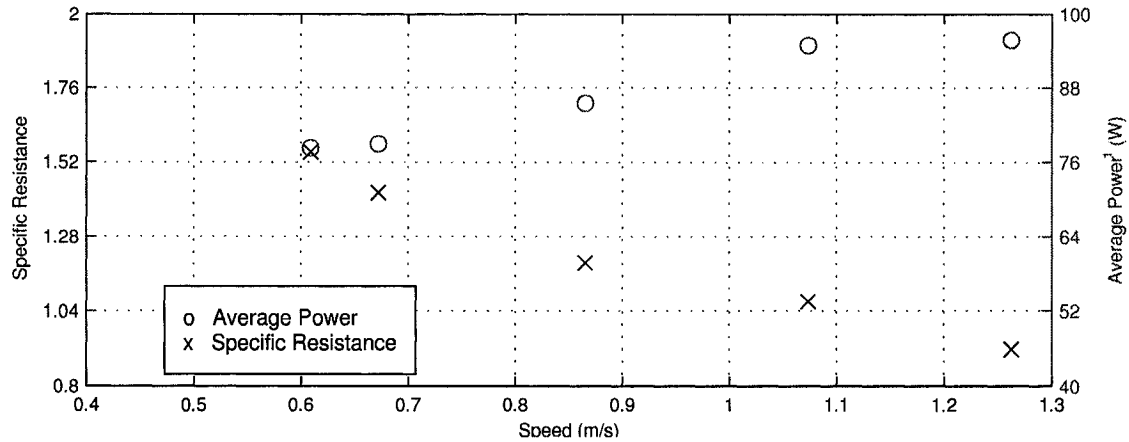

Figure 5.7: Specific resistance and average power versus speed plot for the baseline hardware configuration. [1]The average power is calculated based on the total electrical power output of the batteries.

The best specific resistance values obtained for bipedal RHex were approximately 0.9 for a forward speed of 0.94 m/s using hardware configuration D (see Table 5.6). To put these energy efficiency results in context, Figure 5.8 shows the specific resistance of various vehicles and robots, and for various human tasks. We see that RHex compares favorably to the ARL Scout II, RHex pronking, RHex bounding, and un-optimized RHex tripod gaits. The plot is roughly divided by system type. Passive gravity driven walkers and robots based on such passive walkers, such as the Cornell Biped, appear respectably in the lower left portion of the plot with efficiency values comparable to those of human walking, running, and cycling. Running and hopping robots generally

appear with specific resistance values approximately one to two orders of magnitude higher. Of the systems surveyed, wheeled vehicles offer comparatively high efficiency and speed. However, this data should be viewed with caution because of significant differences in the systems compared. For example, the MIT quadruped is a 25 kg robot powered by an off-board hydraulic pump. The corresponding specific resistance does not reflect the fact that the robot does not carry its power supply. Also, the environments in which each system operates may be different. For example, McGeer's walker is restricted to walking down shallow inclines, powered by gravity.

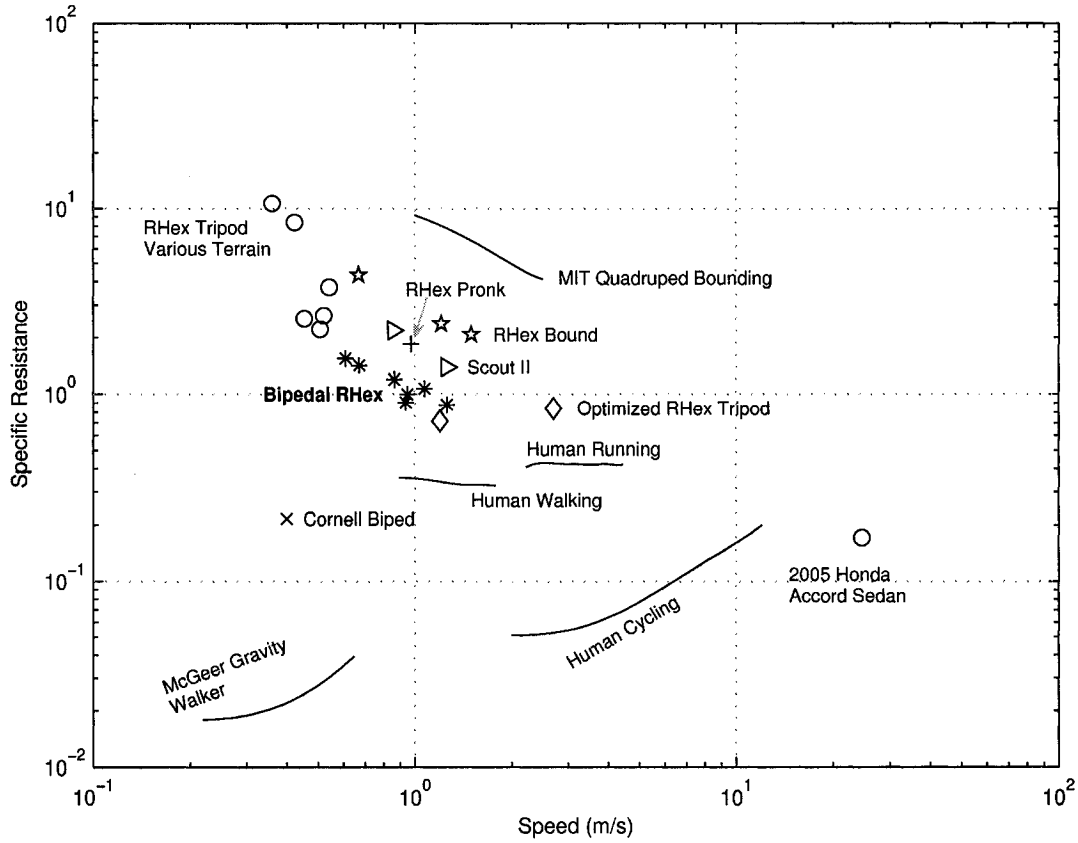

Figure 5.8: Representative specific resistance values for humans, robots, and various vehicles. References: McGeer walker [51]; human walking and running [50]; human cycling [78]; Honda Accord sedan [1] estimated based on EPA highway fuel economy and speed, optimized RHex tripod [94]; MIT quadruped [81] with P_{ave} based on hydraulic pump input only, RHex tripod for various terrain [85]; RHex bound [12]; Cornell biped [16]

Power consumption was analyzed in terms of the leg phase. The first trial of the baseline results is used as a typical data set. Electrical power consumption is tabulated by phase for both legs in Table 5.4(a). Since only the *assumed* phase is known accurately, data from a bench test with the robot legs off the ground is included to get an estimate of the energy required to swing the leg in the flight phase. Electrical energy estimates, E, for each leg j are computed via Equations (5.4) – (5.5), where V_m is the motor terminal voltage, i_{est} is the estimated motor current obtained from Equation (5.1), and q is the stride number:

$$E_{stance,j} = \int_{t_{td_q}}^{t_{lo_q}} |V_m(t) i_{est}(t)| dt \tag{5.4}$$

$$E_{flight,j} = \int_{t_{lo_q}}^{t_{td_{q+1}}} |V_m(t) i_{est}(t)| dt. \tag{5.5}$$

The estimated average power, $\bar{P}$, for each assumed phase and per stride are given by Equations (5.6) to (5.8).

$$\bar{P}_{stance,j} = \frac{E_{stance,j}}{t_{lo_q} - t_{td_q}} \tag{5.6}$$

$$\bar{P}_{flight,j} = \frac{E_{flight,j}}{t_{td_{q+1}} - t_{lo_q}} \tag{5.7}$$

$$\bar{P}_{stride,j} = \frac{E_{flight,j} + E_{stance,j}}{t_{td_{q+1}} - t_{td_q}} \tag{5.8}$$

From Table 5.4(a), we see that power requirement in the flight phase is about 3 times that of stance. Comparing the flight phase for the running experiment and the bench test, we see that the running experiment flight phase power requirements are about 11% higher. Again, this suggests that the leg is on the ground during part of the assumed flight phase.

	Estimated Power $\bar{P}_{stance}$ (W) (Running / Bench Test)	Estimated Power $\bar{P}_{flight}$ (W) (Running / Bench Test)	Estimated Power $\bar{P}_{stride}$ (W) (Running)
Left (leg #3)	7.1 / 0.7	31.5 / 23.5	16.4
Right (leg #6)	11.8 / 1.2	32.3 / 27.2	19.8
Average	9.5 / 1.0	31.9 / 25.4	18.1

(a)

	Power, $\bar{P}$ (W)	Energy, E (J)	Fraction of Total (%)
Stance (estimated)	9.5 (per leg)	3.14	14.3
Flight (estimated)	31.9 (per leg)	6.67	30.4
Legs #1,2,4,5 (measured)	2.1	0.58	2.7
Robot electronics (measured)	42.7	11.55	52.7
Total[1]	81.1	21.93	100.0

(b)

Table 5.4: Electrical energy requirements by leg phase. Estimated values are based on model-based motor current estimation. [1]Note that in order to obtain the estimated total power in the first column, the duty factor must be used to weight the contributions of the stance and flight phases.

In Table 5.4(b), we see that about half of the energy consumed goes to the electronics overhead that includes computation, sensors, and communications, for example. The energy expenditure used to swing the leg during the flight phase is more than 2 times that of stance phase. For this experiment, the average measured battery power was 82.5 W showing a 1.8% error compared to the motor current model-based estimate of 81.1 W, as seen in Table 5.4(b). This suggests that the motor current estimates are reasonably accurate. Flight phase energy requirements are expected to account for an even higher proportion of the energy consumption for the "C" leg configuration, where the leg must cover a $\frac{2\pi-\phi_s}{\pi-\phi_s}$ times larger distance in approximately the same amount of time.

The energy efficiency of the gait depends on both the hardware configuration and the controller parameter values. The effect of the leg trajectory parameters,

for example, will be shown in Section 5.5.2 for hardware configuration D, where the baseline leg trajectory parameters were modified to reduce the specific resistance from 1.05 to 0.90. The data is presented in Table 5.6, p. 72.

5.5 Hardware Modifications

The primary motivation for the hardware modifications presented in this section was to exploit any potential performance advantages in terms of, for example, efficiency, reduced sensitivity to initial conditions and disturbances, and reduced controller parameter sensitivity. Equally important a motivation was to generate insight into the mechanics of this bipedal behavior.

5.5.1 Modified Radial Leg Stiffness

The radial leg stiffness is a key mechanical parameter of the dynamic system being studied. The aim of experimentally investigating the effect of radial leg stiffness (the stiffness between the foot and hip) on the gait is to make the dynamics in the frontal plane more robust by modifying the natural dynamics of the system. In addition, we also seek to determine the sensitivity of the bipedal gait under study to radial leg stiffness. How critical is the value of the radial leg stiffness? This section also includes a discussion of potential ways of determining radial leg stiffness values.

What is the optimal stiffness? As discussed in Chapter 2, the simplest model for running is the planar spring loaded inverted pendulum (SLIP). Even for this simple model, analytical solutions do not exist; the dynamics in the stance phase are non-integrable [30]. Researchers resort to numerical studies or approximations. In bipedal RHex three dimensional dynamics, strongly non-linear leg properties, and rolling contact result in a gait that is vastly more complex than one that can be described by the SLIP model.

Simplifications are commonly employed to design legged robots. For example, the leg stiffness can be chosen so that a desired stance period is achieved based on the approximation of a vertical linear mass-spring oscillator. For example, for a monopod

the corresponding relationship is $t_s = \pi\sqrt{\frac{m}{k}}$, where t_s is the stance period, m is the mass, k is the linear spring stiffness. This type of calculation is difficult to apply to bipedal RHex because of the nonlinear leg stiffness properties and the existence of a double stance phase.

Once again, biological inspiration can serve as an example. Running animals locomote using muscles, tendons, and ligaments to absorb, store, and release elastic energy. Biomechanics studies lump these sources of compliance into a "musculoskeletal" spring, which extends between the foot, or midpoint between the stance feet if more than one foot is on the ground, to the COM. Full and Farley [25] report that runners, trotters, and hoppers using one to three legs per step and having masses ranging over orders of magnitude (e.g. cockroach, 0.001 kg; crab; quail; dog; kangaroo; human; horse, 135 kg) have *relative leg stiffness* values, $k_{rel,leg}$, of approximately 10. The relative leg stiffness is defined as

$$k_{rel,leg} = \frac{1}{n}\frac{\frac{F}{mg}}{\frac{\Delta l}{l}}, \tag{5.9}$$

where l is the hip height, Δl is the compression of the musculoskeletal spring at midstance, F is the peak vertical force measured using a force plate apparatus, n is the number of legs used in stance, and m is the mass of the body. The extensive range of number of legs, posture, body shape, and body mass for which the previous result is applicable lends support for its consideration in the design of legged robots. In addition, this line of reasoning has been employed successfully to determine the leg stiffness for the RHex tripod gait. Substituting bipedal RHex data in Equation (5.9) yields a desired leg stiffness value, $\frac{F}{\Delta l}$, of approximately 5000 N/m. One limitation of this argument is that these results were obtained for gaits with aerial phases.

Using the above results as a guide, experimentation with different leg stiffness values and PD leg tracking gains is a last method to obtain suitable stiffness values. This approach, although arguably the most reliable, must be limited because it is labor intensive, involves leg manufacturing and a very large number of experimental trials. Results from experimentation with different legs are presented in this section.

As shown in Table 5.1, the baseline legs used have a radial stiffness of 1640 N/m. Radial stiffness values cited in that table were obtained from force-displacement data

collected with a specially designed test rig, constructed previously in the Ambulatory Robotics Lab. The legs were tested under pinned end conditions at the hip and at the end of the leg. The radial stiffness was calculated as the force measured for a 25 mm deflection divided by this deflection value. Compared to the baseline stiffness, the aforementioned biomechanics studies suggest stiffer legs. Apart from the baseline legs, two additional sets of legs, with radial stiffness values of 1492 N/m and 2250 N/m, were tested on the robot. This choice was motivated primarily by the desire to find out if the leg stiffness should be increased or decreased. The particular values chosen were based on leg availability.

It was possible to obtain a stable gait with the 1492 N/m legs, but because of repeated mechanical failures due to leg delamination, testing was aborted. Out-of-plane deflections of these legs were visibly much more pronounced compared to the baseline.

It was also possible to obtain a successful gait with the 2250 N/m set of legs. The corresponding results are presented in Table 5.5. Compared to Data Set 3 (baseline legs, v_d=0.9 m/s) of Table 5.2, these results show a 20% improvement in specific resistance. However, it was found that the gait was more sensitive to controller parameter variations, making the tuning procedure more difficult and the gait less robust to initial conditions. Steering and velocity control was also less robust to disturbances.

Data Set Number	Velocity Set-Point (m/s)	Average Speed (m/s)	Average Power (W)	Specific Resistance	Mean Lateral Disp., d (m)	Number of Trials / Success Rate (%)
7	0.90	0.97	80.28	1.00	0.007	10 / 100%[1]

Table 5.5: Radial stiffness test results. [1]Twelve trials were performed but two were discounted because the robot failed to detect both the start and finish lines, despite having crossed them.

Due to the very large parameter space involved in the generation of the gait, it would be very difficult to establish a direct comparison between the gaits obtained with two sets of legs with different radial stiffness. Nevertheless, the tests presented in this section show that the gait is not extremely sensitive to variations in the radial

leg stiffness and that the controller can compensate, to some degree, for radial leg stiffness differences to obtain similar gaits.

5.5.2 Modified Lateral Leg Stiffness

Video analysis of experiments with the baseline hardware indicated that large lateral body deflections were taking place because of out-of-plane leg deflections. Figure 5.9 contains photographs showing out-of-plane leg deflections of the baseline legs. It was also observed that out-of-plane leg deflection effects could cause disturbances in the gait that lead to instability. These observations motivated the design and construction of legs with the same radial stiffness as the baseline legs, but with increased lateral and torsional stiffness. This was accomplished by constructing new composite legs with fewer layers but greater width. The resulting legs have a measured radial stiffness of 1620 N/m, which is nearly identical to the baseline radial stiffness of 1640 N/m. The larger 33.5 mm width, however, yields a theoretical increase in the lateral stiffness by a factor of 2.1 above the baseline.

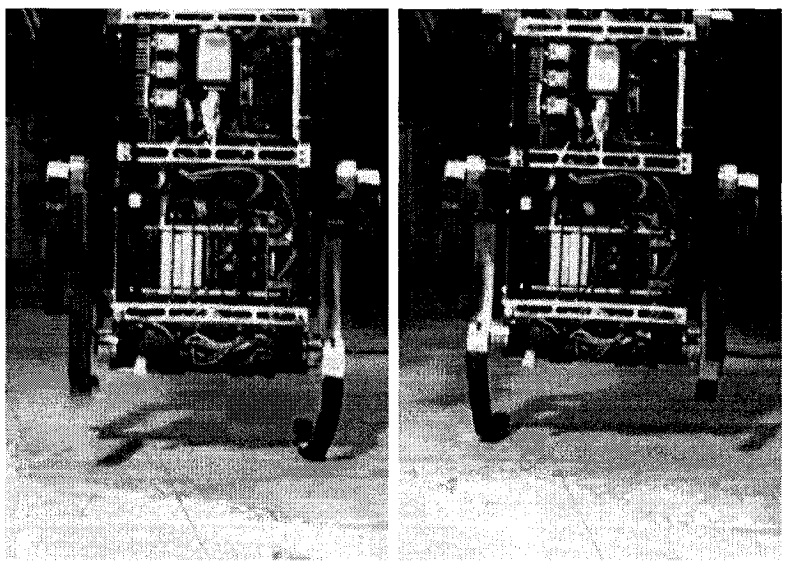

Figure 5.9: Pictures obtained using high frame rate video showing significant out-of-plane deflections of the legs on two successive steps

The wider legs resulted in visibly reduced out-of-plane deflection of the legs, and

lower lateral displacement of the robot during running. Stable roll oscillations were more easily generated when tuning the gait with these legs. It was found that, for a given speed, the duty factor could be decreased and the sweep angle increased more than was possible with the baseline legs. Table 5.6 presents the results obtained. Data Set 8 was obtained using the baseline leg trajectory parameters: $\phi_s(v_d)$=1.005 rad, $\beta(v_d)$=0.617, ϕ_o=-0.07 rad. Data Set 9 was obtained for a leg trajectory parameter set with a lower duty factor and larger sweep angle: $\phi_s(v_d)$=1.005 rad, $\beta(v_d)$=0.617, ϕ_o=-0.07 rad. The latter resulted in a 13% longer stride period and had the benefit of reduced flight phase hip speed requirements. The average hip speed during the flight phase was reduced by 23%, resulting in the hip motors not being required to saturate. This represents an improvement that is especially useful when considering the use of "C" shaped legs, which increase flight phase hip speed requirements. Thus, it was found that legs with an increased lateral stiffness could reduce the amplitude of the lateral displacement oscillation of the robot body, and because these legs allow a more desirable set of leg trajectory parameters to be chosen, these legs represent an improvement for bipedal RHex.

Data Set Number	Velocity Set-Point (m/s)	Average Speed (m/s)	Average Power (W)	Specific Resistance	Mean Lateral Disp., d (m)	Number of Trials / Success Rate (%)
8	0.90	0.98	84.6	1.05	-0.124	2 / 100
9	0.90	0.94	70.0	0.90	-0.165	2 / 100

Table 5.6: Lateral stiffness test results

5.5.3 Integration of, and Experiments with "C" Shaped Legs

Electrically actuated dynamic legged robots push motor limits to their maximum. Bipedal RHex is certainly no exception. This section details a platform upgrade involving the power supply, amplifiers, motors, and gearheads. This redesign draws on experience with the baseline hardware. Results of experiments to date with these legs are also summarized in this section.

As mentioned previously, "C" leg geometry requires the leg angle traversed during

the leg flight phase to be increased by a factor of $\frac{2\pi-\phi_s}{\pi-\phi_s}$, equal to 2.5 based on a nominal sweep angle $\phi_s = 1$ rad. Experiments with the "S" legs determined that the minimum flight phase average speed requirement was 16 rad/s, for a desired forward speed of 0.9 m/s. This translates to an average flight phase speed of 40 rad/s for the "C" shaped legs. Therefore, the following performance specifications were used for the redesign in order to accommodate the "C" shaped legs:

- Maximum output shaft speed > 50 rad/s
- Output shaft stall torque ≥ 4.3 Nm (stall torque of the baseline motor–gearhead assembly based on a gearhead efficiency of 80%)

Each design decision was judged considering the mass added to the robot and the amount of redesign required to accommodate new electronics and mechanical components. Furthermore, thermal considerations were important. Based on the above, Maxon RE30 motors in combination with 14:1 gearheads were chosen. Table 5.7 provides some of the key characteristics of the baseline and upgraded configurations; data sheets can be found in [49]. The battery supply voltage was increased from 24 V to 33.6 V nominal, with the option of using a voltage up to 39.6 V. As a result, it was required to upgrade the custom RHex motor driver board to allow voltages up to 40V. The torque–speed curves for the two configurations are given in Figure 5.10. The upgraded system features the same stall torque as the baseline hardware, but with the capability to operate at significantly higher speeds. Bench tests revealed that the upgraded system can achieve a maximum speed of approximately 58 rad/s while tracking the desired leg position and velocity trajectories.

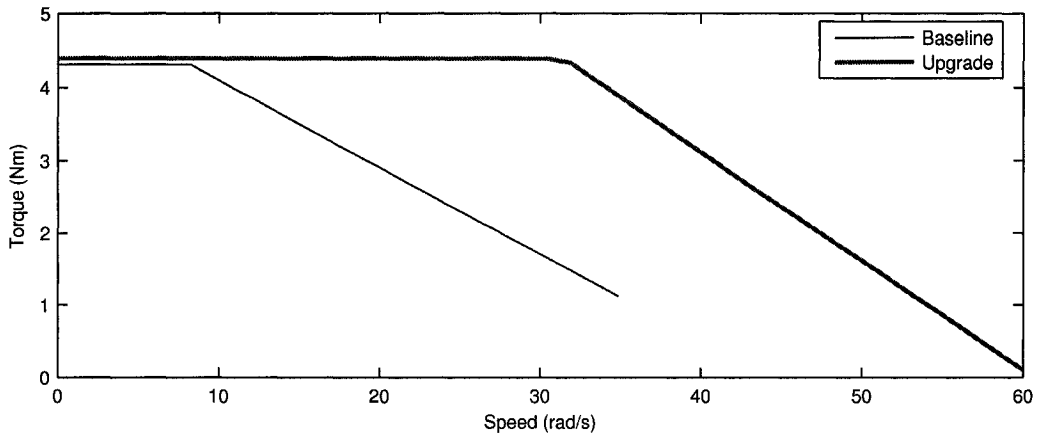

Figure 5.10: Motor torque speed curve based on maximum 10 A current draw and 80% gear efficiency

Component	Property	Baseline Configuration	Upgraded Configuration
Power Supply	Batteries	NiMH, 20 C cells	NiMH, 28 C cells
	Voltage	24 V	33.6 V
	Mass	1210 g	1690 g
Motors	Model	RE25	RE30
	Nominal voltage	18 V	36 V
	Assigned power rating	20 W	60 W
	No load speed @ V_s	13960 rpm	8000 rpm
	Max. allowable speed	11000 rpm	8200 rpm
	Stall torque	0.220 Nm	0.909 Nm
	Terminal resistance	1.33 Ω	1.58 Ω
	Torque constant	0.016 Nm/A	0.0398 Nm/A
	Speed constant	585 rpm/V	240 rpm/V
	Mass	130 g	238 g
Gearhead	Ratio	33:1	13.8:1
	Max. allowable torque	6 Nm	6 Nm
	Mass	162 g	162 g

Table 5.7: Platform upgrade specifications

Preliminary experiments with the "C" leg geometry and the upgraded platform (hardware configuration E) have not yielded a stable gait. As an intermediate step, a stable gait was successfully found for the upgraded platform, but with the "S" leg geometry. Then, based on the corresponding leg trajectory parameters, bench tests

were performed to demonstrate that the robot was capable of tracking the desired position and velocity trajectories required for "C" leg operation. Despite these results, the transition between the "S" and "C" legs has not yet been achieved. Under the above conditions, and assuming the legs are properly balanced, the difference between the "C" and "S" leg trajectories occurs *only* during the *assumed* flight phase where the "C" leg configuration requires higher velocities and accelerations. This suggests, as have previously discussed observations (Section 5.2.1, p. 53; Section 5.3, p. 62), the importance of the overlap between the *actual* stance phase and *assumed* flight phase on the dynamics of the gait. Modification of the flight phase position and velocity trajectories is suggested for future work, in order to make the dynamics around the touchdown and liftoff events similar to those obtained for the "S" shaped legs.

Chapter 6

Simulation Study

This chapter presents a simulation of bipedal RHex created in MSC.ADAMS® and Simulink®. The goal of the simulation was to provide a tool to test new controllers and the utility of additional sensors for bipedal RHex. Simulation also has the potential to provide a controlled environment in which the effect of physical property modifications on gait performance can be studied, without the constraints and cost involved in experimental work. This chapter begins with a summary of the ADAMS/Simulink model. Component models used in the simulation are then presented, along with a description of the important assumptions. A genetic algorithm (GA) used to successfully create a stable bipedal gait is then summarized. Finally, the resulting gait is presented and discussed.

6.1 Bipedal RHex Model and Simulation

Bipedal RHex was simulated using ADAMS and Simulink. This "co-simulation" uses ADAMS to integrate the mechanical dynamics of the system; thus, providing the plant. A discrete-time controller was created in Simulink. Every (simulated) sampling period (T= 1 ms), ADAMS passes the plant outputs to the controller. The controller in Simulink calculates the control inputs to the plant, which are passed back to ADAMS. This creates a discrete-time feedback control system. For more information on how ADAMS and Simulink exchange information see [2]. In the Simulink

controller, the leg trajectory generator, balancing controller, speed controller, leg tracking controller, and forward speed estimation method are the same as those that were implemented on the physical robot.

The ADAMS model of bipedal RHex consists of body and prismatic legs, as shown in Figure 6.1. The limitations and assumptions of such a leg model are discussed in Section 6.2.2. The ADAMS plant inputs are the hip torques: τ_l, τ_r. The required plant outputs are the body pitch angle and rate, and the leg angles and rates: θ, $\dot{\theta}$, $\dot{\phi}_r$, ϕ_r, $\dot{\phi}_l$, ϕ_l. In addition, the stiffness of the leg springs are variable and are calculated in Simulink, as will be discussed in Section 6.2.2.

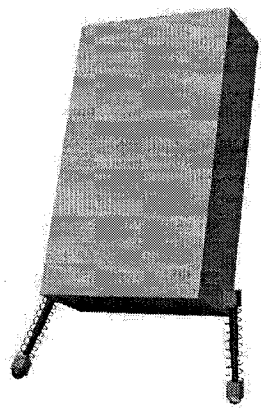

Figure 6.1: MSC.ADAMS model

6.2 Component Models

This section presents models of the robot body, legs, and actuators used in the ADAMS/Simulink simulation outlined in Section 6.1.

6.2.1 Body Model

The robot body is modeled as a rectangular prism with inertia properties (inertial matrix, COM location) obtained from a detailed SolidWorks® CAD model of the robot. The inertia matrix of the robot body, taken at the body COM and aligned with the *xyz* frame (as shown in Figure 3.5(a), p. 28) is approximately diagonal. The

mass and inertia matrix taken at the COM about the xyz axes (see Figure 3.5(a), p. 28) are given in Equations (6.1) and (6.2):

$$m = 8.4 \quad \text{kg} \tag{6.1}$$

$$\mathbf{I} = \begin{bmatrix} 17.80 & 0.21 & 0.00 \\ 0.21 & 6.01 & 0.14 \\ 0.00 & 0.14 & 22.50 \end{bmatrix} \times 10^{-2} \quad \text{kg m}^2. \tag{6.2}$$

In the simulation the small non-diagonal elements of the inertia matrix are set to zero so that the body is symmetric.

6.2.2 Leg Model

Bipedal RHex's half-circular legs (shown in Figure 3.4, p. 26) can deflect in three dimensions. These legs have highly nonlinear stiffness properties. Further complicating the modeling task, is a rolling contact that exists between the leg and the ground (e.g., the foot location, F, moves along the leg). The simulation model considers only sagittal plane leg deflections. This is supported by the results of Section 5.5.2, where it was shown that a leg design reducing out-of-plane leg deflections was beneficial to the gait. In this section, equations for the effective leg length, effective leg angle, and radial leg stiffness are presented. Based on these, the simulation leg model and assumptions are then discussed at the end of this section.

Effective Leg Length and Angle

The effective leg length, l_e, and the effective leg angle, ϕ_e, are shown in Figure 3.5(b), p. 28. Let $2r$ be the length of the leg. Recall that the foot is said to be located at the point of contact between the leg and the ground. Using simple geometric relationships, based on the leg angle ϕ we obtain Equations (6.3) and (6.4):

$$l_e(\phi) = \begin{cases} \sqrt{2}r\sqrt{1+\cos\phi} & \text{if } \phi \geq 0 \\ 2r & \text{if } \phi < 0 \end{cases} \tag{6.3}$$

$$\phi_e(\phi) = \begin{cases} \frac{\phi}{2} & \text{if } \phi \geq 0 \\ \phi & \text{if } \phi < 0 \end{cases}. \tag{6.4}$$

Radial Leg Stiffness

The purpose of this section is to derive the relationship between the radial leg stiffness and the location of the foot. The stiffness of the circular leg is a function of the material properties, cross section geometry, leg radius, and foot location on the leg. The model used to derive the stiffness properties of the leg is shown in Figure 6.2. Let the arc spanned by the leg from the hip to the foot be $\varphi_F \in [0, \pi]$. This model consists of a thin beam with one free end and one pinned end with reaction torque, τ.

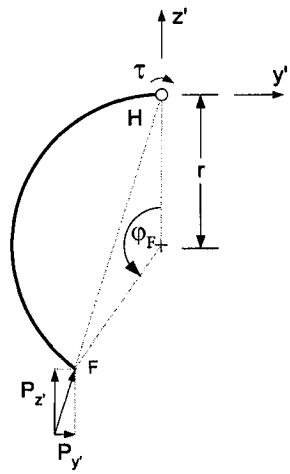

Figure 6.2: Leg stiffness model

The deflection, $\boldsymbol{\delta}$, due to applied force $\mathbf{p}$, was calculated using Castigliano's method [87]. The strain energy, U, contains only a bending term, axial strain and transverse shear strain are negligible for this particular geometry. Let E be the modulus of elasticity of the leg material, $I = \frac{bh^3}{12}$ the second moment of area of the cross section, b the width of the leg, and h the thickness of the leg. Deflections are

found from Equations (6.5)–(6.8):

$$\begin{aligned} \delta_y &= \frac{\partial U}{\partial P_y} && (6.5)\\ &= \int_0^{\varphi_F} \frac{rM}{EI}\frac{\partial M}{\partial P_y} d\varphi && (6.6)\\ \delta_z &= \frac{\partial U}{\partial P_z} && (6.7)\\ &= \int_0^{\varphi_F} \frac{rM}{EI}\frac{\partial M}{\partial P_z} d\varphi. && (6.8) \end{aligned}$$

In this case, the bending moment, M, is a function of φ. Let V be the shear force and let ds be an infinitesimal displacement along the leg. The shear force and bending moment relationships are given by Equations (6.9)–(6.12):

$$\begin{aligned} V &= -P_y \sin\varphi_F + P_z \cos\varphi_F && (6.9)\\ M &= \int V r d\varphi && (6.10)\\ M(0) &= r(1-\cos\varphi_F)P_y - rP_z \sin\varphi_F && (6.11)\\ M(\varphi_F) &= 0 && (6.12) \end{aligned}$$

Let $\mathbf{p} = [P_y \ P_x]^T$ and $\boldsymbol{\delta} = [\delta_y \ \delta_x]^T$. Performing the above integrals, the following force–deflection relationship is obtained:

$$\boldsymbol{\delta} = \mathbf{A}\mathbf{p}, \tag{6.13}$$

where $\mathbf{A}$ is a 2x2 matrix whose elements are:

$$\begin{aligned} a_{11} &= \tfrac{1}{4}(4\varphi_F + 2\varphi_F \cos 2\varphi_F - 3\sin\varphi_F)\\ a_{22} &= \tfrac{1}{4}(4\varphi_F - 2\varphi_F \cos 2\varphi_F - 8\sin\varphi_F + 3\sin 2\varphi_F)\ . \qquad (6.14)\\ a_{12} = a_{21} &= \tfrac{1}{4}(1 - 4\cos\varphi_F + 3\cos 2\varphi_F + 2\varphi_F \sin 2\varphi_F) \end{aligned}$$

Let $\mathbf{p}_r$ be a radial force of magnitude P, and let $\boldsymbol{\delta}_r$ be a radial leg deflection. This radial leg force is applied at the foot and is directed towards the hip. In the leg frame $\mathbf{p}_r$ is

$$\mathbf{p}_r = \left[\ P\sin\left(\tfrac{\pi-\varphi_F}{2}\right) \quad P\cos\left(\tfrac{\pi-\varphi_F}{2}\right) \ \right]^T \tag{6.15}$$

The radial stiffness, k_r, is then

$$k_r = \frac{||\mathbf{p}_r||}{||\boldsymbol{\delta}_r||} \tag{6.16}$$

$$= \frac{P^2}{\boldsymbol{\delta}_r^T \mathbf{p}} \tag{6.17}$$

The radial stiffness increases as the foot location moves away from the tip of the leg. Figure 6.3 contains a plot of the increase in radial stiffness, $k_r(\varphi_F)/k_r(\pi)$, as φ_F is varied from $2\pi/3$ to π radians. Here, $k_r(\pi)$ is the radial stiffness when the foot is located at the tip of the leg. High speed video recordings have shown φ_F to vary between approximately 2.1 and 3.14 rad. Thus, for this range of values, the increase in the radial leg stiffness is very significant, from 1 to 3.5.

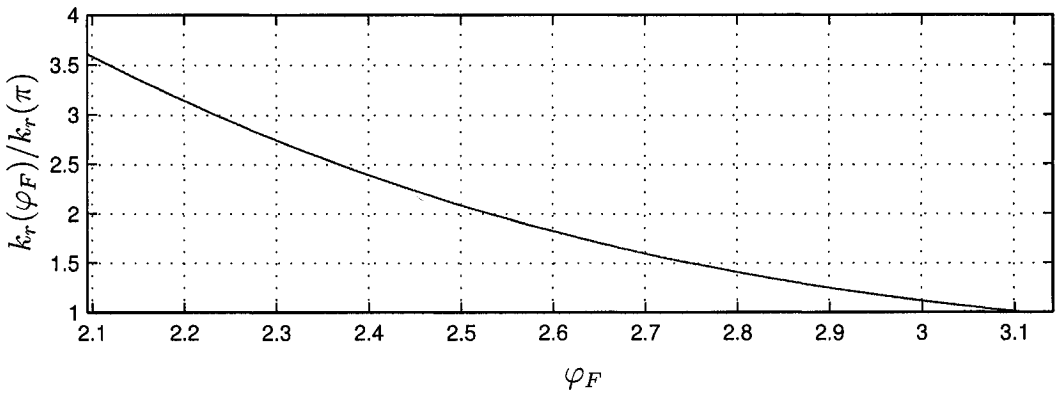

Figure 6.3: Relative radial stiffness, $k_r(\varphi_m)/k_r(\pi)$, of a half circle leg as a function of φ_F

ADAMS Leg Model

In ADAMS the legs are modeled as a prismatic joint and leg spring. The leg spring has a radial stiffness $\frac{k_r(\varphi_m)}{k_r(\pi)} k_r(\pi)$ and free length based on Equation (6.4). For practical implementation reasons, the calculation of the free length of the leg and the radial leg stiffness are performed in Simulink and passed to ADAMS. This simulated leg also includes linear viscous damping. In addition, the leg spring hardens when the leg is in both extension and flight, so that it does not extend significantly beyond

the desired uncompressed length. Thus, in this model, the rolling contact between the foot and the ground is neglected.

More complex leg models pose several problems. Firstly, a flexible curved beam leg can not be simulated in ADAMS because rolling contact along a flexible body is not possible [19]. Secondly, given that the simple model described here runs at approximately 1/40 realtime, added model complexity would result in the model becoming too computationally expensive, especially if iterative optimization algorithms, such as the one described in Section 6.3, are to be used to tune the gait and controller parameters.

6.2.3 Friction and Contact Model

In the ADAMS model the foot is modeled as a small sphere. The mass of the foot was calculated to achieve the desired leg inertia about the hip axis. The friction and contact properties of the unilateral joint formed between the foot and the ground were modeled using the impact and coulomb friction modeling options in ADAMS. Information on the underlying algorithm can be found in [19]. The static and dynamic friction coefficients for RHex on our test track were obtained by conducting a simple experiment: RHex foot material was attached to a weighted plate, which was pulled horizontally with an accurate spring scale. The following static and dynamic coulomb friction coefficients were obtained: $\mu_s = \mu_d = 0.65$.

6.2.4 Actuator Model

The motors, gearheads, and amplifier limits are modeled by a torque–speed curve, given in Figure 6.4. Only torque–speed combinations within the enclosed region are attainable. Let η be the gear efficiency, N the gear ratio, K_t the motor torque constant, and $i_{max,d}$ the maximum desired amplifier output current. Then,

$$\tau_{max} = \eta N K_t i_{max,d} \tag{6.18}$$

is the maximum torque. Similarly, τ_{stall} is the stall torque of the motor-amplifier-gearhead combination, $\tau_{stall} = \eta N K_t i_{max}$. The motor amplifiers on RHex can supply

a maximum of 15 A, resulting in $\tau_{stall} = 6.65$ N m. The maximum speed attainable, the no load speed, is denoted by $\dot{\phi}_{max}$ in the figure.

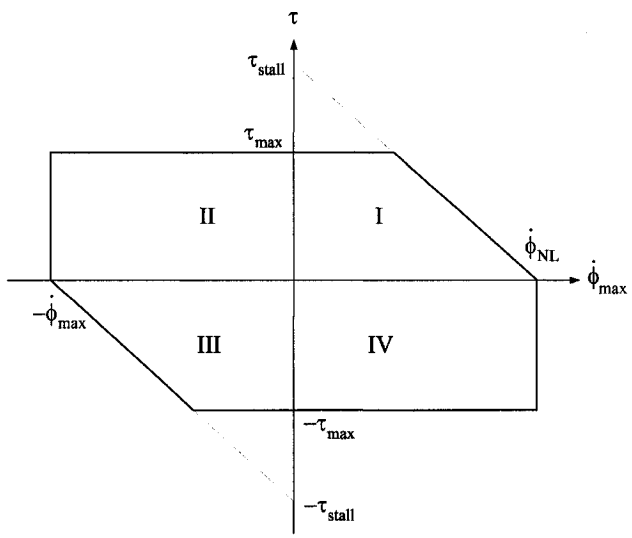

Figure 6.4: Torque speed curve schematic

6.3 Gait and Controller Parameter Tuning: Genetic Algorithm

This section presents details of a genetic algorithm (GA) used to tune gait and controller parameters for the ADAMS/Simulink model of bipedal RHex. As discussed in Chapter 2, genetic algorithms have been used successfully to generate gaits for both real and simulated systems. Key advantages [34] making GAs suitable for legged robot gait development are that they:

- Can deal with large numbers of parameters, continuous or discrete;
- Can optimize parameters with extremely complex cost surfaces;
- Can provide a list of possible solutions;
- Can be used with experimental or numerically generated data.

The parameter tuning problem was formulated as a 10 dimensional optimization problem. The parameters optimized were:

- Constants $c_1 \cdots c_5$ in option A of Table 3.2 (p. 32), required to generate leg trajectory parameters ϕ_o, β, and ϕ_s
- Balance angle, θ_b
- Leg tracking proportional gain, $k_{\phi p}$
- Two PD gains for the inverted pendulum balancing (pitch) controller: $k_{\theta p}$, $k_{\theta d}$
- Proportional gain for the inverted pendulum speed velocity controller: k_{vp}.

The function to be minimized, the *fitness function*, is critical to the outcome of the optimization. After experimentation, the fitness function chosen was

$$\begin{aligned} fitness \;=\; & w_1 \int_0^{t_{end}} |\theta - \theta_d|^2 \, dt + w_2 \int_0^{t_{end}} |v - v_d|^2 \, dt - w_3 \left(t_{end}\right)^{1.5} + \\ & - w_4 \left(\int_0^{t_{end}} v dt \right)^{1.5} + w_5 \left(\int_0^{t_{end}} |\phi_{r,end}| dt + \int_0^{t_{end}} |\phi_{l,end}| dt \right)^{-1} + \text{penalty}. \end{aligned} \tag{6.19}$$

where, t_{end} is the length of the simulation, $w_1 \cdots w_5$ are weighting constants, v is the actual measured forward speed of the robot (measured at the midpoint between the hips), and $\phi_{l,end}$, $\phi_{r,end}$ are the total left and right leg rotations, respectively. Recall that v_d is the desired forward speed, θ is the body pitch angle, θ_d is the desired body pitch angle. The end of the simulation is triggered by a maximum simulation time being reached, a maximum distance being traveled by the robot, or by limits imposed on the body pitch angle, body COM height, or body roll angle being exceeded. The first two terms of Equation (6.19) penalize large pitch and forward speed errors. The third term rewards trials where the robot lasts longer without trigging the end of the simulation. The fourth term rewards trials in which the robot travels greater distance. The leg rotation term in Equation (6.19) was required to heavily penalize solutions not using over-the-hip leg protraction. In addition, a penalty term was added to the fitness function in order to discourage certain parameters from assuming values outside a specified range. This method of constraint handling penalizes a given parameter based on how far it is outside a desired range of values, thus, allowing the algorithm to find unexpected solutions outside the desired parameter range. The

penalty term is calculated via

$$p_j(x_j) = \begin{cases} \kappa_{ll,j}\frac{x_j - ul_j}{ul_j - ll_j} & \text{if } x_j < ll_j \\ \kappa_{ul,j}\frac{ll_j - x_j}{ul_j - ll_j} & \text{if } x_j > ul_j \\ 0 & \text{otherwise} \end{cases} \tag{6.20}$$

$$\text{penalty} = \sum_{i=0}^{10} p_j(x_j) \tag{6.21}$$

where, j is an index indicating the parameter number, x_j is the j^{th} parameter, p_j is the penalty assigned to parameter x_j, ll_j is the lower limit below which a penalty is applied for x_j, ul_j is the upper limit above which a penalty is applied for x_j, and $\kappa_{ll,j}$, $\kappa_{ul,j}$ are the weighting constants. The magnitude of the penalty must be limited because it can negatively affect the ability of the algorithm to converge to a stable gait.

The Matlab Genetic Algorithm and Direct Search toolbox was used to implement the GA. The population size had to be limited because of the computational cost of each trial, a population size of 25 was typical, and the duration of a typical optimization was approximately 50-150 generations.

6.4 Results and Discussion

In this section we present the simulation results obtained with the ADAMS/Simulink model of bipedal RHex. A stable gait could not be obtained with extensive "manual" tuning of the gait and controller parameters. This suggests that the simulation model is even more sensitive to gait and controller parameter variations than the real system. However, the genetic algorithm optimization described in Section 6.3 produced a stable gait over the 7 m distance (approximately 28 strides) allowed by the model. Table 6.2 summarizes key simulation model parameters and Table 6.2 presents a comparison between the simulation and experimental gait and controller parameters.

In table 6.2 we see that the parameters are similar in all cases except for the leg tracking proportional gain $k_{\phi p}$, and to some extent the leg trajectory parameters.

Parameter	Value	Units
Leg Properties		
Uncompressed leg length	0.165	m
Radial stiffness, $k_r(\pi)$	1640	N/m
Radial viscous damping	125	N/(m/s)
Static friction coefficient, μ_s	0.65	
Dynamic friction coefficient, μ_d	0.65	
Mass moment of inertia about hip axis, $I_{Leg_{xx}}$	0.0055	N m^2
Actuator Limitations		
Stall torque	6.65	N m
Maximum torque	6.65	N m
Hip motor no load speed	100	rad/s
Robot Geometry		
Hip spacing	0.3	m

Table 6.1: Simulation parameters

These differences are assumed to be largely attributable to the un-modeled rolling contact that exists between the leg and the ground. The larger value of the leg tracking P gain and the smaller sweep angle appear to be required to help get the leg "under" the robot without the aid of rolling.

Table 6.3 summarizes the simulated gait. The power and specific resistance numbers are comparable to the values obtained in experiment, see Table 5.2, p. 59.

Figure 6.5 shows the leg velocities, positions, and torques over two strides. We observe that good tracking is achieved of both the position and velocity trajectories. It is clear from the abrupt changes in the leg velocity plot that the touchdown event occurs about 10 ms before the *assumed* touchdown event. Recall that in experiment the actual touchdown event was observed to occur slightly after the assumed touchdown event. The leg velocity plot also indicates a good correspondence between the actual and assumed liftoff events. In contrast, assumed liftoff events occurred during the actual stance phase in experiment.

The leg trajectory parameters are plotted in Figure 6.6 along with the resulting stride period. The relatively constant parameters indicate good gait stability. The

Parameter	Simulation Value	Experimental Value
Controller Parameters		
Balancing P gain, $k_{\theta p}$	36.1	35
Balancing D gain, $k_{\theta d}$	0.4	0.4
Balance angle, θ_b	1.43	1.47
Speed P gain, k_{vp}	0.064	0.055
Leg tracking P gain, $k_{\phi p}$	20.0	4.6
Leg tracking D gain, $k_{\phi d}$	0.39	0.50
Leg Trajectory Parameters		
Duty factor, β	0.69 - $0.02\dot{\phi}_d$	0.785 - $0.028\dot{\phi}_d$
Offset, ϕ_o	0.18	-0.07
Sweep angle, ϕ_s	0.36 + $0.038\dot{\phi}_d$	0.84 + $0.0275\dot{\phi}_d$

Table 6.2: Controller and gait parameters

Velocity Set-Point (m/s)	Average Speed (m/s)	Average Power[1] (W)	Mechanical Specific Resistance	Specific Resistance[2]
0.91	0.88	96	1.33	1.91

Table 6.3: Simulation gait summary. [1]Average power is based on the actuator input alone. [2]Specific resistance based on an electronics overhead of 42.7W, as obtained for the real robot.

average duty factor is equal to approximately 0.6. Thus, a double stance phase, of similar duration as was found in experiment, exists. The average stride period is approximately 0.2 s, 26% lower than in experiment.

Body pitch, roll, and yaw angles are plotted in Figure 6.7. The error in the pitch angle is typically less than 3°, indicating that the body pitch successfully tracks the desired angle. The roll angle is stable, but the mean value is non zero. This is due to non-zero initial conditions. The roll oscillation amplitude is small, approximately 2°, as compared to 4-6° in experiments. This is the result of the shorter stride period in simulation, which reduces the duration of the single support stance phase. The yaw angle plot is qualitatively similar to that obtained in experiment. It shows that the robot's forward direction is stable, without any yaw angle feedback control.

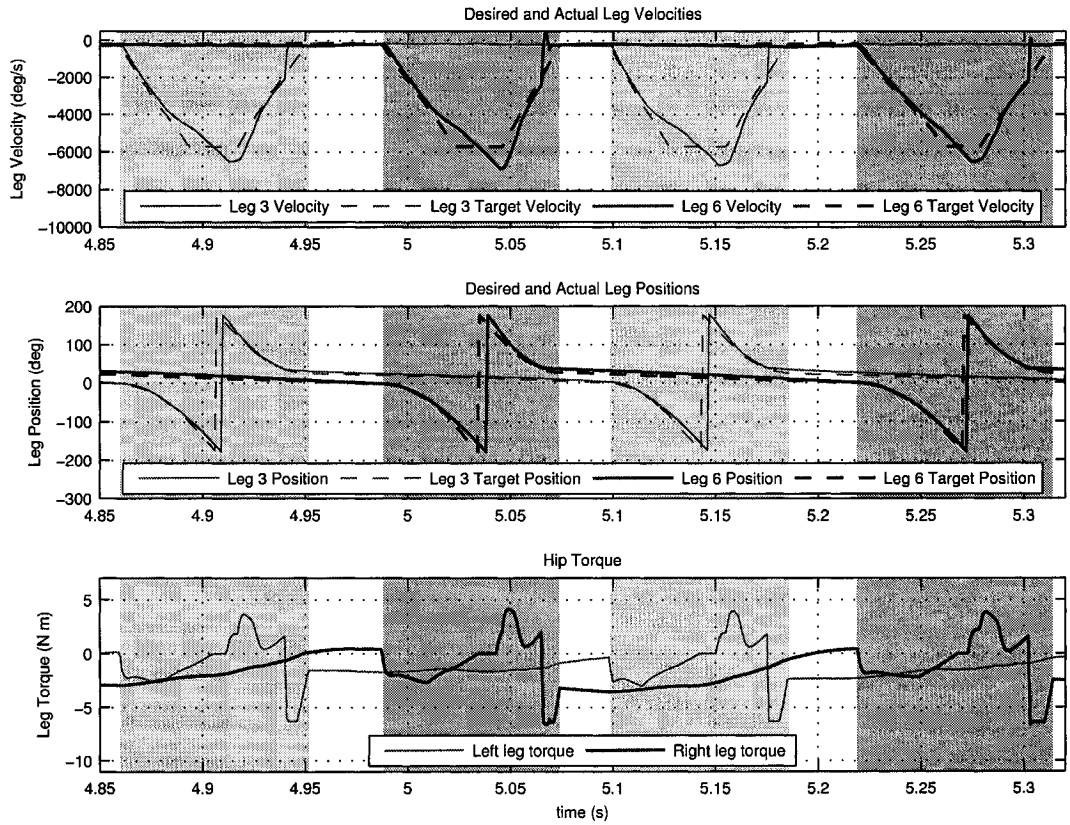

Figure 6.5: Simulation leg velocity, position, and hip torque plots

Figure 6.7 also includes a plot of the forward speed, desired forward speed, and estimated forward speed. The error in the average speed was 3%, showing good speed control. Although the estimated forward velocity lags the actual forward velocity, the error is generally less than 0.2 m/s.

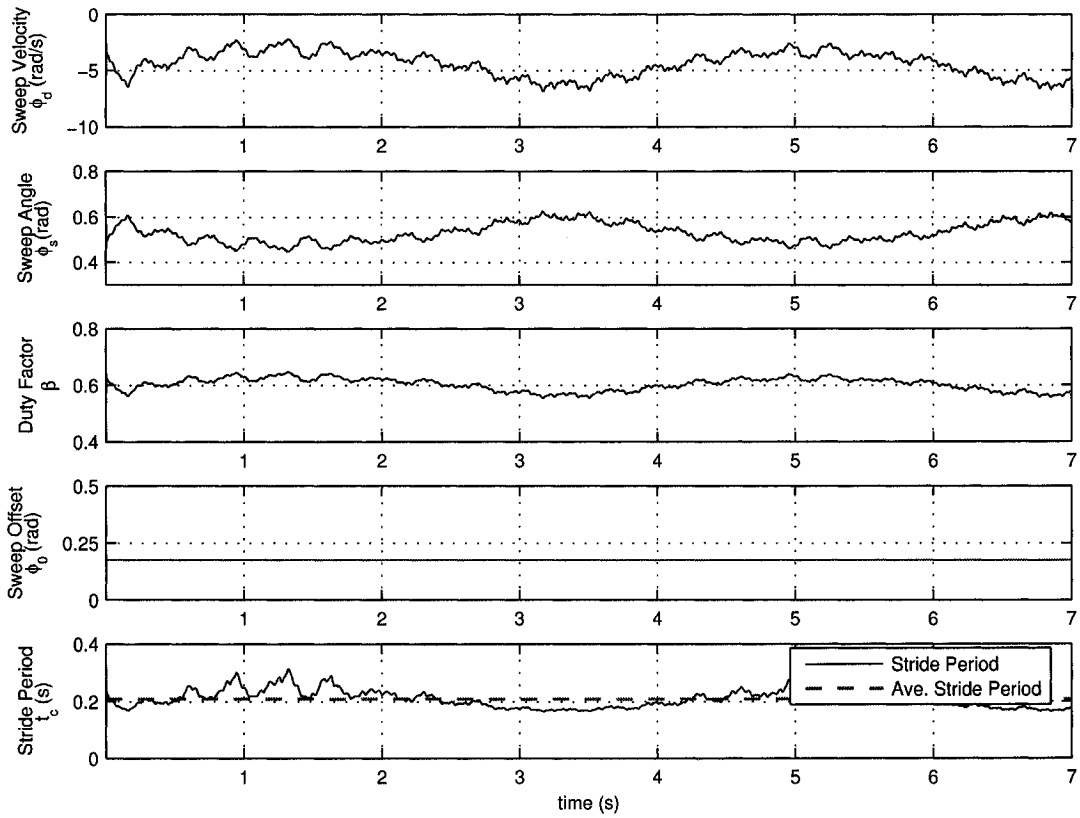

Figure 6.6: Leg trajectory parameter and stride period plot

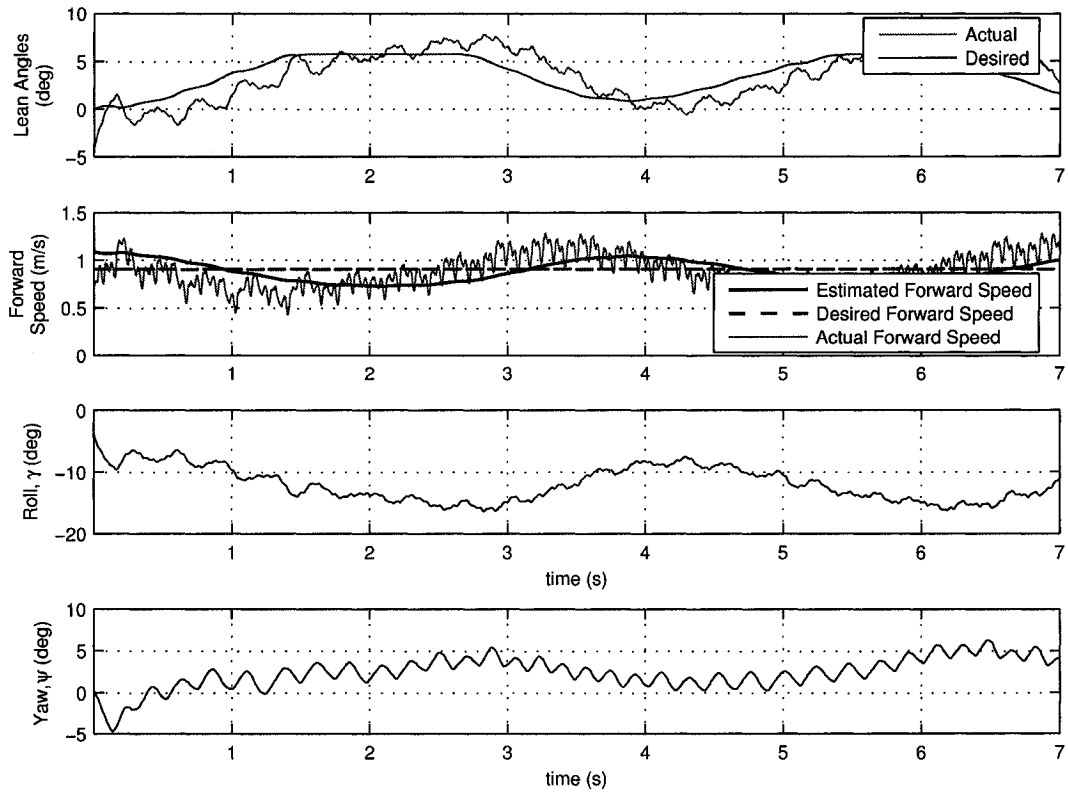

Figure 6.7: Simulation body pitch angle, forward speed, roll angle, and yaw angle plot

In summary, a stable gait was successfully obtained in simulation. It was found that it was more difficult to tune a gait in simulation than in experiment. However, the feasibility of optimization methods, such as the genetic algorithm presented above, partially compensate for this difficulty. Furthermore, although qualitative and quantitative similarities exist between simulation and experiment, the difference in the required leg tracking gains and leg trajectory parameters suggests that the simulation model can be further improved. The use of this simulation of bipedal RHex to study new controllers, additional sensors, and physical parameter modifications is suggested for future work.

Chapter 7

Conclusions

7.1 Summary and Conclusions

This thesis presented the development of a novel, three dimensional, bipedal running gait for the RHex robot, a cockroach-inspired hexapod robot capable of range of behaviors, including hexapedal walking, running, and stair climbing. The behavior presented in this thesis uses only two actuated degrees of freedom (DOF), one per compliant leg – the minimal number of actuated DOF required for a dynamically stabilized biped. The benefits of such a simple actuation approach are reduced system cost and weight, and improved reliability. To the author's knowledge, there are no previous (2D or 3D) bipeds with only one actuated degree of freedom per leg capable of dynamic running.

In Chapter 3, a pitch and forward speed controller was presented. This sagittal plane controller included three proportional derivative (PD) control laws for pitch, forward speed, and leg tracking. A leg trajectory generation scheme, parameterized by four leg trajectory parameters, was presented in detail. Suitable relationships for the leg trajectory parameters were also given. It was found that a forward speed measurement was not required to stabilize the forward speed of the robot – a simple forward speed estimation scheme based on the desired sweep velocity was sufficient.

In terms of sensing, it was found that only pitch and leg angle sensing are required. Based on the pragmatic stability criteria presented in this thesis, the resulting

gait had a 50% success rate, with failures due to the robot veering off the test track. However, with the addition of yaw angle feedback, a steering controller improved the repeatability of the gait (for the baseline hardware configuration) to 100% over 30 trials (Table 5.2, p. 59). The steering controller, which differentially modifies the leg trajectory parameters between the two legs, was presented in Chapter 4. This chapter also included a discussion of gait and controller parameter tuning, a critical issue for the success of the gait. It was found that stable running is very sensitive to controller and gait parameter variations and that the tuning procedure required was labor intensive and dependent on the operator's skill.

Body roll stability was discussed in Chapter 4. Roll stability was analyzed in terms of the dimensionless moment of inertia, which was found to have a value above unity, indicating that roll oscillations may not be passively stable, under the stated assumptions. However, the forced response, which includes a short double stance period, was experimentally shown to have stable roll oscillations without active roll angle control. In addition, it was found experimentally that vertical and lateral oscillations do not require active control.

Chapter 5 presented experimental results. With the baseline configuration, forward speed control was demonstrated for 0.64, 0.86, and 1.15 m/s set-points. The mean velocity error of the average speed was 4.3%, for 30 trials. The minimum and maximum speeds obtained were 0.57 and 1.26 m/s, respectively. However, the gait and controller parameters were not tuned explicitly to maximize the range of forward speeds possible. Specific resistance values ranged from 0.9 to 1.55, comparing favorably to the ARL Scout II, RHex bounding, and RHex pronking, among other robots.

Experiments were performed to determine the effect of the radial leg stiffness on the gait. It was found that stable bipedal gaits could be obtained for all the radial stiffness values tested (1492, 1640, 2250 N/m). However, because of the effect of the large number of gait and controller parameters on stability and energy efficiency, it was difficult to directly compare the gaits obtained with sets of legs of different radial stiffness. However the results indicate that the controller can compensate, to some degree, for different radial leg stiffness values.

Motivated by video recordings showing significant out-of-plane leg deflections, wider legs with the same radial stiffness as the baseline legs, but with approximately twice the lateral leg stiffness were designed and fabricated. These legs resulted in visibly reduced lateral body oscillations and allowed for a set of leg trajectory parameters to be chosen that significantly reduced flight phase hip speed requirements. These legs were also used to generate a 0.94 m/s gait with a specific resistance of 0.9, the lowest value presented in this thesis.

The results presented in this thesis used "S" shaped legs, as opposed to the regular "C" shaped legs used on RHex (see Figure 3.4, p. 26). This "S" shape leg configuration reduces the actuator speed requirements when not in stance, but otherwise does not fundamentally change the dynamics or control of the system. Preliminary results using a hardware upgrade designed to accommodate "C" leg operation were summarized in Chapter 5. However, in preliminary tests "C" leg operation was not attained.

Finally, Chapter 6 presented a simulation of bipedal RHex that successfully produced a stable gait. A genetic algorithm optimization was employed to obtain a stable gait, when manual tuning was not successful. The results suggest that the model can be further improved by accounting for rolling between the leg and ground. The simulation gait was qualitatively similar to those produced in experiment. Furthermore, with few exceptions, the simulation gait displays quantitative similarities to experimental gaits.

7.2 Recommendations and Future Work

Several recommendations for future work are suggested in terms of experimental work, platform design, and simulation.

The preliminary results obtained with the upgraded platform (Section 5.5.3, p. 72) show potential for "C" shaped leg operation. Modification of the flight phase position and velocity trajectories is suggested, in order to make the dynamics around touchdown and liftoff events similar to those obtained for the "S" shaped legs. Once "C" shaped leg operation is accomplished, bipedal mode could be further integrated

into RHex's already large behavioral repertoire by creating transitional behaviors between hexapedal and bipedal running. Such behaviors would allow increased step and obstacle clearance capabilities for the RHex robot due to the raised COM of the bipedal RHex.

In terms of experimental work, it is suggested that Controller #2 (Section 3.2.3, p. 34) be experimentally tested and the results compared to those presented in this thesis for Controller #1.

It is expected that mass distribution modifications could improve the performance of the gait and simplify the control task by making the passive dynamics of the system more suitable to the gait. Modification of the hip spacing is another option. One suggested approach would be to use the middle legs instead of the back legs on RHex to achieve a bipedal gait. In this case, the dimensionless inertia in the roll plane would be approximately 0.25. In this configuration, an added benefit would be that because of the approximately symmetric nature of the body about a vertical plane through the middle hips, the front and rear legs could be replaced by small, temporary "training wheels" that would contact the ground when the pitch angle is either too large or too small. This could make optimization algorithms such as in [94] feasible because it is expected that a sufficiently high percentage of trials would make it across a test track. In addition, the training wheels could also be used to provide reward/punishment feedback for optimization algorithms. The goal of such an optimization would be to obtain a gait where the "training wheels" never contact the ground. The results could then be compared to those presented in this thesis to generate insight into both gaits.

In terms of the platform design, it would be useful to incorporate changes that make the platform more amenable to an increased level of sensing and more detailed modeling. Such changes could allow more sophisticated controllers to be implemented. In particular, leg geometry and leg sensing is of interest. An example of such work, intended to improve hexapedal walking and running, is in progress for the RHex robot [48]. In this work instrumented, compliant, four-bar legs with point feet are employed in conjunction with wireless data transmission from the legs to the robot. However, alternative approaches could be taken.

Finally, simulation work has the potential to be useful in controller development, sensor selection, and as a tool to study the effect of physical parameters on the gait. For these reasons, future simulation work is recommended. In particular, a more complete leg model that does not neglect the rolling contact is suggested. However, because the intermittent and rolling contact present between the ground and the flexible leg cannot be accurately modeled with MSC.ADAMS, an alternative simulation environment should be explored.

Bibliography

[1] Honda Accord. Honda Motor Company. `http://automobiles.honda.com/models/specifications_full_specs.asp?ModelName=Accord+Sedan`, Accessed June 25, 2005.

[2] ADAMS/Controls, MSC.Software Corporation, `http://www.mscsoftware.com/products/products_detail.cfm?PI=428`, Accessed June 25, 2005.

[3] R.M. Alexander. The gaits of bipedal and quadrupedal animals. *Int J Robot Res*, 3(2):49–59, 1984.

[4] R.M. Alexander. Three uses of springs in legged locomotion. *Int J Robot Res*, 9(2):53–61, 1990.

[5] R. Altendorfer, U. Saranli, H. Komsuoglu, D.E. Koditschek, H.B. Brown Jr., M. Buehler, N. Moore, D. McMordie, and R.J. Full. Evidence for spring loaded inverted pendulum running in a hexapod robot. In *Proceedings of the International Symposium on Experimental Robotics*, December 2000.

[6] T. Arakawa and T. Fukuda. Natural motion trajectory generation of biped locomotion robot using genetic algorithm through energy optimization. In *IEEE International Conference on Systems, Man and Cybernetics*, pages 1495–1500, 1996.

[7] Ambulatory Robotics Lab. McGill University. `http://www.cim.mcgill.ca/~arlweb`, Accessed June 25, 2005.

[8] Fujitsu Automation. Humanoid robot. `http://www.automation.fujitsu.com/products/products0731.html`, Accessed June 25, 2005.

[9] J. Bares and D. Wettergreen. Dante II: Technical description, results and lessons learned. *Int J Robot Res*, 18(7):621–649, 1999.

[10] K. Berns. Walking machine calalogue. `http://www.walking-machines.org/`, Accessed June 25, 2005.

[11] D. Campbell. Bounding and stair descent in the hexapod RHex. Master's thesis, McGill University, February 2004.

[12] D. Campbell and M. Buehler. *Preliminary Bounding Experiments in a Dynamic Hexapod*, volume Experimental Robotics VIII of *Lecture Notes in Control and Information Sciences*, pages 612–621. Springer-Verlag, 2003.

[13] G.A. Cavagna, H. Thys, and A. Zamboni. The sources of external work in level walking and running. *J Physiol*, 262:639–657, 1976.

[14] C. Chevallereau, G. Abba, Y. Aoustin, F. Plestan, E.R. Westervelt, C. Canudas de Wit, and J.W. Grizzle. Rabbit: A testbed for advanced control theory. *IEEE Control Systems Magazine*, June 2003. Paper Number CSM-02-038.

[15] J.H. Choi and J.W. Grizzle. Planar bipedal robot with foot rotation (pre-print). In *American Control Conference*, pages 4909–4916, September 2005.

[16] S.H. Collins, A. Ruina, R. Tedrake, and M. Wisse. Efficient bipedal robots based on passive-dynamic walkers. *Science*, 307:1082–1085, February 2005.

[17] S.H. Collins, M. Wisse, and A. Ruina. A three-dimensional passive-dynamic walking robot with two legs and knees. *Int J Robot Res*, 20(7):607–615, July 2001.

[18] Honda Corporation. Say hello to asimo. `http://asimo.honda.com`, Accessed June 25, 2005.

[19] MSC Software Corporation. Using ADAMS/Solver. ADAMS/VIEW Documentation, 2003.

[20] P. Kaufman (Dir.). Rising sun. Film, 20th Century Fox Home Entertainment, 1993.

[21] C.T. Farley, J. Glasheen, and T.A. McMahon. Running springs: speed and animal size. *J Exp Biol*, 185(1):71–86, 1993.

[22] M. Fujita. Aibo: Toward the era of digital creatures. *Int J Robot Res*, 20(10):781–795, 2001.

[23] T. Fukuda, R. Michelini, V. Potkonjak, S. Tzafestas, K. Valavanis, and M. Vukobratovic. How far away is artificial man? *IEEE Robotics and Automation Magazine*, 8(1):66–73, March 2001.

[24] R.J. Full, K. Autumn, J.I. Chung, and A. Ahn. Rapid negotiation of rough terrain by the death-head cockroach. *Am Zool*, 38:81A, 1998.

[25] R.J. Full and C.T. Farley. *Biomechanics and Neural Control of Posture and Movement*, chapter 13, pages 193–205. New York: Springer Verlay, 2000.

[26] R.J. Full and D.E. Koditschek. Templates and anchors: Neuromechanical hypotheses of legged locomotion on land. *Exp Biol*, 202:3325–3332, 1999.

[27] R.J. Full and M.S. Tu. Mechanics of a rapid running insect: two-, four-, and six-legged locomotion. *J Exp Biol.*, (156):215–231, 1991.

[28] G. Gabrielli and TH. von Kármán. What price speed? *Mech Eng*, 72:775–781, 1950.

[29] L. Geppert. Qrio, the robot that could. *IEEE Spectrum*, 41(5):34–37, May 2004.

[30] H. Geyer, A. Seyfarth, and R. Blickhan. Spring-mass running: simple approximate solution and application to gait stability. *J. Theor. Biol.*, 232(3):315–328, 2004.

[31] A. Goswami. Postural stability of biped robots and the foot rotation indicator point. *Int J Robot Res*, 18(6):523–533, June 1999.

[32] P. Gregorio, M. Ahmadi, and M. Buehler. Design, control, and energetics of an electrically actuated legged robot. *IEEE Transactions on Systems, Man, and Cybernetics*, 27B(4):626–634, August 1997.

[33] V.S. Gurfinkel, E.V. Gurfinkel, A. Shneider, E.A. Devjanin, A.V. Lensky, and L.G. Shitilman. Walking robot with supervisory control. *Mech Mach Theory*, 16:31–36, 1981.

[34] R.L. Haupt and S.E. Haupt. *Practical Genetic Algorithms.* New York: John Wiley, 1998.

[35] H. Herr, G.T. Huang, and T.A. McMahon. A model of scale effects in mammalian quadrupedal running. *J Exp Biol*, (205):959–967, 2002.

[36] M. Hildebrand. Symmetrical gaits of horses. *Science*, 150:701–708, 1965.

[37] K. Hirai, M. Hirose, Y. Haikawa, and T. Takenaka. The development of honda humanoid robot. In *IEEE Int. Conf. Robotics and Automation (ICRA'98)*, pages 1321–1326, 1998.

[38] S. Hirose and Y. Umetani. The basic motion regulation system for quadruped walking vehicle. In *American Society of Mechanical Engineers, 80-DET-3*, 1980.

[39] University of Michigan J. Grizzle. Web site: `http://www.eecs.umich.edu/~grizzle/`, Accessed June 25, 2005.

[40] M. Gienger K. Lffler and F. Pfeiffer. Sensors and control concept of walking "Johnnie". *Int J Robot Res*, 22(3):229–239, March 2003.

[41] S. Kajita, T. Nagasaki, K. Kaneko, Y. Kazuhito, and K. Tanie. A hop towards running humanoid biped. In *IEEE Int. Conf. Robotics and Automation (ICRA'04)*, pages 629–635, 2004.

[42] K. Kaneko, F. Kanehiro, S. Kajita, H. Hirukawa, T. Kawasaki, M. Hirata, K. Akachi, and T. Isozumi. Humanoid robot HRP-2. In *Proc IEEE Int Conf Robotics and Automation (ICRA'04)*, pages 1083–1090, April 2004.

[43] T. Kato, A. Takanishi, G. Naito, and I. Kato. The realization of the quasi-dynamic walking by the biped walking machine. In *Proceedings of the International Symposium on Theory and Practice and Manipulators, ROMANSY*, pages 341–351, 1981.

[44] E. Klavins and U. Saranli. Object-oriented state machines. *Embedded Systems Programming*, 15(5), May 2002.

[45] N. Kohl and P. Stone. Policy gradient reinforcement learning for fast quadrupedal locomotion. In *IEEE Int. Conf. Robotics and Automation (ICRA'04)*, pages 2619–2624, 2004.

[46] H. Komsuoglu, D. McMordie, U. Saranli, N. Moore, M. Buehler, and D.E. Koditschek. Proprioception based behavioral advances in hexapod robot. In *Proceedings of the IEEE Int. Conf. on Robotics and Automation*, pages pp 3650 – 3655, Seoul, Korea, May 21-26, 2001.

[47] Leg Lab, Massachusetts Institute of Technology. `http://www.ai.mit.edu/projects/leglab/`, Accessed June 25, 2005.

[48] P.-C. Lin, H. Komsuoglu, and D.E. Kodistchek. A leg configuration sensory system for dynamical body state estimates in a hexapod robot. In *IEEE Int. Conf. Robotics and Automation (ICRA'03)*, volume 1, pages 1391 – 1396, September 2003.

[49] Maxon Precision Motors, inc., `http://www.maxonmotorusa.com/products/`, Accessed June 25, 2005.

[50] W.D. McArdle, F.I. Katch, and V.L. Katch. *Exercise physiology : Energy, Nutrition, and Human Performance.* Lippincott Williams and Wilkins, 2001.

[51] T. McGeer. Passive dynamic walking. *Int J Robot Res*, 9(2):63–82, April 1990.

[52] R.B. McGhee. Robot locomotion. In R.M. Herman, S. Grillner, P.S.G. Stein, and D.G. Stuart, editors, *Neural Control of Locomotion*, pages 237–264. Plenum Press, 1976.

[53] T.A. McMahon. Mechanics of locomotion. *Int J Robot Res*, 3(2):4–29, 1984.

[54] T.A. McMahon. The role of compliance in mammalian running gaits. *J Exp Biol*, 115:263–282, 1985.

[55] T.A. McMahon and G.C. Cheng. The mechanics of running: How does stiffness couple with speed? *J Biomech*, (23 Sup. 1):65–78, 1990.

[56] D. McMordie. Towards pronking with a hexapod robot. Master's thesis, McGill University, 2002.

[57] D. McMordie. Towards pronking with a hexapod robot. Master's thesis, McGill University, July 2002.

[58] D. McMordie and M. Buehler. Towards pronking with a hexapod robot. In *4th Int. Conf. Climbing and Walking Robots (CLAWAR'01)*, pages 659–666, 2001.

[59] D. McMordie, C. Prahacs, and M. Buehler. Towards a dynamic actuator model for a hexapod robot. In *IEEE Int. Conf. Robotics and Automation (ICRA'03)*, volume 1, pages 1386 – 1390, September 2003.

[60] H. Miura and I. Shimoyama. Dynamic walk of a biped. *Int J Robot Res*, 3(2):60–74, Summer 1984.

[61] E.Z. Moore and M. Buehler. Stable stair climbing in a simple hexapod. In *4th Int. Conf. Climbing and Walking Robots*, pages 603–610, 2001.

[62] E.Z. Moore, D. Campbell, F. Grimminger, and M. Buehler. Reliable stair climbing in the simple hexapod RHex. In *IEEE Int. Conf. Robotics and Automation (ICRA'02)*, pages 2222–2227, 2002.

[63] K.N. Murphy. Trotting and bounding in a simple planar model. Technical Report CMU-LL-4-1985, The Robotics Institute, Carnegie Mellon University, Pittsburgh, PA, USA, February 1985.

[64] K.N. Murphy and M. Raibert. Trotting and bounding in a planar two-legged model. In K Kedzior A Morecki, G Bianchi, editor, *5th Symposium on Theory and Practice of Robots and Manipulators*, pages 411–420. MIT Press, Cambridge MA, 1984.

[65] R.R. Murphy. Trial by fire [rescue robots]. *IEEE Robotics and Automation Magazine*, 11(3):50–61, 2004.

[66] California Institute of Technology NASA Jet Propulsion Laboratory. Mars exploration rover mission. `http://marsrovers.jpl.nasa.gov/home/`, Accessed June 25, 2005, 2004.

[67] K. Nishiwaki, T. Sugihara, S. Kagami, F. Kanehiro, M. Inaba, and H. Inoue. Design and development of research platform for perception-action integration in humanoid robot : H6. In *IEEE/RSJ International Conference on Intelligent Robots and Systems (IROS'00)*, volume 3, pages 1559–1564, 2000.

[68] K.i Nishiwaki, S. Kagami, Y. Kuniyoshi, M. Inaba, and H. Inoue. Online generation of humanoid walking motion based on a fast generation method of motion pattern that follows desired zmp. In *IEEE Int. Conf. Robotics and Automation (ICRA'98)*, pages 1321–1326, 1998.

[69] J.-H. Kim; J.-H. Oh. Realization of dynamic walking for the humanoid robot platform khr-1. *Adv Robotics*, 18(7):749–768, August 2004.

[70] Polypedal Lab, University of California Berkeley. `http://polypedal.berkeley.edu`, Accessed December 16, 2003.

[71] J.M. Porta and E. Celaya. Efficient gait generation using reinforcement learning. In *4th Int. Conf. on Climbing and Walking Robots (CLAWAR)*, pages 411–418, 2001.

[72] I. Poulakakis. On the passive dynamics of quadrupedal running. Master's thesis, McGill University, 2002.

[73] I. Poulakakis, J.A. Smith, and M. Buehler. Modeling and Experiments of Untethered Quadrupedal Running with a Bounding Gait: The Scout II Robot. *Int. J. of Robot Res.*, 24(4):239–256, 2005.

[74] C. Prahacs, A. Saunders, M.K. Smith, D. McMordie, and M. Buehler. Towards legged amphibious mobile robotics. In *Proceedings of the Inaugural Canadian Design Engineering Network (CDEN) Design Conference*, Montreal, Canada, June 29–30 2004.

[75] J. Pratt. Virtual model control of a biped walking robot. Master's thesis, Massachusetts Institute of Technology, Cambridge, Massachusetts, 1995.

[76] J. Pratt, C.-M. Chew, A. Torres, P. Dilworth, and G. Pratt. Virtual model control: An intuitive approach for bipedal locomotion. *Int J Robot Res*, 20(2):129–143, 2001.

[77] J. Pratt, P. Dilworth, and G. Pratt. Virtual model control of a bipedal robot. In *IEEE Int. Conf. Robotics and Automation (ICRA'97)*, 1997.

[78] L.G.C.E. Pugh. The relation of oxygen intake and speed in competition cycling and comparative observations on the bicycle ergometer. *J. Physiol.*, 241:795–808, 1974.

[79] Biped robot rabbit. `http://robot-rabbit.lag.ensieg.inpg.fr/English/`, Accessed June 25, 2005.

[80] M. Raibert. *Legged Robots That Balance.* MIT Press, 1986.

[81] M. Raibert, H.B. Brown, M. Chepponis, J. Koechling, J.K. Hodgins, D. Dustman, W.K. Brennan, D.S. Barrett, C.M. Thompson, J.D. Hebert, W. Lee, and L. Borvansky. Dynamically stable legged locomotion. Technical report, MIT Artificial Intelligence Laboratory, 1989.

[82] M.H. Raibert and J.K. Hodgins. *In Encyclopedia of Artificial Intelligence.* Wiley: New York, 1992.

[83] N. Robertson. Meet packbot: The newest recruit. `http://archives.cnn.com/2002/TECH/science/08/01/packbot/`, August 1, 2002. Accessed June 25, 2005.

[84] U. Saranli. *Dynamic Locomotion with a Hexapod Robot.* PhD thesis, University of Michigan, 2002.

[85] U. Saranli, M. Buehler, and D.E. Koditschek. RHex: A simple and highly mobile hexapod robot. *Int J Robot Res*, 20(7):616–631, July 2001.

[86] U. Saranli and D.E. Koditschek. Back flips with a hexapedal robot. In *IEEE Int. Conf. Robotics and Automation (ICRA'02)*, pages 2209–2215, 2002.

[87] R. Solecki and R.J. Conant. *Advanced Mechanics of Materials.* Oxford University Press, 2002.

[88] S. Song and K.J. Waldron. *Machines that walk.* MIT Press, Cambridge, MA, 1989.

[89] World's first running humanoid robot. Press Release, Sony Corporation, December 18, 2003. `http://www.sony.net/SonyInfo/News/Press/200312/03-060E/`, Accessed June 25, 2005.

[90] R. Tedrake and H.S. Seung. Improved dynamic stability using reinforcement learning. In *5th Int. Conf. on Climbing and Walking Robots (CLAWAR)*, pages 341–348, 2002.

[91] R.L. Tedrake. *Applied Optimal Control for Dynamically Stable Legged Locomotion.* PhD thesis, Massachusetts Institute of Technology, 2004.

[92] The robot with a hidden agenda. European Union Research Commission. `http://europa.eu.int/comm/research/success/en/ind/0277e.html`, Accessed June 25, 2005.

[93] M. Vukobratovic and A. A. Frank. On the gait stability of biped machines. *IEEE T Automat Contr*, 15(6):678–679, December 1970.

[94] J.D. Weingarten, G.A.D. Lopes, M. Buehler, R.E. Groff, and D.E. Koditschek. Automated gait adaptation for legged robots. In *IEEE Int. Conf. Robotics and Automation (ICRA'04)*, volume 3, pages 2153 – 2158, 2004.

[95] E. Westervelt. *Toward a Coherent Framework for the Control of Planar Biped Locomotion.* PhD thesis, University of Michigan, 2003.

[96] G. Zeglin and H.B. Brown. Control of a bow leg hopping robot. In *IEEE Int. Conf. Robotics and Automation (ICRA'98)*, Leuven, Belgium, May 1998.